



UCL

**Clinical Applications
of Electrical Impedance Tomography
in Stroke and Traumatic Brain Injury**

Nir Goren

A thesis submitted for the degree of

Doctor of Philosophy

Of

University College London

Department of Medical Physics and Biomedical Engineering

University College London

May 2020

Declaration

I, Nir Goren, confirm that the work presented in this thesis is my own. Where information has been derived from other sources, I confirm that this has been indicated in the thesis.


Signature

May 7, 2020
Date

Acknowledgements

Carrying out doctoral research is a fascinating and demanding journey, which I feel very privileged to have been able to undertake. Relocating with family to another country where another language is spoken, increases the hurdles to be overcome. I have many wonderful people to thank for making this journey possible.

I thank firstly my supervisor Professor David Holder for giving me the opportunity to join the UCL-EIT group, and for believing in me throughout the very long journey to complete this research project. I am incredibly grateful to Professor Jem Hebden, my second supervisor who has always made himself available to me unconditionally during the tough times as well as the good times. His support has been priceless. I also wish to thank Professor Gary Royle, for his support and practical guidance.


I feel very privileged to have had the opportunity to have been a member of the UCL-EIT group, a group of very talented and extremely nice people. I am forever indebted to Dr James Avery who from the start, answered my endless trivial physical questions with infinite patience and kindness. I thank Dr Kirill Aristovich who taught me all about reconstructions. I thank Dr Markus Jehl for his assistance with reconstructions, and for creatively adapting his electrode corrections algorithm. I am also grateful to Dr Tom Dowrick, for his technical support, Dr Brett Packham for his guidance given my physiologist background, to Dr Gustavo Sato do Santos for his assistance with statistics and provision of moral support and understanding of what it is like changing countries with a family to complete a PhD. I thank Dr Anna Witkowska-Wrobel for assistance with human studies and for sharing observations. I express my appreciation to Dr Mayo Faulkner, Dr Sana and Ilya Torotin who lent me their scalps for hours, and shared opinions and perspectives. I want to thank Eleanor Mackle who joined me for a charmed summer at UCL HASU to collect data, and for a tedious winter of skimming papers.

I am very grateful to Professor David Werring for instigating the positive collaboration with the UCLH stroke research team. I thank Renuka Erande for her professional approach to my EIT exception requests, and her wonderful research team: Caroline H., Caroline W., Azra, Krishna, Emma, and Maria, for helping me to recruit stroke patients. I was privileged to meet stroke patients who consented to take part in our

clinical study during tough times. Meeting these people and hearing their stories was one of the most meaningful human experiences I have ever had.

Surviving in London with two small sons would not have been possible without the generosity and vision of my parents-in-law Terry and Isaac Van der Horst, and my parents Yigal and Elisheva. I also thank my older brother Shai for his encouragement and statistical advice. I am grateful to all my family and friends in Israel and England for walking with me with end-less patience and love.

I am also grateful for the support of the organizations who saw us struggling and reached out: the Anglo Israel Association (AIA), the Bnai B'rith Leo Baeck Lodge and the Ian Karten Charitable Trust. I owe special thanks to Julia Samuel who reached out to us together with Ernest Kochmann, and who helped me with proofreading of the re-written thesis manuscript.

Last, but so so not least I thank my three little stars Itamar, Uri, and Alona, for sharing their daddy with brain research for the last eight years and Shira- my true love, and life partner - Thank you for always believing in me even when I had doubts, for literally supporting me in sickness and in health, and for going to the other side of the world and back with me for this. TODA .

Abstract

Electrical Impedance Tomography (EIT) is a medical imaging technology which uses voltage measurements on the boundaries to reconstruct internal conductivity changes. When applied to imaging brain function, EIT is challenged by the unique geometry of the head and the high variability in the conductivities of brain tissue. Stroke and Traumatic Brain Injury (TBI) are two of the leading causes of death and long-term disability worldwide. It has been suggested that EIT, which is already in clinical use primarily as a means of assessing lung function, could be used as a pre-hospital diagnostic tool for stroke and TBI, and for bedside monitoring for brain injury patients.

The main aim of this PhD thesis is to bring the application of EIT in brain injury closer to regular clinical use. Chapter 1 introduces the concepts of EIT, stroke and TBI, and provides a comprehensive review of clinically relevant neuroimaging techniques and the current state of brain EIT. Chapter 2 presents the results of a series of lab experiments designed to investigate the characteristics and mechanisms of drift in measured boundary voltages, which is the key technical barrier to brain monitoring with EIT. Experiments were conducted on lab phantoms, vegetable skin, and healthy human subjects. Chapter 3 describes a feasibility study of monitoring for brain injury with EIT over several hours, using noise recorded on real healthy volunteers. This study also compares the performance of different electrode types. Chapter 4 presents a clinical pilot study performed on acute stroke patients. Multi-frequency (MF) EIT data were recorded on patients and healthy controls to create the first of its kind clinical EIT dataset to be used as a resource for future research for the EIT community. Finally, the ability to identify stroke patients is demonstrated on the clinical EIT dataset.

Impact statement

The main goal of this PhD research work is to drive forward the clinical use of electrical impedance tomography (EIT) in brain injury to provide better early diagnosis and continuous monitoring of stroke and traumatic brain injury (TBI). As such, the primary potential beneficiaries are patients. The main outcomes of this work are new insights into EIT applied to the brain, and a new and unique clinical stroke EIT database.

New insights were generated concerning three crucial diagnostic applications of EIT: as a non-invasive, safe, affordable, bedside, monitoring tool for a secondary brain injury after head trauma or first stroke; the ability to verify brain injury/stroke on-site; and the ability to distinguish between the two types of stroke (ischaemic or haemorrhagic). This work has already yielded a peer-review paper reporting on the new stroke-EIT dataset [69]. This work will yield several more peer-review scientific publications:

- Observations on drift in baseline EIT measurements recorded on phantoms, vegetable skins, and human subjects.
- A feasibility study of TD-EIT monitoring for brain injury using simulated lesions with added realistic noise.
- Stroke identification using electrical impedance spectroscopy measurements in an acute stroke population.

Insights were gained by applying new concepts in a series of laboratory and clinical experiments. A database was established by collecting high quality data in acute stroke patients, which has been fully anonymised and openly shared online, and is available as a research resource to support further work on brain injury detection and type classification.

This is a multidisciplinary project, and as such its outcomes will potentially benefit relevant academic communities in both healthcare engineering and medicine, as well as biomedical industries. Within academia, the data and results, as well as methods used here for the first time, will support further studies in the field of brain EIT. The wider field of EIT for medical applications (such as lung monitoring and breast cancer diagnosis) could also utilise the insights and techniques resulting from this study. The research field of Electrical Impedance Spectroscopy (EIS) could also benefit from the EIT stroke database, as this consists of multi-frequency data. Related imaging tech-

nologies, such as optical or microwave imaging, which are targeting similar clinical applications, would benefit from knowledge gained here regarding common technical challenges, such as drift in baseline measurements, asymmetry analysis, and tissue spectra classification.

Outside academia, biomedical research and medical devices companies will be able to use the open database to drive their research forward. Once published, this demonstration of brain injury detection could encourage investment in those companies and hopefully also in further academic research.

Table of Contents

Table of Contents	11
1 Introduction	15
1.1 Overview	15
1.2 Introduction to Electrical Impedance Tomography (EIT)	17
1.2.1 Electrical Impedance	17
1.2.2 Bio-impedance	17
1.2.3 Bio-impedance of Brain Lesions	18
1.2.4 Electrical impedance tomography (EIT).....	21
1.2.5 Image reconstruction in EIT.....	25
1.2.6 Imaging Modalities	26
1.2.7 Sources of Errors in EIT	27
1.2.8 EIT Research from Idea to Clinical Uses	29
1.3 Stroke	31
1.3.1 Stroke Epidemiology	31
1.3.2 Pathophysiology of Stroke and Delayed Bleeding	31
1.3.3 The Burden of Stroke Mimics	32
1.3.4 Current Principles of Stroke Management.....	33
1.4 Traumatic Brain Imaging (TBI)	36
1.4.1 TBI Epidemiology	36
1.4.2 Pathophysiology of TBI and Delayed Bleeding.....	36
1.4.3 Principles of TBI management	37
1.5 Intracranial bleeds.....	39
1.6 Medical Techniques for Brain Injury Monitoring	44
1.6.1 Bedside Invasive Cerebral Monitoring.....	44
1.6.2 Non-Bedside Non-invasive Cerebral Monitoring.....	46
1.6.3 Pre-hospital and Non-invasive Bedside Cerebral Monitoring.....	48
1.6.4 The Multi-Modality Monitoring (MMM) approach and EIT Relevancy.....	55
1.7 Summary of Relevant EIT and EIS Literature	57
1.7.1 Fundamental Brain EIT Studies.....	57
1.7.2 Recent Brain EIT Studies	58
1.7.3 EIT for Brain Injury (Stroke and TBI)	60
1.7.4 EI Spectroscopy and Brain Symmetry Studies	62

1.8	The Aims of this Research Project	67
1.9	Statement of Originality.....	69
2	Investigation of Boundary Voltage Drift.....	71
2.1	Introduction.....	71
2.2	Rationale	72
2.3	Purpose	72
2.4	Experiment Design.....	73
2.4.1	Recording Types	73
2.4.2	Electrode Montage and Current Injection Protocols.....	75
2.4.3	BV Processing	76
2.4.4	Additional Data Parameters	78
2.4.5	Electrodes Movement Elimination (EME) by Reconstructing Changes in BV which are directly related to Electrode Movement.....	79
2.5	Method.....	80
2.5.1	Electrode Types	80
2.5.2	Data Collection.....	81
2.5.3	Data Processing and Statistical Analysis.....	83
2.5.4	Drift Elimination Trial	85
2.6	Results.....	86
2.6.1	BV Noise and Drift Comparison Between Electrode Types.....	86
2.6.2	BV Noise and Drift Characteristics in Resistor Phantom	88
2.6.3	BV Noise and Drift Characteristics in Head-shaped Tank	88
2.6.4	BV Noise and Drift Characteristics in Marrow	89
2.6.5	BV Noise and Drift Characteristics in Humans	93
2.7	Discussion	101
2.7.1	Summary of Results.....	101
2.7.2	Significance of Findings	102
2.7.3	Study Limitations.....	105
2.7.4	Conclusions and Future Work	106
3	Feasibility of Brain Injury Detection with TD-EIT.....	107
3.1	Introduction.....	107
3.2	Rationale	107
3.3	Purpose	108
3.4	Experiment Design.....	109

3.5	Method.....	111
3.5.1	Simulated Lesions	111
3.5.2	Real Drift Samples.....	112
3.5.3	Data Cleaning.....	113
3.5.4	Combining Simulated and Recorded BV.....	113
3.5.5	Image Reconstruction.....	113
3.5.6	Image Quality Assessment	115
3.5.7	Reconstructions' Meta-Data.....	116
3.6	Results.....	118
3.7	Discussion.....	120
3.7.1	Summary of Results	120
3.7.2	Significance of Findings.....	120
3.7.3	Conclusions and Future Work.....	122
4	EIT Clinical Study at UCL Hospital Hyper Acute Stroke Unit (HASU)	123
4.1	Introduction	123
4.2	Rationale.....	127
4.3	Purpose	127
4.4	Experiment Design.....	128
4.5	Method.....	133
4.5.1	Data Collection	133
4.5.2	Data Processing	139
4.5.3	Datasets for Statistical Analysis:	141
4.5.4	Statistical Analysis	142
4.6	Results.....	143
4.6.1	Standing BV	143
4.6.2	BV Left-Right Symmetry	143
4.6.3	Spectral Ratio (SR).....	145
4.6.4	Spectral Ratio Symmetry	145
4.6.5	Spectral Ratio Symmetry with Dry Electrode Locations Only	145
4.7	Discussion.....	147
4.7.1	Summary of Results	147
4.7.2	Significance of Findings.....	148
4.7.3	Conclusions.....	151
4.7.4	Study Limitations	152
4.7.5	Future Work.....	152

5 Discussion and Future Work	153
5.1 Summary of Studies.....	153
5.2 Discussion.....	154
5.2.1 Drift in TD-EIT.....	155
5.2.2 Feasibility of TD-EIT in Monitoring Head Injury	156
5.2.3 The UCLH Stroke-EIT Dataset and EIS for Stroke Diagnosis	156
5.3 Recommendations for Future Work.....	157
5.3.1 Drift Investigations for TD-EIT.....	157
5.3.2 EIS for Stroke and TBI Applications	158
Acronyms	161
References.....	163

1 Introduction

1.1 Overview

This document describes the work I undertook as part of my doctoral studies at the Department of Medical Physics and Biomedical Engineering at University College London (UCL).

Electrical Impedance Tomography (EIT) is a non-invasive medical imaging technique using the injection of low electrical currents and measuring voltage changes on the surface of the body under investigation, in order to reconstruct tomographic images. These images represent changes in tissue conductivities within the body. Inside the head, these changes could be the result of various conditions. EIT has been used in medical research for more than two decades. Several clinical applications have been suggested over the years, for example gastric emptying function, breast tumour detection, and lung ventilation [31], but its main clinical use currently is for lung function [63]. In relation to the brain, EIT is presently being researched for stroke detection [49,50], locating epileptic foci in epilepsy patients [57,156], imaging fast neuronal activity [10], and detecting spreading depression in the cortex [24].

In stroke and traumatic brain injury (TBI) patients, correct, swift diagnosis after onset, is crucial for a better prognosis [3,120]. Between 80-85% of strokes have been shown to be ischaemic and the remainder haemorrhagic. Confirmation of a stroke occurrence and the elimination of the possibility of an intracranial bleed is critical to ensure that a patient is sent to a stroke unit with imaging and thrombolysis abilities. Confirmation of a Large Vessel Occlusion (LVO) is vital for a better patient outcome with the patient diverted if necessary, to a stroke centre with endovascular capabilities [93,71]. Secondary bleeding into the primary infarcted area occurs in a significant proportion of cases, and is one of the most common, dangerous complications [110,7]. In moderate to severe TBI patients, confirming brain injury and its type at the scene will give the patient better survival chances. A delayed onset of intracranial bleeding could also occur and might even prove fatal [42,48,64,111]. Secondary bleeding could occur hours or even weeks after injury, and could also be misdiagnosed during hospital admission, even where a patient undergoes a CT scan of the head.

It has been suggested that EIT could be used in pre-hospital diagnosis and classification of brain injury [135,166,13], and in the monitoring of stroke and TBI patients

to detect secondary intracranial bleeding early [109,159], which has led to this current study. In addition to its theoretical ability to detect such vital changes, EIT has the potential to be a portable bedside low-cost solution for such cases. A patient, who is considered to be at risk of these issues after a preliminary assessment, could then be connected to a set of electrodes mounted on the scalp within minutes by a paramedic at the point-of-care or by a nurse in hospital. These would be connected to a portable device the size of a laptop computer in the ambulance or at the hospital bedside, providing images and alerting staff to any changes.

This document comprises an introductory chapter, three chapters describing the experimental work and its results, and a concluding chapter. The introduction provides an overview of bio-impedance and electrical impedance tomography, its principles, modalities and limitations, followed by background information on stroke and TBI, its management and secondary intracranial bleeding types. The final part of the chapter reviews existing methods for monitoring stroke and TBI patients, relevant recent EIT studies on which this study is based and discusses the relative advantages of EIT.

The second chapter describes the work done to explore the principal technical barrier behind the feasibility of using EIT as a monitoring tool for stroke and TBI. A series of laboratory experiments were conducted in humans and phantoms to characterise and investigate the drift in baseline voltage measurements. The third chapter reports on a feasibility study which employed a combination of computer simulations with real noise recorded with EIT from healthy subjects in the lab. The goal of the study was to explore whether EIT monitoring with existing instrumentation and algorithms is indeed possible with realistic drifts.

The fourth chapter reports on an extensive clinical study on acute stroke patients at University College London Hospital. It describes the process of data collection, the unique dataset created, and the subsequent data analysis. This data collection was informed by the results outlined in chapters two and three, and in addition by recent animal work done by members of the UCL EIT Group which has also explored the feasibility of EIT for assessment of stroke and TBI [49,50].

The final chapter summarises the findings of this project and the conclusions stemming from the experimental work and reviews the potential for future work in this area.

1.2 Introduction to Electrical Impedance Tomography (EIT)

1.2.1 Electrical Impedance – Basic Definitions

Electrical impedance (Z) is the measure of opposition of an electrical circuit. In pure Direct Current (DC) circuits, the impedance is the resistance ($Z = R$). In an alternating current (AC) circuits where capacitance (C) could be involved, a lag phase (also called phase angle, Φ) might be introduced where measured voltage is lagging behind the injected current. This turns impedance into a complex entity ($Z = R + iX$) where Z represents the absolute impedance (also called Modulus), and iX the imaginary part. i is the imaginary unit and X represents the reactance of the circuit. Reactance ($X = 1/\omega C$) is inversely proportional to frequency ($\omega = 2\pi f$), assuming capacitance is a fixed electrical property [79]. The inverse resistance for DC is Conductance (σ), which is the ability of a material to conduct electrical current and is equal to $1/R$. For AC, the equivalence of conductance is admittance which equals to $1/Z$. In many EIT studies, such as that reported here, a change in the conductivity of tissues is calculated instead of a change in resistivity.

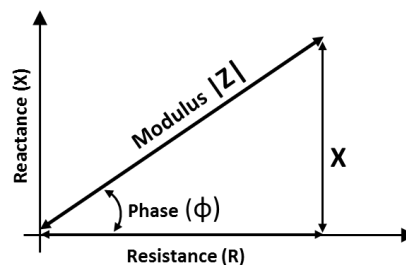


Figure 1-1: Impedance in the Complex Plane. A representation of the impedance as a combination of its amplitude and phase angle

1.2.2 Bio-impedance

Bio-impedance, which is fundamental to EIT applications, refers to the way the electrical characteristics of biological tissue change in response to an applied electrical current. As these differ from one tissue to another, bio-impedance allows us to distinguish between different tissues types and between histologic variants of the same tissue by applying electrical current and examining their dielectric properties. Biological tissue can be modelled as an electrical circuit consisting of resistors and capacitors (RC circuit). Intracellular and extracellular spaces, mainly consisting of ionic fluids, are represented as resistors. A lipid cell membrane on the other hand, is an electrical insulator with capacitive qualities [79].

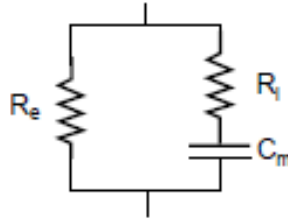


Figure 1-2: A Cell modelled as a basic RC Circuit. R_i and R_e are the resistances of the intracellular- and extracellular-space, and C_m is the membrane capacitance [79].

Tissue impedance changes with frequency as the capacitive reactance is frequency dependent. At low frequencies (< 100 Hz) current cannot penetrate a cell's membrane and will flow only through the extracellular space. As frequency increases, more current will cross the membrane and flow into the intracellular space. Thus, the resistive component of the impedance will decrease and the reactive component (phase angle) will increase. At very high frequencies, the reactance will become negligible and drop back towards zero, leaving only a resistive impedance with lower magnitude. This means that overall, Z decreases with frequency [79]. This typical behaviour of biological tissue impedance over frequencies is often demonstrated in what is termed a *Cole-Cole* plot, named after Cole and Cole who extensively studied the frequency response of dielectrics. Figure 1.3 is an extension of the resistance-reactance plot in the complex plane (figure 1.1). Instead of a single point for a measurement at one frequency, the values for a range of frequencies are all superimposed.

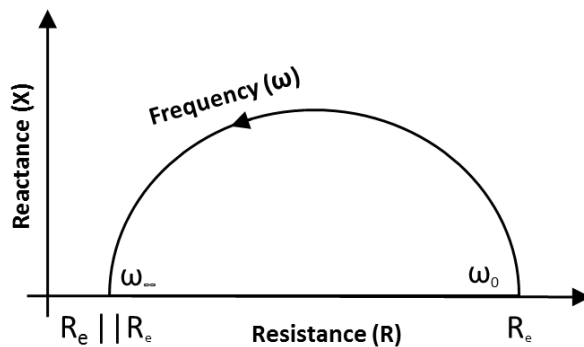


Figure 1-3: Idealized Cole-Cole Plot of Biological Tissue.

1.2.3 Bio-impedance of Brain Lesions

The human head consists of many different tissues, but is commonly modelled in terms of seven main tissue types: white matter, grey matter, cerebrospinal fluid (CSF), dura matter, skull, scalp, blood, and air (ears, mouth, and nose cavities). Oth-

er tissues, such as pia matter or blood vessels are omitted as their overall volumes are negligible or they are too spread out to be effectively modelled.

Establishing the precise conductivity values of tissues *in-vivo* is a complicated task, and although a rich literature exists, there is no consensus about those values. This is mainly due to the lack of uniformity in the design of such studies. As a review by Horesh [82] demonstrates, blood has a very different conductivity to most other head tissues, with an increase of 60 to 360% compared to brain tissues, or around a 60% decrease compared to CSF (table 1.1).

Tissue	Conductivity at 1 kHz (S/m)
Skull	0.018
Scalp	0.44
CSF	1.79
Dura matter	0.44
Grey matter	0.3
White matter	0.15
Air	0.001
Blood	0.7

Table 1-1: Summary of Approximate Head Tissue Conductivities at Low Frequencies, Used in this PhD Work. Adapted from Horesh PhD thesis, 2006 [82].

The values mentioned in the table above were used for simulations and image reconstructions in this thesis, as this proved to be the best source at the time. A recent work by McCann *et al* [113] was published in 2019, thoroughly reviewing the reported values of human head tissue conductivity. Comparing the above values to McCann's review confirmed that all of them are within the reported range. However, brain (grey and white matters) were in the lower range of the reported values while skull conductivity was at the higher end of the scale. Therefore, the Brain-to-Skull Conductivity Ration (BSCR), which is an important factor for EIT was slightly lower than the reported range. The review also concluded that conductivity varies significantly with different pathologies, and that conductivity of skull, white matter, and BSCR significantly correlates with age.

Grey matter comprises most of the cortex in the brain. The impedance of healthy grey matter is due to the conductive ionic extra-cellular and intra-cellular compartments, so there is a substantial change of conductivity with frequency (see 1.2.2). In contrast, blood behaves like an aqueous ionic solution up to 1 MHz so has a very flat frequency response [12,19]. In ischaemic grey matter, extracellular water moves into the intracellular space. As a result, the low frequency conductivity is reduced, but the

properties are similar at higher frequencies approaching 1 MHz. There are therefore large differences in conductivity over frequency between blood, normal brain tissue and ischaemic brain tissue which could be useful for MF-EIT.

When intracranial bleeding occurs (e.g. haematoma, haemorrhage, or haemorrhagic transformations) blood displaces other tissues, such as dura, grey or white matter, and CSF. In any type of bleeding lesion, the decrease in impedance is expected to be drastic as blood is much more conductive than other brain tissues and the impedance changes very little with frequency [82,49]. However, Mainwaring *et al* [58] found a mean conductivity difference of around 0.02 S/m during injection of 1 ml of blood in a piglet brain, an order of magnitude less than would be expected from the values mentioned above. It is possible the injected blood diffused over a larger area than intended, or ischaemia secondary to the injected blood into the white matter may have caused an impedance change in the opposite direction, cancelling out some of the change due to the blood.

Wang *et al* [159] recently found contradictory results between recordings of a haemorrhagic-like perturbation in a head-shaped tank with an open and closed skull. During recording using Time-Difference EIT, a decrease in impedance was observed with no skull present, while an increase in impedance was recorded in a similar setup with a skull. They speculated that this was due to a change in intracranial pressure. Yang *et al* [168], explored impedance spectra from a rabbits' *in-vivo* haemorrhagic stroke model. They also reported an increased impedance spectrum after the injection of autologous blood into the rabbit's brain. These findings were explained in terms of a reduction of CSF volume in the head, and/or ischaemia of the brain tissue squeezed by a pool of blood.

Dai *et al* [41] further investigated these findings in rabbits. Using 16 electrodes at 50 KHz, they injected autologous nonheparinized blood into 12 rabbits with open crania, and to 12 rabbits with intact crania. In this study, blood was injected for 150 seconds and both local impedance (the ICH area) and the whole brain impedance were monitored for 3 hours. They found that when the cranium was open, the impedance of the ICH area where the blood was injected, as well as the whole brain impedance, decreased relative to the amount of blood being injected. With an intact cranium, while the impedance of the area without ICH continued to increase, the impedance of the ICH area decreased within twenty seconds of the blood being injected. This then remained almost unchanged, and the whole brain impedance had a small fall before notably increasing. Therefore, when conducting experiments into

EIT of intracranial bleeding, care must be taken not to overestimate the contrast that blood represents in the brain, and not to dismiss findings that differ from those that are expected.

Unlike blood, ischaemic brain tissue caused by deprivation of oxygen supply, tends to exhibit an increase in impedance with time. The difference in conductivity between healthy and ischaemic brain tissue will increase over minutes and hours after the onset of a stroke. A very recent study published by Cao *et al* [33] monitored the impedance change of ischaemia in an animal model using 15 rats (10 ischaemia, 5 control) with open crania. They applied 8 electrodes and monitored a right MCA ischaemic lesion over 2 hours. Rats with ischaemia presented with both significant continuous increase in resistivity of the whole brain, and significant increasing difference between the impedance of the two hemispheres over time, in comparison with the control rats with healthy brains.

The change in conductivity as a function of frequency, however, is quite similar for both ischaemic and healthy brain tissue [82,49,170], making differentiation between the two over frequency very challenging.

1.2.4 Electrical impedance tomography (EIT)

In electric impedance tomography (EIT), a low amplitude alternating current is injected into the body under investigation, and voltage is measured with surface electrodes. Measured boundary voltages (BV) are then used, together with prior knowledge about the electrical properties of biological tissues to calculate a map of conductivity changes ($\Delta\sigma$) inside the body. This map can then be translated into a tomographic image.

A common EIT device - Includes: a) An electronics box containing a constant current source and voltage recording amplifier; b) a head box containing a switch board, connectors, leads and electrodes; and c) a PC / laptop – with software controlling the injection protocol, storing, demodulating the recorded signal, and reconstructing images.



Figure 1-4: The UCL ScouseTom EIT System in Tank Experiment

A custom EIT system is used by the UCL EIT group for the development of EIT applications. It is known as the “ScouseTom” [17]. This has two main components: a current source and a voltage measurement unit. Both are commercially available, off-the-shelf-units: a Keithley 6221 current source, and a Biosemi ActiveTwo EEG amplifier (figures 1.4,1.5). This kind of system is particularly useful during methodological development as it is modular and flexible to use. The ScouseTom was the system used throughout this research project.

Current Injection - Keithley 6221 Current Source

- Designed for semiconductor testing
- Frequency: 0.001Hz to 100kHz
- Amplitude: 2pA to 200mA
- Output Impedance: $\sim 10^{14}\Omega$
- Output Noise: $< 1 \text{ mV}_{\text{RMS}}$ (5 mV_{pp})
- Very stable across load and frequency
- MATLAB/LabView Compatible
- Can produce composite waveforms



Voltage Recording - BioSemi ActiveTwo EEG Amplifier

- Allows for simultaneous sampling of all channels
- Entire waveforms is captured for offline processing
- 24-bit ADC
- Max Sampling Frequency: 3kHz
- Channels: 256
- Input range: -1048 to +1048 mV
- Input Impedance: 200M Ω
- Input Noise: 2.0 μV RMS



Figure 1-5: Commercial Components of the ScouseTom EIT system

Methods for use of Two, Three, and Four Terminals – Using four terminals (or four electrodes), current is injected via two electrodes and voltage is recorded by the two other electrodes. The two terminals method uses the same pair of electrodes through which to inject the current and record the voltage. When using three terminals one electrode is shared. Most instruments now use the four-terminal method which is less sensitive to systematic errors and to changes in contact impedance [25]. Theoretically, if the input impedance of the recording amplifiers is sufficiently high, the contact impedance for the injecting pair becomes irrelevant and the contact impedance of the recording pair becomes negligible.

Current Injection and Measurement Protocols – Using this system, sinusoidal current, with an amplitude and frequency typically in the hundreds μA and KHz ranges, is injected between a pair of electrodes, referred to as an injection, and voltages are

measured at all electrodes in parallel in relation to a common reference electrode [17,69]. A protocol specifies the current amplitude, frequency, and injecting electrode pattern. Injected amplitude is limited as a function of frequency in accordance with safety regulations IEC 60601 [88]. The principal challenge when injecting the head is the shunting effect due to the scalp being much more conductive than the skull, and the CSF beneath the skull also being much more conductive than the cortex. Injecting electrodes on opposite sides of the head (i.e. 180° apart) can drive the current through deeper brain areas than adjacent electrodes which drive the current closer to the surface. A mix is often used to sample the whole head [55,107].

A protocol which was previously designed by the UCL-EIT group for stroke applications, is called the '**Spiral16**' protocol and was used in chapter 2 of this thesis [55]. It uses a 16-electrode montage based on the EEG 10-20 electrode system (figure 2.5) and the four terminals method. The protocol includes a series of 34 current injections while recording simultaneously from all 16 electrodes with common reference. Injections are a mixture of opposite and adjacent to optimize current patterns going through the head, and ordered in a spiral pattern hence the name of the protocol. Each injection lasted 100 mS, and a measurements frame was completed every 3.4 seconds.

Another protocol used in this thesis is the '*Drift Elimination 16*' ('**DE16**') protocol designed for the drift investigations in chapter 2. The '*DE16*' protocol took injecting pairs with maximised distance between the electrodes. The maximum spanning tree of the given 16 electrodes set-up was used to achieve this. This method was tested and validated before, using a 32-electrode set-up in a head-shaped tank [91]. 15 independent injections were added with 19 redundant less optimal injections (34 injections in total) to provide more information, to improve image reconstruction, and for better stability in cases of a noisy environment of baseline drifts. Each current injection was 100 mS long, keeping sampling rate of 1/3.4 seconds as with the '*Spiral16*' protocol. A variant of the '*DE16*', the '**Marrow DE 16**' was designed for Marrow experiments (see chapter 2). It comprised of 34 polar injections specially designed for this setup to match the *DE16* sampling rate in human subjects.

Applying the same principles, a different protocol described in chapter 4 was adopted. Using a montage of 32 electrodes on stroke patients, 31 injections in total were chosen to optimise the overall magnitude of the voltages recorded, and the number of independent measurements [107]. This protocol was named '**OP32**'.

Data Collection and Demodulation - The injection protocol creates sets of EIT measurement combinations. A given combination is defined by the injecting pair and the measuring pair of electrodes. Knowing the amplitude and frequency, each combination is in fact a single EIT measurement used as a data point in a series of measurements over time or at different frequencies. A single EIT measurement is the demodulated voltage amplitude at a single electrode, averaged over a certain number of periods of the waveform (figure 1.6). Assuming an injection is made by a pair of electrodes and recordings are made using all other pairs, some of the combinations are using the two terminals or three terminals method (also called “injecting combinations”) but most of the combinations use the pure four terminals method. When a protocol cycle is completed, the size of the final set of data, usually termed a ‘frame’, depends on the number of electrodes and the number of injections. For example, for 16 electrodes and 34 injections, one data frame contains 544 measurements. “Injecting combinations” are more sensitive to measurement errors, hence are usually omitted and not used for subsequent image reconstruction.

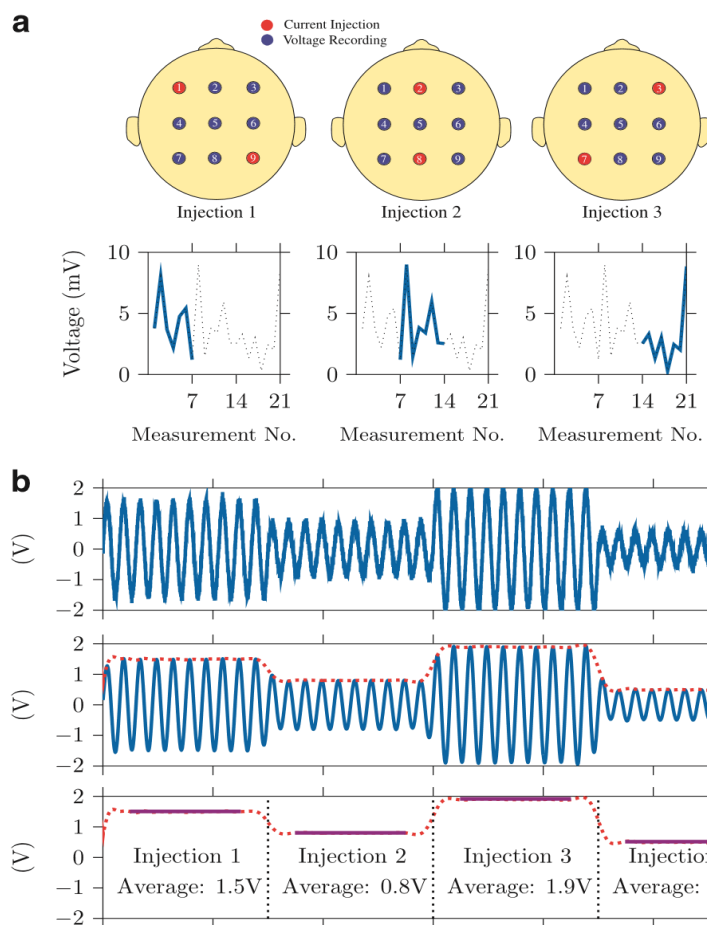


Figure 1-6: EIT Data Collection and Demodulation Process [69]. **a)** Simplified EIT data collection with three current injection pairs out of nine total electrodes. For each injection pair, voltage recordings are made on the remaining seven electrodes, to produce a total of 21 measurements in this example. **b)** Data processing pipeline on a single electrode in this example for four different injection pairs. *Top:* Raw data are imported from Bio-semi BDF file, *middle:* filtering around the injection frequency and demodulation using the Hilbert transform (red line). *bottom:* segmentation into individual injections and averaging. The edges of the waveform are excluded from averaging to remove switching and filtering artefacts.

1.2.5 Image reconstruction in EIT

The purpose of EIT is to reconstruct the impedance (or resistivity) distribution within the body using BV measurements. However, since it is simpler to implement when injecting current and measuring voltage, conductivity which is the inverse of resistivity, is reconstructed. Tikhonov regularization-based method approaches to EIT image reconstruction were developed in the 1980s and are often used in EIT medical applications [154,76]. The central idea is to split the problem into ‘forward’ and ‘inverse’ problems.

The Forward Problem - Predicting BVs given a known input current is called the forward problem. Solving it requires prior knowledge of the (head) geometry and the conductivities of the different tissues. For simple geometrical shapes, an analytical solution could be derived, but for a complex organ such as the head, a detailed model needs to be created. A Finite Element Model (FEM) represents the head as a mesh of small voxels to which electrical properties are assigned, and thus allows the forward problem to be solved numerically. Linear difference EIT, such as time-difference where the impact of a change in conductivity on the BV is linearised, uses the change as the data. Hence, instead of mapping the absolute conductivities σ to BV, the changes in conductivity ($\Delta\sigma$) is mapped with changes in BV (ΔV). This forward problem can be represented as:

$$\Delta V = J \cdot \Delta\sigma$$

where J is the sensitivity matrix (also called Jacobian), where

$$J_{ik} = \partial \Delta V_i / \partial X_k$$

represents the sensitivity of measurement i to a change in voxel k in the voxels vector X . A typical forward solution will start by simulating voltages for all FEM elements based on the current injection protocol and assigned conductivity values, and continues by calculating the sensitivity matrix J , based on those simulated voltages.

The Inverse Problem - Is to estimate the changes in internal conductivity ($\Delta\sigma$) from the changes in BV (ΔV). Hence, the following inverse equation needs to be solved:

$$\Delta\sigma = J^\dagger \cdot \Delta V$$

where J^\dagger is the pseudo-inverse of the sensitivity matrix J . This is known as the inverse problem. The solution to it, $\Delta\sigma$, represents the map of electrical changes which occurred in the body under investigation, which is then used for clinical interpretation.

In practice, the number of voxels (or elements) in the mesh is often of the order of millions while the number of BV measurements is around a few hundred. This means that many combinations of mesh values could result with similar measurements, which makes the inverse problem severely ill-posed. Being ill posed also makes the inverse problem very sensitive to noise, as small changes in BV measurements can result in large changes in reconstructed conductivity. Hence, the sensitivity matrix must be regularised using prior information, improving the smoothness of the solution. Both 0th and 1st order Tikhonov regularisation seek to minimize the equation:

$$\| V_{estimated} - V_{measured} \|^2 + \lambda \| \Psi(\Delta\sigma) \|^2$$

Where $\Psi(X)$ is a penalty function operating on the calculated conductivities, and λ is a hyperparameter. The goal is to match simulated BV to the measured BV while ‘punishing’ voxels with high magnitude. The hyperparameter λ (> 0) is the relative weight between the two terms above, and is estimated using the measured data [103]. 0th order Tikhonov apply the penalty directly to the estimated conductivities, while 1st order applies the penalty to the first derivative of the estimated conductivities.

In this thesis, zeroth order Tikhonov regularisation was applied in chapter 3 as it makes no assumptions on the reconstructed conductivities, other than assuming limited changes. The approach used to apply the zeroth order Tikhonov regularisation was to compute the Singular Value Decomposition (SVD) and to dampen the small singular values with the regularisation parameter when computing the pseudo inverse of J . This approach is often used in EIT [19,76, 80,103,154].

1.2.6 Imaging Modalities

In EIT, there are in principle three approaches: *Absolute EIT*, where the image is based on a single set of BV measurements without a reference dataset; *Multi-Frequency EIT (MF-EIT)* where an image representing a change in conductivity is reconstructed based on the difference between two sets of BV measurements recorded at the same point in time with different frequencies; and *Time-Difference EIT (TD-EIT)* where an image is reconstructed based on the difference between two sets of BV measurements taken at two different time points, with the same frequency. Both Absolute and MF-EIT avoid the need for a reference measurement (i.e. obtained without the pathology), which is of a great value for medical applications where a baseline measurement for the patient before she/he was admitted is rarely available.

However, despite this major advantage and despite having been proposed over two decades ago, these two EIT modalities still require further development before they can be employed clinically. Absolute imaging requires very precise modelling of the object, which is currently only possible with simple geometries. The principle challenge for MF-EIT is that changes over frequency, unlike changes over time, are non-linear and difficult to predict. Packham *et al* [129] showed that when imaging stroke-like perturbations in a head-shaped tank with a heterogeneous background, TD-EIT performed better than linear MF-EIT algorithms. These were tested without skull and scalp components which would attenuate the measured signal dramatically. Nevertheless, recent progress has been made with advanced MF reconstruction algorithms. Malone *et al* [107,108] developed a MF fraction algorithm, which uses prior knowledge of tissue conductivities and the spatial distribution of the tissues within the volume to represent each element in the FEM as a combination of tissues. This algorithm has been proven to work for 2D tank experiments with an ischaemic-like perturbation and homogeneous background. It also provided better quality images over linear FD-EIT algorithms, in simulations of non-linear cases. Zhou *et al* [173] presented an update to the fraction algorithm by using a constrained Total Variation Regularization Algorithm to achieve sharper image boundaries and better spatial resolution. Yang *et al* [87], presented a novel spectral decomposition FD imaging algorithm (SD-FD) for stroke EIT, using blind source separation methods such as PCA and ICA to separate different tissues reconstructions of the same case. This was proven to work for the 2D simulation of ICH, and later for 2D head tank measurements containing scalp and skull-like tissues, and a non-homogeneous background with an ischaemic stroke-like perturbation.

Both fraction and SD-FD techniques show promise for MF-EIT to work in the future, and algorithms are currently being optimized in order to make them applicable to clinical studies. Until then, TD appears to be the most robust EIT imaging modality.

1.2.7 Sources of Errors in EIT

As mentioned earlier, EIT is highly ill posed and sensitive to errors. Throughout the process there are several possible sources of errors that could damage image quality. Errors could originate from the instrumentation itself, from the way measurements are acquired, and from the modelling process as part of the image reconstruction. Some errors are more dominant in MF-EIT and are cancelled out when performing TD-EIT, and vice versa. The main sources for error can be summarised:

Instrumentation Errors - are errors which every EIT system introduces to varying degrees since instrumentation is never completely perfect. Various mechanisms and electronic components could introduce noise to the injected current and/or to the recorded BV. These are described in detail by Boone and Holder [25].

Measurement Errors – are errors introduced during measurement due to factors in the close contact area between the electrodes and the subject's scalp. This is usually called Contact Impedance (CI). CI includes the electrodes, the skin, and the conductive medium between them, which is usually gel. Although CI is measured as a single value, various factors could change in any of the three components, and effectively change the CI [112]. Uncertainties around the CI could introduce two types of errors to the process; one on the injection side where the actual current flowing into the body is miscalculated, and one on the recording side where measured BV is not fully representing the actual impedance change inside the body. Change in CI over time usually occurs. It is suspected to be the main cause for drift in baseline BV values. CI-related drift is long known to have a negative effect on image quality [23], and is a key factor in TD-EIT applications.

Electrode impedance is dependent on its material, size, and shape. Factors influencing gel conductivity are the substance's components and its ion concentrations. Skin impedance can depend on whether the *stratum corneum*, the highly resistive upper layer of the epidermis, has been mechanically removed, or by a change in ion concentration (caused by sweat, for example). These factors and the electrode-gel-skin interface are broadly described by McAdams *et al* [112]. External factors around the contact area, such as temperature, dehydration of the gel or the skin, mechanical pressure holding the electrode in place, and movement of the subject could also affect CI [112].

Modelling Errors – Solving the forward and inverse problems may also introduce errors. For example, these could derive from practical compromises in the meshing procedure. In the studies described in this work, a FEM mesh was created from a CT and MRI image taken from an unknown subject. Differences between head and brain anatomy of different individuals are sometimes significant, and reconstructing images with measurements taken from one subject using a FEM mesh obtained from another's head can cause errors [90]. This is not relevant to computer simulations or mechanical phantom studies. The resolution of the mesh (i.e. the number of elements in it) is also a factor for precision. While a larger number of elements give

higher spatial precision, it also creates a significant computational burden, and so an optimal compromise needs to be found between precision and computation time.

When solving the forward and inverse problems, conductivity values for the tissues are assigned to the different mesh elements. As mentioned earlier those values are close but probably not completely accurate. The error in those conductivities could also introduce errors. Another modelling factor is the isotropy of the tissue. Tissues could be modelled as having isotropic or non-isotropic conductivities. In reality, some of the tissues are not isotropic, but since such a model of the head is not practical, all tissues are modelled as isotropic which introduces another potential source of inaccuracy [4]. Electrodes size and shape could also cause modelling errors [27].

1.2.8 EIT Research from Idea to Clinical Uses

Since EIT is not yet a clinically mature field, every new application idea has to go through a full research and development (R&D) process. The first stage is very often a *computer simulation study*, where current patterns and boundary voltage measurement are being simulated in software, here using FEM techniques. Parameters such as tissue conductivity, current injection amplitude and frequency, electrode locations et al can be selected by the researcher; forward and inverse solutions are then computed, and images are reconstructed. When this appears to be satisfactory, the next stage is a mechanical phantom (*tank study*) where a static model of the application is being tested. Here, a phantom with a well-defined (e.g. head shaped tank) geometry with or without modelled skull and scalp is built and filled with saline or biological material as a background. Currents are injected and BVs are recorded. This simulates only part of the complexity of real-life measurements but tests the application in conditions where systematic noise exists and some of the tissue complexity is modelled to reflect aspects of a real-life application. When tank studies show encouraging results, it is common to explore *animal models* as the next step before trying the technique on humans. A living animal presents much greater complexity than tank studies. The UCL-EIT group often use rats as a model animal, although other groups have used rabbits, cats, and pigs. Animal studies offer the ability to control the characteristics of the lesion under investigation, such as size, location, and the exact time of introduction. It also offers the opportunity to acquire measurements without the skull in place, which reduces the level of complexity. Finally, when animal studies have proved satisfactory, the next challenge is testing on *human* subjects.

These four types of studies or stages of R&D: *simulation*, *tank*, *animal* and *human* studies are a natural development. However, the real dynamic of R&D is often less

straightforward, but much more iterative. When problems occur the process usually goes back a step or two, e.g. for further instrumentation or algorithm improvement. After a round of improvements, the process restarts from the most relevant stage.

1.3 Stroke

Stroke is a major health problem and estimated to cost the English economy alone approximately £7 billion per year [1]. Stroke can be briefly defined as an acute focal neurological deficit resulting from vascular disease [102]. It is caused by a lack of oxygen to part of the brain. It has two main subcategories: ischaemic stroke (IS) and haemorrhagic stroke (HS). Transient ischaemic attack (TIA) is defined as stroke symptoms and signs that resolve within 24 hours, and a non-disabling stroke is defined as a stroke with symptoms that last for more than 24 hours but later resolves, leaving no permanent disability [1].

1.3.1 Stroke Epidemiology

Approximately 56 million deaths occur annually worldwide. Approximately 5.5 million deaths are attributable annually to a stroke which accounts for nearly 10% of all deaths worldwide [121]. Each year, approximately 110,000 people in England, 11,000 people in Wales and 4,000 people in Northern Ireland suffer a first or recurrent stroke. Most people survive a first stroke but are often left with significant morbidity. Around 20,000 people suffer a TIA every year in England. It is thought that approximately 1 million people in the UK are living with the effects of strokes [2]. A recent study of stroke epidemiology in China between 1980 and 2017 by the World Stroke Association (WSO) pointed out 11 different studies with an average prevalence of nearly 900 per 100,000 over that entire time-period. It also stated a mortality of 154.7 per 100,000 [85]. Global stroke statistics published by the WSO in 2019 reported an incidence of 145/ 100,000 in India, and a yearly mortality rate of 216/ 100,000 in Russia [95].

1.3.2 Pathophysiology of Stroke and Delayed Bleeding

An ischaemic stroke (IS) occurs where blood supply is interrupted by a blood clot. This type accounts for 80-85% of all stroke cases, while a haemorrhagic stroke (HS) is caused by a vascular rupture. Primary treatment for IS involves clot dissolving agents, although this could be dangerous or even fatal for haemorrhagic stroke patients. HS are treated using other techniques, including surgical intervention to remove blood collection and to reduce Intracranial pressure (ICP) [102].

Haemorrhagic Transformations (HT) - HT is a secondary bleed into an already existing lesion. It is one of the major complications of IS and is associated with poor outcomes [7,110]. HT has a broad spectrum and its severity ranges from a minor pe-

techtial haemorrhage within infarcted tissue to a large-volume haematoma extending beyond the borders of the initial infarction. HT could develop as soon as a few hours after an IS, but could also develop later, up to a few weeks after the IS. The physiological mechanism of HT relies on two main processes. A metabolic molecular cascade, which starts minutes after the onset of ischaemia, brings disruption to the blood-brain barrier (BBB). In addition, an inflammatory response due to ischaemia damages cerebrovascular anatomy and its auto-regulatory capacity. HT occurs in a significant proportion of patients following IS. Over the last 20 years several studies have attempted to assess the prevalence of HT among acute IS patients. Direct comparison between those studies is complicated as they differ in design, eligibility criteria, IS severity, patients' demographics etc. Based on those studies, HT with no clinical symptoms occurs in 30-40% of first-ever IS cases, and symptomatic HT occurs in an additional 5-10% of the cases [21,126,146]. Clot dissolving agents increase the risk for HT, as do mechanical procedures for re-canalizing blood vessels, thus treating IS involves increasing the risk for HT. Furthermore, there is a trend toward increasing HT rates as the time between IS onset and vessel recanalization increases [7,146].

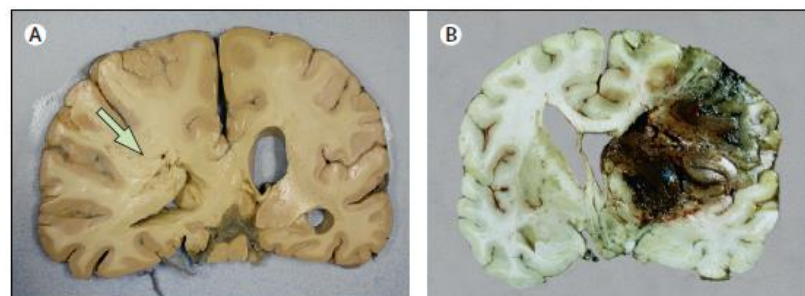


Figure 1-7: Haemorrhagic Transformation after Ischaemic Stroke. Slices of brain from autopsy showing (A) an area of infarction involving the middle cerebral artery territory (arrow) and (B) a different IS case where a haemorrhagic transformation in the cerebral hemisphere is visible [21].

Haematoma Expansion (HE) - HE is an increase of an existing haematoma by more than 33% or more than 12.5 ml in volume. It is a common and severe complication of HS. Studies suggest that more than 50% of HS patients will develop HE within the first 24 hours, most of them within the first 3 hours. HE is often associated with early neurological deterioration and is an independent predictor of poor outcome and increased mortality [20,131].

1.3.3 The Burden of Stroke Mimics

An acute ischemic diagnosis is not always straightforward, since there are several disorders, that present with an acute neurological deficit so imitating a stroke, hence

the stroke mimics. Stroke mimics are non-vascular conditions that present with an acute neurological deficit simulating acute stroke and represent a significant percentage of all acute stroke hospital admissions. The most common clinical stroke mimics includes psychiatric disorder, seizures, postictal paralysis, toxic metabolic disturbances, brain tumour, infections, and migraine [58]. Stroke mimics often become ‘false positive’ stroke diagnoses. On the other hand, and more rarely, an acute stroke may have an atypical clinical presentation that simulates other disorders; these are termed stroke “chameleons”. These might become a ‘false negative’ stroke diagnosis.

Both phenomena emphasize the need for accurate stroke identification. A recent study in Norway in 2017 by Faiz & Labberton et al [58] recorded all admissions to a stroke unit over 12 months in a large-scale hospital. From a total of 1881 admissions, 719 were diagnosed as stroke mimics (38.2%). They found also stroke mimic patients to be significantly younger than TIA and stroke patients ($p < .001$), and a higher proportion of women ($p = 0.009$). Earlier studies from the US and the UK found very similar results [67,116]. The Norwegian study calculated that by 2050, the incidence of stroke mimics will increase by 89% for men and by 72% for women. They concluded that by accounting for the expected population growth by 2050, admissions for stroke mimics will increase substantially, and that stroke evaluation strategies must change to counterbalance this expected trend.

1.3.4 Current Principles of Stroke Management

At the Scene and in the Emergency Department – The first important principle is rapid recognition of symptoms and diagnosis. Diagnosis of stroke at the scene is effectively done with the FAST (Face, Arm, Speech, and Time) Test [124]. If a stroke is suspected, the patient has to be directed to a hospital with a stroke unit. Furthermore, if a Large Vessel Occlusion (LVO) is suspected then it is preferable to direct the patient straight to a stroke centre with endovascular capabilities even if it is a little longer ride [71,93]. In the emergency unit, rapid diagnosis is done using the ROSIER (Recognition of Stroke in the Emergency Room) scaling tool [123], which is based on features from the medical history and physical examination of the patient. The National Institutes of Health Stroke Scale (NIHSS) is also a very common scale originally developed as a communication tool for stroke research [30], but adopted as a diagnostic and status monitoring tool for stroke patients worldwide. The NIHSS is composed of 11 elements, each of which scores a specific ability between 0 and 4. Its minimal score of zero is for no stroke symptoms and its maximum is 42 [117]. If a

stroke is suspected, the patient should be admitted directly to a specialist acute stroke unit, if available. TIA patients are being assessed for their risk of having a subsequent stroke using the ABCD2 tool [68]. A score 4 and above, or people with crescendo TIA (two or more TIAs in a week) are at high risk, and should be assessed for urgent (within 24 hours) imaging: diffusion-weighted MRI or CT and if needed carotid endarterectomy and carotid stenting.

Thrombolysis and Mechanical Thrombectomy – After initial screening, patients are assessed for immediate (the next slot within 1 hour) or ASAP (within 24 hours) brain imaging. After immediate imaging, if HS is ruled out and other medical parameters permit, thrombolysis with recombinant tissue plasminogen activator (tPA) should be administered by trained staff with compatible monitoring equipment, to monitor for complications in situ. At this point, comorbidities are evaluated, and further treatment is considered, such as Aspirin and anticoagulation, or a reversion of coagulation in patients with HS. It is only then that patients are assessed as to their need for surgery, as neurosurgical treatment is beneficial for selected patients with HS or severe middle cerebral artery infarction [1,29]. The maintenance of Cerebral Blood Flow (CBF) and oxygenation to prevent further brain damage after a stroke is another important aspect in the treatment of stroke patients. Where needed, supplemental oxygen is given, and blood pressure and sugar levels are managed. In an acute stroke unit, nutrition and hydration are kept under close scrutiny, and patients are encouraged to mobilise themselves and are helped to sit up.

HT and HE Management - HT patient management depends on the amount of bleeding, associated symptoms, primary IS characteristics, and any patient comorbidities. Interventions to restrict HE and HT include haemostatic therapy, cautious lowering of high blood pressure, and quick reversal of prior anticoagulation. Balancing the patient's antithrombotic and anticoagulant therapies are dictated by the circumstances of the IS and subsequent HT. The decision to restart antithrombotic therapy after HT depends on the risk of subsequent arterial or venous thromboembolism, the risk of recurrent HT, and the clinical state of the patient. Anticoagulation should be considered in patients with a very high risk of thromboembolism or when there are definite indications for these drugs. Clot evacuation might be needed in deteriorating patients. For patients presenting with lobar clots >30 ml and within 1 cm of the surface, evacuation of the HT by standard craniotomy may be considered. For patients with cerebellar haemorrhage >3 cm who are deteriorating neurologically or having brainstem compression and/or hydrocephalus from ventricular obstruction, surgical removal of the haemorrhage as soon as possible is recommended. Minimal

invasive surgery is a promising option, and is the subject of a few ongoing studies [\[20,21\]](#).

1.4 Traumatic Brain Imaging (TBI)

Traumatic brain injury (TBI) is an insult or trauma to the brain caused by external mechanical forces, whereas head injury is a generic term referring to injuries affecting not only the brain but also other structures of the head [96]. The UK National Institute for Health and Care Excellence (NICE) guidelines refers to head injury as any trauma to the head other than superficial injuries to the face [3].

1.4.1 TBI Epidemiology

Epidemiology reports from the UK, the US, and Europe, vary largely and are sometimes hard to compare, as reviews differ in definitions and scope. The reason for the difference in numbers and statistics is often because the brain injury and head injury areas overlap. There is, however, a consensus that TBI is one of the leading causes of death and long-term disability. Looking at the general picture, these reports suggest that in western countries approximately 1000 people per 100,000 attend Accident and Emergency E units (A&E) with TBI every year; approximately 250 of them are admitted to hospital, and 10 per 100,000 die [96,97,147].

In the UK, head injury is the most common cause of death and disability in people under 40 years of age. Between one third to one half of those attending A&E units are under 15 years old. 95% of TBI cases are defined as mild whereas 5% are defined as moderate or severe. Therefore, emergency departments see many patients with mild head injuries and need to identify the very small number who will go on to have serious acute intracranial complications. Approximately 40% of patients presenting in coma with severe TBI die and a further 20% survive with major disability, whereas patients with moderate TBI have approximately 10%–20% risk of death or severe disability [96].

1.4.2 Pathophysiology of TBI and Delayed Bleeding

Brain injury following trauma includes the immediate, or primary, injury caused at the moment of impact, and any secondary injury developing in the first few hours or days after the impact [84]. Secondary injury could involve cellular ischaemia, activation of inflammatory cascades, cell swelling and vasogenic oedema. Brain swelling caused by those mechanisms within the rigid confines of the skull, results in raised intracranial pressure (ICP) and reduces cerebral perfusion pressure (CPP). A vicious circle starts when this in turn worsens cerebral ischaemia. TBI is usually sub divided into focal, diffuse, and penetrating brain injury. Blunt trauma usually results in focal inju-

ries, while angular or rotational acceleration–deceleration forces (such as in high-speed road car accidents) cause diffuse injury. Both types of injury may coexist [96]. In TBI where closed skull fracture is present and it is not depressed, specific treatment is rarely required and healing occurs spontaneously; however, open and depressed fractures require surgical intervention [84].

Delayed Onset Lesions after TBI - Most TBI injuries are detectable in the first CT scan in the emergency unit, where a detailed screening protocol is used to decide who should be scanned and with what urgency. However, a delayed onset of intracranial lesions is a well-known phenomenon and has been recognized and documented worldwide. Cases of delayed Extradural Haematoma (EDH), Subdural Haematoma (SDH), and Intracerebral Haemorrhage (ICH) have been reported and published [42,48,64,111]. In these cases, patients with a normal initial CT scan, a Glasgow coma scale (GCS) of 15 out of 15, and with no alarming clinical signs, deteriorate clinically and present significant findings in a later CT scan. In some cases, the delayed injury was severe and even resulted in death.

No comprehensive epidemiology study was found to enable the accurate determination of the prevalence or incidence of this phenomenon. This is possibly due to its complicated nature as it includes many injury types, diverse personal backgrounds and TBI circumstances, alongside different triage and treatment protocols worldwide. Numbers in serial reports of delayed EDH and ICH ranged from 5% to 30% depending on the primary injury degree, and point at lower numbers of delayed SDH [111]. In those reports, the time scale for the development of a delayed onset injury is generally within the first 2-3 days after impact, but in some cases many days or even weeks after. An educated estimate relying on existing literature could be that around 5-10% of moderate and severe TBI cases will develop a significant additional lesion which was not visible in the initial imaging. Although very rare, a delayed onset could also occur in mild TBI patients.

1.4.3 Principles of TBI management

At the Scene - Management follows trauma and life support principles with the assessment and treatment of the most urgent problems systematically. Patients who are comatose or who have deteriorating consciousness should have their airway secured (intubated if necessary), to secure adequate oxygenation and ventilation. Fluid replacement is important to avoid hypotension. Spinal immobilisation should be maintained until clinical assessment and/or imaging studies indicate that it can be removed [96]. Pain should be treated in order to prevent ICP elevation. In cases

where patients present with GCS \leq 8, a designated emergency unit should be prepared [84].

Glasgow Coma Scale (GCS) – This widely used neurological scale measures the level of consciousness of a person after a brain injury as well as in any subsequent assessment. Published in 1974 by Teasdale and Jennett [149], its maximum score is 15 (originally 14) and is composed of three tests: eye (E, max score- 4), verbal (V, max score- 5), and motor responses (M, max score- 6). The minimum GCS score is 3 (deep coma or death), and an example of a GCS report would be: “GCS 13 = E4 V4 M5 at 11:45”. The current GCS has different versions for adults and children.

In A&E - The treatment goal is to control ICP and maintain an adequate CPP in order to meet the demands of the injured brain [96]. Trained staff assess the need for an urgent CT scan according to NICE criteria set for adults and children. The primary imaging modality is CT whilst MRI is used when there is insufficient information from the CT scan to take clinical decisions. After initial triage and imaging, patients are considered for admission and additional observation, or discharge back to the community. Patients with imaging findings, a GCS under 15, persistent vomiting, a severe headache and other clinical concerns are considered for admission [3].

Admission to Hospital Wards and Neuroscience Units - There is increasing recognition that patients with severe and moderate TBI should be managed in neuroscience units (NSU), regardless of the absence or presence of any need for neurosurgical intervention. However, this is not always possible due to current resource constraints, in terms of neuroscience beds and staff. In such cases, ongoing liaison with NSU over clinical management is essential. The objective of hospital admission for patients who do not require transfer to a NSU is to continue neurological observations, allow time for symptom improvement, and to identify the small subset of patients who deteriorate [96].

Observation - NICE guidelines define what should be a minimal check-up while under observation, and how often the examination should be repeated. If a patient is deteriorating, a further CT scan should be considered and a clinical reassessment should be organised. When the CT scan is normal but the GCS is less than 15 after 24 hours, another CT or MRI should be considered. Staff specialising in paediatric head injuries are essential to accurately observe infants. Most patients recover without specific or specialist intervention, but others experience long-term disability or even die from the effects of complications that could potentially be minimised or avoided with early detection and appropriate treatment [3].

1.5 Intracranial bleeds

Intracranial bleeds are usually categorised according to their location and nature. Sometimes a certain type of bleed can result from either a TBI or a stroke, and for other types it is usually the result of just one of them. It is important to note the main bleed type characteristics [73,84,137].

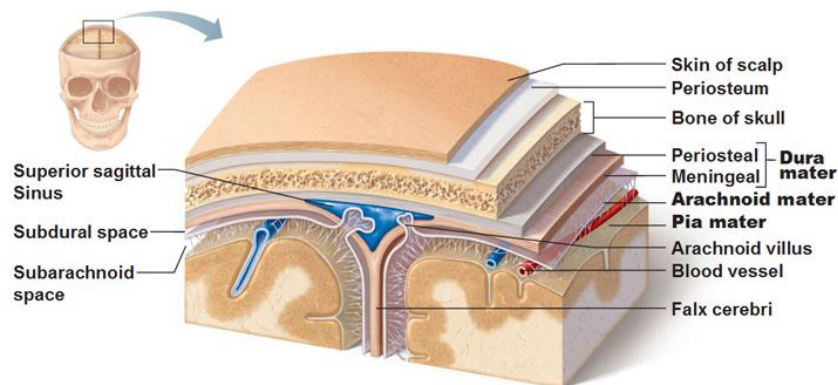


Figure 1-8: Brain Protective Layers. Image from www.antranik.org.

Extradural Haematoma (EDH) - Is an accumulation of blood in the extradural space between the inner side of the skull and the Dura Mater. It is typically shaped like a biconvex lens. Most (90%) are associated with skull fracture and are caused by an injury to the middle meningeal artery. They therefore affect the parietal and temporo-parietal brain areas. EDH occurs in 1-3% of all TBI cases. Volumes could be up to 75cm^3 , and surgical intervention is recommended for lesions from 15 mm in thickness or 30 cm^3 in volume. EDH usually develops between minutes to 8 hours from impact. It is more common in patients ages 6-10 and 20-30 years of age and is four times more common in men. Patients often experience rapid recovery after impact and then a quick deterioration (a lucid interval). Outcomes depend on the level of consciousness at the time of surgery, with mortality approaching 20% if the patient is unconscious prior to surgery. EDH is more associated with TBI.

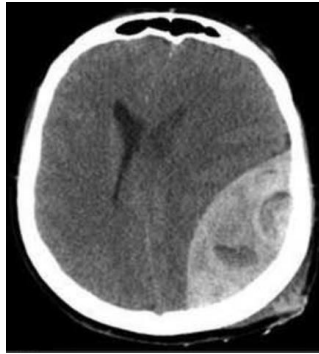


Figure 1-9: Extra-Dural Haematoma (EDH). Acute EDH with biconvex shape [96].

Subdural Haematoma (SDH) - Is an accumulation of blood between the inner side of the Dura and the arachnoid layer. It is caused either by the tearing of cortical veins when the haematoma is commonly frontal, or of small arteries when more often it is in temporo-parietal areas. It typically forms in a crescent shape, but could also appear as a thin layer following the tentorium when chronic. Most patients with acute SDHs also have some other form of brain injury and their prognosis is worse than those with EDHs. Acute SDH develops within 3 days, sub-acute SDH within 3 weeks, and chronic SDH can develop weeks or months after a head injury. The original injury may be minor, and the patient may not remember it as a particularly dramatic event. For sub-acute or chronic states, CT is sometimes insufficient and an MRI scan is needed. Chronic SDH incidence is ~1.7 per 100,000. It increases with age to 7 per 100,000 after the age of 70. Surgical evacuation is recommended for haematomas from 10 mm in thickness. SDH is more associated with TBI.

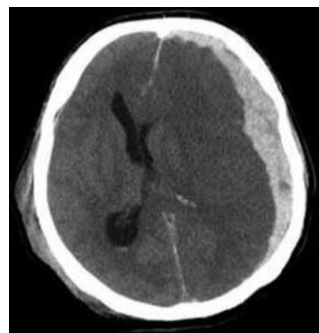


Figure 1-10: Sub-Dural Haematoma. Acute SDH with typical crescent shape [96].

Subarachnoid Haemorrhage (SAH) – Is a bleed into the subarachnoid space between the arachnoid membrane and the Pia Mater. It is seen in 30–40% of patients with severe TBI, usually near a skull fracture, and its presence indicates a potentially worse outcome. Most spontaneous SAHs (strokes) are due to a small aneurism, which usually occurs close to the circle of Willis junctions. A SAH could develop over

minutes up to days. Major complications are re-bleeding and vasospasm, and sudden death occurs in up to 10% of the spontaneous SAH cases. A typical symptom of spontaneous SAH is a thunderclap headache. SAH is associated with both a stroke and TBI.

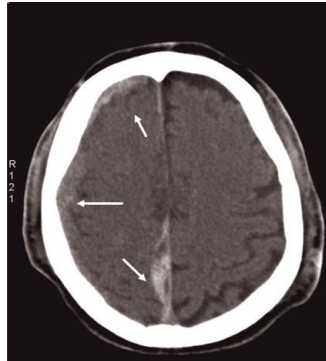


Figure 1-11: Subarachnoid Haemorrhage. Traumatic SAH, arrows show right anterior and lateral subdural blood collections and parafalcine subarachnoid collection [84].

Haemorrhagic Contusions and Lacerations (HCL) – Are superficial multiple discrete areas of small haemorrhage (< 2 cm²) and usually appear in the frontal and temporal lobes. It is typically caused by venous injury when brain hits skull bone at the site of impact and then the opposite side during deceleration. The term contusion is used when the Pia Mater has not been breached, and laceration when the Pia Mater is torn. Local areas of contusion with no or minimal blood flow are common after severe TBI and the centre of the contusion is often irreversibly damaged. However, areas around the contusion (*penumbra*) are associated with localised cerebral oedema and have survival potential if the oxygen supply to this region is maintained. Focal contusions can be associated with cerebral oedema and raised ICP leading to a delayed neurological deterioration and may need surgical evacuation. HCL could appear soon after impact. It could also have a delayed onset up to 48 hours after impact, and is more often associated with TBI.

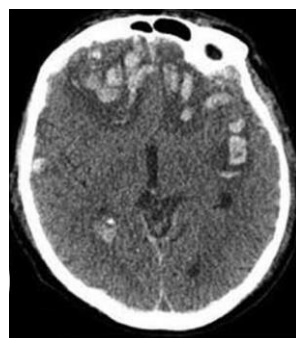


Figure 1-12: Haemorrhagic Contusions. Contusions in frontal and temporal lobes [96].

Intracerebral Haemorrhage (ICH) – Is an accumulation of blood within the brain. It differs from HCL in size (> 2 cm²) and in blood content as in ICH most of the lesion is blood and not oedema. It occurs in around 15% of severe TBI cases, and in 10-15% of all stroke cases. It is typically located in cerebral cortex (80%), and usually in the frontal and temporal lobes. Other typical locations are the basal ganglia and the cerebellum. An ICH with 20-30 ml in volume is considered massive, and when over 60 ml is fatal within 30 days in 90% of cases. Small studies looking into the growth of ICH over time suggests that ICH increase by approximately 25% within an hour of the initial CT scan, and around 10% more within 24 hours. Its typical shape is spherical or close to spherical. ICH is more common in men, in black and in Japanese people, and is associated with both stroke and TBI.

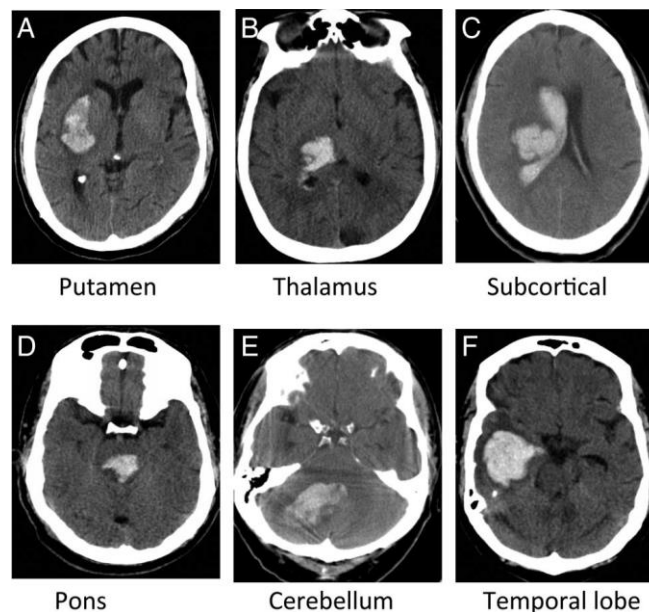


Figure 1-13: Intracerebral Haemorrhage (ICH). Typical locations of hypertensive ICH are putamen(A), thalamus (B), subcortical white matter (C), pons (D) and cerebellum (E). Thalamic and subcortical haemorrhages often extend into ventricles (B and C). Cerebral amyloid angiopathy, drug abuse or vascular anomaly often causes lobar haemorrhage (F) [46].

Interventricular Haemorrhage (IVH) – Is a bleed into one of the brain ventricles which are normally filled with CSF, usually as a result of an ICH overflow. It is common in premature babies in the first few days after birth, but also occurs in adults as a result of TBI or HS. It occurs in 35% of moderate and severe TBI cases, and is often associated with other injury types, as it is usually attributed to extensive force on impact. It is therefore associated with poor outcomes. IVH could produce a dilated ventricle and increased ICP, and blood clots in the CSF causing hydrocephalus. IVH is associated with both stroke and TBI.

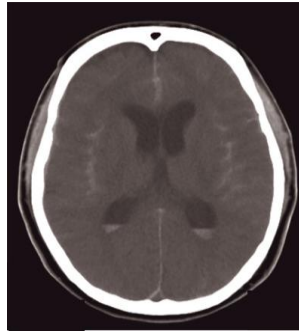


Figure 1-14: Intraventricular Haemorrhage. Diffuse subarachnoid and intraventricular blood collection [102].

Diffuse Axonal Injury (DAI) – Is as its name suggests a diffuse injury. A severe DAI has three main components: a focal lesion in the Corpus Callosum, often associated with traumatic intraventricular haemorrhage (IVH); focal lesions in the brainstem; and very small scattered haemorrhages, mainly along the midline. DAI is attributed with shearing nerve fibres at the junction between the grey and white matter. Surgical intervention is recommended when the lesion is larger than 25 cm³ and there is a midline shift of more than 5 mm, or when the main lesion is more than 50 cm³. DAI involves a mechanism at the cellular level which begins on impact, and sometimes only finishes 24 hours after the impact. DAI occurs in 50-60% of severe TBI cases. Patients are often in deep coma although only small scattered lesions are visible in images, and the ICP is normal. The mortality for severe DAI is around 50% and it is the most common cause of coma, a vegetative state, and subsequent disability. DAI is closely associated with TBI.

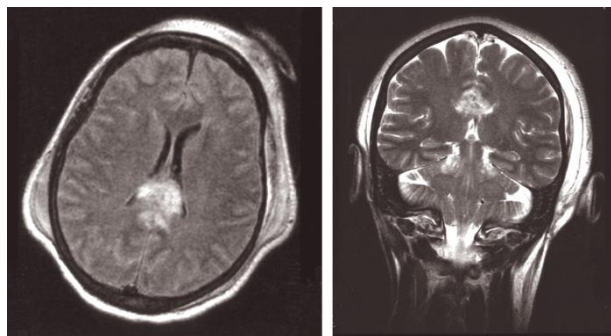


Figure 1-15: Diffuse Axonal Injury (DAI). DAI showing extensive haemorrhagic change in the region of the Splenium [84].

1.6 Medical Techniques for Brain Injury Monitoring

As secondary insults to the injured brain can originate from either systemic or cerebral sources, monitoring to detect these insults must have both systemic and cerebral components. Systemic variables such as blood pressure, sugars and gases are routinely monitored in the neuro-intensive care unit (NICU). The goal of monitoring the injured brain is to enable the detection of harmful physiological events before they cause irreversible damage to the brain. Like the systematic parameters, ICP, CPP, CBF, inflammation, metabolism, and seizures are also being monitored in the NICU allowing diagnosis and effective treatment while providing 'on-line' feedback to guide interventions. Through these interventions, the clinician aims to minimize secondary injury in order to optimise patient management and outcome. It is therefore important to review available monitoring systems applicable after stroke and TBI [38,153].

1.6.1 Bedside Invasive Cerebral Monitoring

Invasive cerebral monitoring involves the insertion of a group of intracranial sensors into the patient's head to enable the continuous monitoring of parameters which are undetectable in imaging. These drastic measures are carefully considered and used only in severe brain injury cases as they carry inherent risks such as infection and secondary insults, involving neuro surgical procedures. These measures are unavailable in smaller hospitals with no neurological Intensive Care Unit.

The first and most common monitored parameter is *Intracranial Pressure (ICP)*. When ICP is raised, CPP will be compromised and can cause secondary focal or global ischemia. The 'gold standard' technique for invasive ICP monitoring is a catheter positioned with its tip in the lateral ventricle connected to a standard pressure transducer. The advantages of this technique are that it can be calibrated periodically, and could also be used simultaneously for CSF drainage if necessary. Another optional technique is placing a transducer-tipped system in the brain parenchyma, subdural area, or subarachnoid space. This is done either through a skull bolt on the NICU, or by a 'Burr hole' neurosurgical procedure with minimal infection and complication rates.

Cerebral Blood Flow (CBF) is another parameter monitored using invasive probes measuring temperature. The power necessary to generate this increase in temperature is related to the tissue's ability to transfer heat, which is directly proportional to the rate of CBF. While still requiring further investigations, it has been suggested that

it could be used to prevent secondary ischaemia after TBI. The limitations of this technique are its localised nature, and its sensitivity to calibration.

Monitoring jugular venous oxygen saturation (**Sjv_{o2}**) is a technique used to estimate the balance between global cerebral oxygen delivery and its utilisation in the brain. A catheter is inserted into the dominant internal jugular vein and then advanced to the jugular bulb. Once the catheter is in place, measurement can be made either continuously using a fibre-optic probe or by directly aspirating blood samples and using an oximeter. The main advantage of this method is that it can reflect global cerebral oxygenation, but there is evidence suggesting that it is too slow for indicating ischaemia. It also carries risks of pneumothorax, arterial puncture, thrombosis, and infection. For monitoring focal tissue oxygen tension (**pBrO₂**), invasive probes were developed utilizing a closed polarographic cell with reversible electrochemical electrodes. Oxygen, which has diffused from the brain tissue across a semi-permeable membrane, produces a flow of electrical current directly proportional to the oxygen concentration. This represents the balance between oxygen delivery and cellular oxygen consumption. This has proven to be an effective measure for secondary ischaemia in TBI patients.

Cerebrovascular Auto-regulation - Is frequently impaired after TBI and is associated with poor outcomes. Continuous monitoring of this parameter may predict patients at risk of secondary injury and may help to define individual treatment targets. Monitoring this parameter is mostly achieved by continuously computing the correlation between systemic blood pressure and either ICP or pBrO₂, thus assessing the cerebral response to spontaneous fluctuations in blood pressure.

Cerebral Micro Dialysis (CMD) – is a well-established laboratory tool, increasingly used for bedside clinical monitoring. This is performed with a catheter positioned close to 'at-risk' tissue, measuring dialysate concentrations of glucose, lactate, pyruvate, glycerol, and glutamate. The lactate/pyruvate ratio can indicate aerobic/anaerobic glycolysis due to hypoxia and ischemia or an energy crisis. In addition, glutamate and glycerol are biochemical markers of cell damage and cell death. CMD is becoming an established tool providing on-line analysis of brain tissue biochemistry assisting clinical decision-making whilst a patient is in neuro-intensive care. This includes CPP management, hyperventilation guidance, and the appropriateness of extensive surgical procedures. This technique is limited to worse case strokes only despite being reliable and accurate.

1.6.2 Non-Bedside Non-invasive Cerebral Monitoring

This group of techniques includes two of the well-known 'gold standard' imaging modalities: Computed Tomography (**CT**), and Magnetic Resonance Imaging (**MRI**). Other techniques included in this group are Single Photon Emission Computed Tomography (**SPECT**), and Positron Emission Tomography (**PET**). This group of imaging techniques with vascular imaging (angiography) provide very high-resolution brain tissue structure images. The main drawbacks of these imaging systems are that they are immobile, being large pieces of machinery with some using ionising radiation (a problem with severely ill patients) and are expensive. They therefore cannot provide continuous monitoring.

CT is x-ray based tomographic imaging technique, considered to be one of the 'gold standard' methods. CT scanners have become standard in hospitals and medical centres. CT is used mainly for first assessment, being considerably cheaper than MRI. Standard CT protocols are effective to demonstrate structural changes both in bone and brain tissue. CT could miss features due to beam hardening effects, or when one or more dimensions of a lesion are smaller than the resolution window, especially in the brain stem and spinal cord, as in DAI.

Xenon-enhanced CT is a CT technique which utilizes a stable non-radioactive gas mixture containing Xe, an indicator capable of crossing the blood brain barrier. This provides rapid access to both structural and quantitative CBF data using equipment that is readily available. The study can be repeated within a short period of time allowing the use of CT as a non-invasive CBF monitoring tool. This technique is not applicable to all patients. For example, it is difficult to perform in patients with associated pulmonary pathology.

CT Perfusion is another CT technique used for brain injury monitoring. It involves sequential acquisition of data during the intravenous administration of iodinated contrast material. It provides parametric images of cerebral blood volume (CBV), mean transit time (MTT), CBF, and CT angiography alongside regular structural CT data. It is a widely accessible, rapid, and accurate technique for monitoring after head injury, and assessing cerebral vasospasm after SAH. It is limited, however, by the radiation dose volume of contrast agent that can be safely administered [37].

Portable CT is another CT variant, unique in this group for being mobile. A few devices have been developed and are currently in trials. This could be used in the NICU for brain monitoring. The advantage is the patient does not need to be transported, useful particularly for those on ventilators and vasoactive drips. Bedside acquisition of CBF data is a particularly significant improvement; important parameter

monitoring such as tissue oxygenation or local CBF using different monitors can remain in place during the study and can be validated with the tomographic data. In contrast with stationary CT, the time from decision to scan is shorter, while the images are only slightly lower quality [34]. Portable CT does require a relatively large bedside space and is expensive as a bedside device.

MRI is the second 'gold standard' imaging method, using strong magnetic fields and its gradients to generate tomographic images. It can be used for structural imaging for first assessment when CT is not available, or when greater sensitivity to white matter lesions is required. However, MRI is less accessible than CT which is therefore preferable in the acute injury phase. It can also be used for functional imaging (*fMRI*), and is ionizing radiation free. Differences in imaging contrast between normal and injured brains are dependent on the particular MRI pulse sequence employed. By employing a variety of different MRI sequences, the extent of a brain injury can be demonstrated in high resolution across the brain. For instance, *Gradient Echo* and Fluid Attenuation Inversion Recovery (*FLAIR*) sequences are highly sensitive to DAI.

Perfusion MRI uses rapid sequential *susceptibility-weighted* imaging after an injection of MRI contrast medium. *Diffusion-weighted (DWI)* images the microscopic movement of water. Perfusion/ Diffusion mismatch has been used to diagnose early cerebral ischaemia [37].

SPECT uses radioactive isotopes, to image the emitted gamma rays. SPECT is a relatively simple and inexpensive technique to assess cerebral perfusion, as the isotopes taken into the brain result in gamma ray intensity which is proportional to CBF. However, the images produced are of relatively low resolution. Its main limitations are the use of ionising radiation and its low spatial resolution [37].

PET is another form of nuclear imaging, based upon the detection of photon pairs. Positron-emitting isotopes are administered to the patient via IV or inhalation. Emitted positrons are annihilated in a collision with an electron resulting in the release of energy in the form of two photons (gamma rays) released at an angle of 180° to each other and detected externally using a ring of detectors which measure coincidence. Simultaneous events are used to reconstruct the isotope distribution. PET is a research tool which is relatively expensive and not universally available. Despite this, it has been successfully used to investigate changes in physiology after head injury in terms of CBF, oxygen, and glucose metabolism. PET studies can be repeated and used to assess changes in physiology. Its main limitations are ionising radiation, high cost, and low spatial resolution [37].

1.6.3 Pre-hospital and Non-invasive Bedside Cerebral Monitoring

The following section reviews technologies and devices of mobile non-invasive brain monitoring, the group to which EIT belongs. This review includes both peer-review literature and internet websites of medical technology companies, as some of the developments occur in the medical devices industry outside of academia. Information from company websites and press releases are often vague to protect intellectual property and business strategies. Sometimes, the status of a technology company (i.e. capital invested, or number of employees) is an indicator of the maturity of the technology. This section tries to draw as complete a picture as possible.

Transcranial Doppler Ultrasonography (TCD) - Uses low frequency (~ 2 MHz) ultrasound waves to derive CBF velocity from the Doppler shift caused by red blood cells moving through the field of view. Access to cerebral blood vessels is achieved by identifying cranial “windows” through which the ultrasound beam can penetrate the skull without being too dampened. This technique traditionally relied on highly skilled operators. The three traditional transcranial windows are transtemporal, transorbital, and transforaminal. TCD is quite widely used to diagnose and monitor cerebral vasospasm after SAH, and has also been used for ICP monitoring [153,39]. Commercially, The Lucid™ Robotic System (Neural Analytics, Inc. <https://www.neuralanalytics.com>) is a combination of TCD ultrasound, robotics, and machine learning designed to non-invasively measure and display brain blood flow information under the guidance of a professional user. Its machine learning abilities are designed to identify specific disease states, and preliminary press publications claim that it is able to identify large vessels occlusion (LVO) with 91% sensitivity and 85% specificity [158].



Figure 1-16: Novel TCD Device. The Lucid™ (from neuralanalytics.com)

Optic Nerve Sheath Diameter (ONSD) – Is a non-invasive method for ICP measurement. It is applied by measuring the nerve sheath diameter with ultrasound and

has been shown to be an accurate non-invasive bedside diagnostic tool for ICP [32]. The optic nerve sheath is contiguous with the meninges of the central nervous system and is encased with the subarachnoid membrane. When ICP increases, CSF from the subarachnoid space accumulates in the optic nerve sheath and thus widens it. This was also established with CT and MRI imaging methods [139]. ONSD is easy and available but limited as it is not continuous and cannot always be applied, such as in the case of patients with chronic ocular disease and malignant hypertension.

Electroencephalography (EEG) - Uses scalp electrodes connected to amplifiers and filters to detect intracranial electrical activity, which is displayed as positive or negative deflections (y axis) on a line and is recorded versus time (x axis). Continuous EEG (cEEG) is used for monitoring seizures (especially non-convulsive seizures) and for titrating anticonvulsant drugs. It is also used for detection of vasospasms after SAH. Quantitative EEG (qEEG) where large data are quantified by computer could help with data analysis and decision making. Traditional EEG methods have proved limited. Drawbacks include cumbersome set-ups, operator dependency, poor spatial resolution, and it is artefact sensitive [153,94]. However, recent studies targeting pre-hospital stroke triage used a much simpler set-up. In 2019, Gottlibe et al [70] used an off-the-shelf consumer EEG device, the MUSE brainwave sensor device by Interaxon Inc. (Toronto, Ontario, Canada) containing 4 dry electrodes for the forehead, to identify stroke. They recorded EEG data between 0-220 Hz for ten minutes on thirty-three ischaemic stroke patients and 25 healthy subjects. Using the revised Brain Symmetry Index (BSI) which uses Fourier series to detect asymmetries in spectral power between the two cerebral hemispheres, they found a significant difference between the two groups (BSI score of stroke patients was 0.36 ± 0.25 , while healthy controls score was 0.17 ± 0.1 , Mean \pm STD, $p < 0.05$). Commercially, AlphaStroke® developed by Forest Devices, Inc. (<https://forestdevices.com/>) utilises EEG with a strong focus on the initial triage of stroke patients, based on the asymmetry in EEG signal between hemispheres. It is indicated for stroke detection in any environment including prehospital, outpatient clinics, nursing facilities, and emergency departments [158]. Another company, BrainScope (<https://brainscope.com/>) developed the BrainScope® One to assess mild TBI, including functional and structural injury, using a small set of electrodes placed on frontal and temporal regions, within minutes of data recording. More than fifteen peer reviewed studies were conducted by BrainScope [28].



Figure 1-17: Novel EEG Setups for Stroke Diagnosis. Left: the BrainScope (from brain-scope.com), Right: the AlphaStroke (from forestdevices.com)

Near Infrared Spectroscopy (NIRS) – Uses the transmission and absorption of near infrared light (700–1000 nm) as it passes through tissue. Oxygenated and deoxygenated haemoglobin have different absorption spectra. Advances have allowed measurement of absolute concentrations of oxy-haemoglobin and de-oxy-haemoglobin. Being a safe and simple method, and despite depth limitations, NIRS has the potential to provide continuous non-invasive measurement of cerebral haemodynamic and metabolic parameters over multiple regions of interest with high temporal resolution [141,153]. In acute stroke patients, NIRS studies reflected reduced brain tissue oxygen saturation on the side with stroke compared to the contralateral hemisphere [119]. Commercially, the Infrascanner® developed by Infrascan, Inc. (<https://infrascanner.com>) is a handheld device used for diagnosing intracranial bleeds. The device uses a specific wavelength of 805 nm which is sensitive only to blood volume and not to blood oxygenation level. Extravascular blood (such as in an acute haematoma), absorbs NIR light more than intravascular blood (such as in a healthy brain) due to a greater concentration of haemoglobin. Infrascanner compares the left and right side of the brain in four different areas (eight measurements) and detects asymmetries (absorbance of NIR light is greater on the side of bleed). A full scan takes less than 2 minutes. Eighteen peer-reviewed publications have been reported by Infrascan [87]. In one such study out of a cohort of 431 patients including 122 cases of haematoma, the Infrascanner demonstrated high sensitivity (88%) and specificity (91%) in detecting hematomas > 3.5 cc in volume and <2.5 cm from the surface of the brain. The device has been cleared by the American Food and Drug Administration (FDA) to be used as a screening tool and as an adjunct to the standard diagnostic procedures [18]. NIRS as a method has also been approved by the FDA for patients at risk of reduced-flow or no-flow ischemic states, but not to be used as a sole basis of diagnosis.



Figure 1-18: Novel NIRS Device. a) Infrascanner 2000 handheld battery-operated sensor, front and back. b) Disposable cap with light guides for NIR laser and detector positioned over scalp. c) An optional docking station for data backup and/or battery recharge. d) Home screen. e) Preparation screen at the beginning of a session. f) Typical measurements completed at frontal lobe at two locations. g) Measurements completed at parietal lobe with simulated head trauma. [18]

Microwave Imaging (MWI) – Is based on measurements and analysis of backscattered microwave signals transmitted through the head. The signals are affected by biological tissues and scattered due to the dielectric contrast between different tissues [118]. Antennae are distributed over the entire head to achieve high detection sensitivity. Typically, each antenna is used in turn as a transmitter while remaining antennae are in a receiving mode, resulting in a large number of measurements. MWI has much in common with EIT: it addresses similar reconstruction problems and surface coupling issues, uses similar reconstruction algorithms, and targets the same medical applications. Clinical studies of pre-hospital stroke classifications are now in progress and are producing encouraging results for differentiating between stroke types using classification algorithms based on frequency difference measurements [130]. The use of MWI for post stroke monitoring is currently being investigated and simulation studies suggest that monitoring the progression of lesions in stroke is feasible [138].

Being an ill-posed method, MWI is highly sensitive to measurement errors and demands a high signal-to-noise ratio for images to be of acceptable quality [118]. MWI has the potential to be a low-cost, bedside, non-invasive, non-ionising monitoring technique. The human skull poses less of a problem for it with its use of microwaves in comparison with EIT. Commercially, there are three known devices

using MW technology for stroke and TBI, covering most of the applications covered by this thesis: pre-hospital confirmation of stroke/ TBI, stroke type classification, and brain injury monitoring in hospital settings. All three are in the early stages of commercial development. The three devices are: the Swedish Strokefinder™ developed by Medfield Diagnostics, AB. (<http://www.medfielddiagnostics.com>) which is the result of some of the studies mentioned above, the American EMTensor developed by EMTensor, Inc. (<https://www.emtensor.com>), and the Australian EMvision developed by EMvision Medical Devices, Ltd. (<https://www.emvision.com.au>).



Figure 1-19: Novel MWI Devices. a) The StrokeFinder MD100 (from medfielddiagnostics.com). b) The EMvision (from EMvision.com). c) The EMTensor (from EMTensor.com).

Radio Frequency – A technology called Volumetric Impedance Phase Shift (VIPS) is developed by the MedTech company Cerebrotech medical systems (<http://www.cerebrotechmedical.com>). It has recently published a clinical study reaching a promising milestone. The VIPS device, called Visor, functions by transmitting an array of varying frequencies (30-300 MHz) of low energy radio waves from each side of the back of the head to a receiver in the forehead portion of the device. Radio waves of different frequencies are modified differently as they pass through the tissue, depending on the type and fluid properties of the tissue, producing a unique signature for varied brain pathologies. Mean Bioimpedance Asymmetry (MBA) is calculated within 30 seconds of data collection. Large territory strokes caused by Emergent Large Vessel Occlusion (ELVO) are currently being targeted for the purpose of more efficient pre-hospital triage, allowing patients with ELVO to be sent directly to specialist stroke centres with mechanical thrombectomy capabilities. In a

peer-reviewed study published in 2018 [93], 235 patients were recruited across three cohorts with a variety of acute neurological conditions including 57 cases of severe stroke, 26 cases of small stroke, 73 other neurological conditions, and 79 healthy volunteers. The VIPS MBA score allowed to efficiently separate severe stroke from healthy and from the general recruited patients population, both with Area Under the ROC Curve (AUC) of 0.95.

Another commercial device utilizing electromagnetic energy in the RF spectrum has recently started to be developed by Sense Neuro Diagnostics (<https://senseneuro.com>) using similar principles to the MWI devices described earlier. The Sense device is using an antenna array, measures and analyses the scattering and absorbance of transmitted RF signal, by brain tissues. A single data frame collection is completed in less than a minute, and its first intended use is for long term monitoring for changes in brain injured patients.



Figure 1-20: Novel RF-based Devices. Left: The Visor device (from cerebrotechmedical.com), Right: The Sense device (from senseneuro.com).

Chemical Biomarkers – Are molecules which can cross the brain blood barrier (BBB). After brain injury tracing them in the bloodstream could be used to diagnose stroke and to discriminate between haemorrhage and ischaemia. NR2 peptide, a product of proteolytic degradation of the N-methyl-D-aspartate (NMDA) receptor, could potentially be a diagnostic marker for ischaemic stroke. Dambinova et al (2012) ran a clinical study of simple blood tests in 192 acute stroke patients (101 strokes, 91 stroke mimics) and found a peak concentration of NR2 peptide at 12 hours after symptom onset. With a concentration cut off set at 1.0 µg/L they were able to separate strokes from mimics with a sensitivity of 92% and specificity of 96% [43]. Stanca et al (2015) investigated the possibility of discriminating between stroke types using a combination of two biomarkers: Glial Fibrillary Acidic Protein (GFAP) and antibodies against NMDA receptors. They took blood from 72 stroke patients and 52 healthy controls at 12, 24, 28, 72 hours and 1 and 2 weeks after onset. The combination between the peak concentration of the two after 12 hours allowed differentiation

between haemorrhage and ischaemia with a sensitivity of 94% and a specificity of 91%. [143]. The possibility of using biomarkers for diagnosing concussion is also being studied [44]. This type of diagnosis has great potential to become widely available and at much lower cost compared to MRI and CT. Its main limitations are being non-continuous and sensitive to co-existing neurological disorders. Commercially, fast implementation of bloodstream carried biomarkers is in the research and development stages by the Russian company DRD (<https://drdbiotech.ru/>).

Accelerometers – Pulse blood enters the right brain hemisphere a few milliseconds prior to the pulse entering the left hemisphere due to the slightly asymmetrical locations of the internal carotid arteries relative to the heart. A highly sensitive array of accelerometers is located around the head and monitors this pulsation pattern. Studies suggest that this pattern alters in patients with brain injuries. A study by Smith et al, 2015 [142] measuring accelerometers' data patterns in healthy individuals and patients confirmed that with different degrees of vasospasms using TCD, and accelerometers data from healthy controls, allowed the identification of vasospasms in a prospective cohort of 58 patients with a sensitivity of 81% and negative predictive value of 61%. Another 2015 study, by Auerbach et al, [14] followed a similar design but aimed to detect concussion. In a cohort of 82 high-school football players, accelerometer data enabled concussion to be detected with a sensitivity of 76.9% and a specificity of 87%. Commercially, The BrainPulse™ device, developed by Jan Medical, Inc. (<https://www.janmedical.com>) is targeting these applications.



Figure 1-21: Nobel Accelerometers-based Device. The BrainPulse One (from janmedical.com).

Electromagnetic Tomography (EMT) – A growing body of evidence in the literature is describing experimental work utilizing the change in electrical impedance induced by magnetic fields created around the body. The main theoretical advantage of EMT over EIT is its ability to overcome skull resistivity. There is a variety of hardware designs and measuring techniques under the group of electromagnetic induction methods. According to the literature, the main group studying its applications in brain injury is the Chinese Third Medical University group. Studies describe preliminary

promising results in simulations, mechanical phantom feasibility studies, and animal work of ICH model in rabbits [98,127,128,164].

Digital Health Sensing – New approaches for early detection of stroke include utilizing sensors and software on smartphones (m-health) and sensors embedded in electrical devices connected to the internet (IoT). Proposed concepts and preliminary data suggest these approaches might be beneficial to populations at risk and to the health system as a whole [72,145].

Mobile Stroke Unit (MSU) - An impressive innovation designed to address the challenge of shortening onset-to-needle-time in stroke patients is the use of Mobile Stroke Units (MSU) [59,163]. An MSU is a large ambulance equipped with a mobile CT scanner, small laboratory, telemedicine, medication, and medical staff (paramedics and/or clinicians). The MSU concept was first trialled clinically in 2008 in the USA, and now there are more than 20 similar programs worldwide at different stages of trials (figure 1.22). Although results from large scale well-balanced clinical studies have yet to be published, preliminary evaluations provide very positive clinical results and proven cost-effectiveness [47,74,75,52]. A similar concept is the stroke helicopter (“Helistroke”) which is already subject to feasibility studies [86]. These types of stroke solutions are very likely to encourage further research and development of advanced diagnostic and monitoring solutions for stroke.

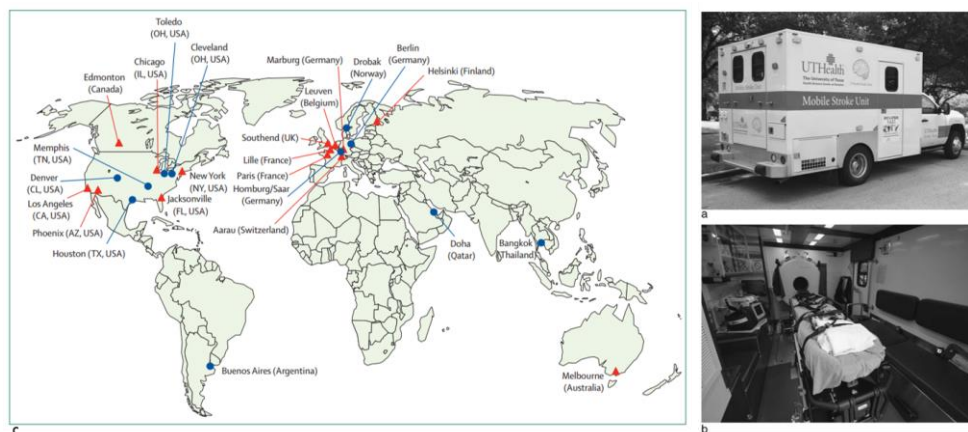


Figure 1-22: Mobile Stroke Unit (MSU). a) Exterior of the Mobile Stroke Unit [74] b) Interior of the Mobile Stroke Unit [74] c) Mobile Stroke Unit research projects; blue circles indicate sites with active MSUs and red triangles indicate sites in which such projects are in the state of implementation [59].

1.6.4 The Multi-Modality Monitoring (MMM) approach and EIT Relevancy

This PhD research deals with the application of EIT to the detection of brain injury. As brain injury is a complicated condition, EIT might prove to be only a part of the solution in the first stage.

Non-bedside techniques such as CT and MRI offer much higher resolution images/ data, but cannot provide continuous monitoring, are rarely available outside hospitals, and are much more expensive. Invasive techniques, however, could be applied at the bedside, but are much riskier to patients, and are beneficial only in severe cases where the potential benefit outweighs the risk.

An optimal monitoring technique would be non-invasive, mobile, affordable and compatible with bedside operation, such as EIT. Having reviewed the many monitoring techniques currently available or under development, it is clear that no single method offers a perfect solution for covering all aspects and possible cases of monitoring after a brain insult. The challenge is therefore to integrate monitoring systems in order to combine their strengths, and allow greater confidence in decision-making. This is the Multi-Modality Monitoring (MMM) approach. MMM may allow a greater understanding of individual pathophysiology and the delivery of tailored treatment strategies instead of applying general treatment policies [144]. EIT could become an important component of the MMM strategy, and still, needs to prove its effectiveness as a monitoring method for brain injury.

1.7 Summary of Relevant EIT and EIS Literature

Imaging brain functions using EIT has been under investigation for nearly three decades. Historically, most of this work has taken place at UCL, as described in detail by Holder and Tidswell (2005) [81]. Most of the relevant work on which this study is based was aimed at stroke pre-hospital identification and classification in order to administer antithrombotic drugs as soon as possible to ischaemic stroke patients. Nevertheless, relevant progress with reconstruction algorithms and instrumentation has been made with other applications, especially with epilepsy [77,78,156,157,161] and fast neural activity imaging [9,10,60,61].

1.7.1 Fundamental Brain EIT Studies

Almost 20 years ago, brain EIT began to employ FEM based imaging methods for better representation of the anatomically complex human brain [19]. A few years later Romsauerova et al (2006) ran a technical-clinical study to characterize the UCLH Mk 2 MF-EIT system and considered 7 patients with three types of pathologies, of which one type, Arteriovenous Malformation (AVM), mimicked the impedance characteristics of a haemorrhage. Data were collected for the range of 16 KHz – 64 KHz and reconstructions were made with a linear frequency difference method and with a new compartment-wise algorithm. For the first algorithm, there were no reproducible or recognizable changes in the images when compared to the known pathologies on MRI. For the latter algorithm, there were no significant differences between lesion areas with respect to mirror areas in six out of seven cases. Instrumentation accuracy of 0.1% was set as the technical target to improve in future studies [135]. This study strongly suggested that MF EIT is not a straightforward approach, and that further instrumentation and algorithm improvements were needed. Nevertheless, it employed innovative analysis methods for MF data, which was later adopted in this study for MF data collected in the acute stroke ward.

Early computer simulations of TD monitoring by Boone and Holder in 1996 [23] established the effect of drift in contact impedance (CI) over time on EIT image quality. A linear drift of 2% was found to be sufficient to cause noticeable image distortion. At 5% the original image was almost lost. After more than 10% drift, significant artefacts were observed in the image. Drift in CI might be the principal cause of drift in BV, which is the main technical challenge addressed in this study. The work done by McAdams et al (1996) [112] explored the mechanism and the different factors underlying CI, describing the different components of electrode-gel-skin interface. It also

suggested that skin impedance might be the largest component of the three in the band of 1-10 KHz, and recommended that aggressive gels (>> 5% ions concentration) should not be used on the skin, for the long-term monitoring of bed-ridden patients.

A study of EIT headsets by Tidswell et al (2003) compared the performances of four scalp electrode arrays: conventional EEG Ag/AgCl cup electrodes, Easycap, geodesic head net, and Physiometrix E-net, for use in EIT on humans. Measurements were taken over a few minutes' timescale from a novel head phantom with marrow skin, and from healthy human subjects. Baseline noise, SNR, and CI were compared. The Physiometrix headnet (today called the Hydrodot) was found to be the least noisy, having only $4.5 \pm 0.6\%$ of the measurements with more than 1% noise [150]. With the exception of the geodesic head net, which could not be used over several hours, the other electrode types were considered for evaluation in this thesis work.

A clinical study by Fabrizi et al (2006) aimed to detect and localize epilepsy seizures foci in epilepsy patients while monitoring over hours with TD-EIT. They tested 22 seizures in 7 patients. Estimated local impedance changes were around 10% and the BV changes were around 0.1%. The changes occurred over a few minutes; recordings were made with the UCLH Mk 1b at 38.4 KHz and 2.2 mA. Images were generated using a realistic head-shaped four-layer model (scalp, skull, CSF, brain) consisting of a 136,000-element head mesh, and a linear tSVD reconstruction algorithm. No reproducible images could be reconstructed even though changes in BV were higher than expected [57]. However, the study confirmed the feasibility of recording over several hours with EIT for monitoring purposes, and of combining EEG and EIT simultaneously. A further study by Fabrizi et al (2009) established the current injection protocol used as a starting point in the study presented in this thesis (the "spiral 16" protocol) and the method for comparing image quality [55].

1.7.2 Recent Brain EIT Studies

A study reported by Packham et al (2012) examined the possibility of four different linear Frequency Difference (FD) algorithms to reconstruct images from a realistic head shape 3D tank with a complex background simulating ischaemic stroke-like lesion. The local impedance changes were of $\sim 20\%$. Although weighted FD algorithms (WFD and WFD Adjacent) were superior to the simple linear algorithms (FD and FD Adjacent), images reconstructed with a TD algorithm yielded a smaller error and were preferable to those generated using the FD algorithms. Given that this study

was performed before testing with a more realistic set-up including skull and scalp, the results strongly indicated that FD-EIT applications based on linear algorithms still required further development before they could be applied to patients [129]. As part of developing the next generation of FD algorithms, research has been directed toward non-linear FD algorithms by Malone et al [107,108] and Yang et al [169], as previously described.

Research has proceeded over the years in other relevant aspects of EIT. In the earlier clinical studies of Romsauerova and Fabrizi mentioned above, the UCLH Mk2 and Mk1b were used respectively [57,135]. Instrumentation was developed and tested in a few iterative cycles, and then compared for use in clinical studies, including the UCLH Mk 2.5 and the KHU Mk 1 [134,56]. For the purposes of brain EIT research, engineers in the UCL EIT group recently developed the ScouseTom system, as described by Avery et al (2017). Using off-the-shelf components and local hardware and software design which is widely available online, a highly versatile and reproducible MF-EIT system [17] has been produced, and is used for the studies reported here. As part of supporting open brain EIT research, Avery *et al* (2017) have published a recipe for generating a reproducible 3D printed head-shaped tank based on real CT and MRI scans and designed with a realistic conductivity distribution [16]. This tank was also used in the work reported here.

Additional tools developed by the UCL-EIT group include a method for rapidly extracting patient specific FEM meshes from CT and MRI [155,90], and a new and improved tool for efficiently running forward models [92]. Jehl et al (2016) investigated the need for patient-specific meshes for more accurate reconstructions [90]. Using simulations, they concluded that for TD applications this is unnecessary and that a general head mesh was as effective as a patient-specific head mesh. Again, Jehl et al (2015-16), established a reconstruction algorithm for the correction of electrode modelling errors using an Electrode Boundary Jacobian (EBJ). This method was validated in TD-EIT reconstructions with simulated data and 3D head-shaped tank [91] and later in MF-EIT with realistic head model simulated data [89]. These advancements in brain EIT research, allowed this work to try again for TD-EIT and MF electrical impedance monitoring applied to stroke and TBI which had failed in previous clinical studies [57,135].

1.7.3 EIT for Brain Injury (Stroke and TBI)

The idea of monitoring brain injuries with EIT is not new, and first appeared in the published literature many years ago. In 1987, Murphy reported an attempt to detect IVH using EIT in a new-born infant [122]. More recently, Manwaring et al (2013) used a swine model of head injury and a novel combined ICP/EIT sensor to find consistent evidence for intracerebral injuries. EIT and ICP monitoring were facilitated using a ring of disposal Ag/AgCl electrodes on the scalp, and one intracerebral ICP sensor/EIT electrode combination, for about 30 minutes [109]. A human study by Dai et al (2013) dealing with in vivo imaging of influx and efflux of irrigating fluid (5% dextrose in water), with scalp electrodes during the twist-drill drainage operation in patients with SDH, concluded that intracranial resistivity changes in humans were detectable and quantifiable with EIT [40].

Dowrick et al (2016) investigated the possibility of TD-EIT imaging of ischaemic and haemorrhagic stroke in rat stroke models. Using an array of 40 spring-loaded gold-plated electrodes on an anesthetized rat's skull, they injected a 150 μ A current at 2 KHz and recorded before, during, and after introducing the animal with stroke. Reconstructions with a 4-million element mesh and 0th order Tikhonov regularization yielded three successful images out of seven ICH cases, but did not include any of seven ischaemic stroke cases. [90]. To investigate the possibility of MF-EIT for imaging stroke, Dowrick et al also studied the in-vivo impedance spectra of healthy brain, ischaemic, and clotted blood in four rats. They characterized the spectra of these stroke tissues over the frequency range 0-3 KHz, and found a flat spectrum for clotted blood between 250 Hz and 3 KHz, while healthy and ischaemic brain impedance increased at a similar linear rate and with a constant difference of 5-10% between them [49]. Using the UCL ScouseTom, they also found a maximum phase angle of < 0.5 degree which implied the imaginary part is negligible.

Over the last few years, the EIT research group at the Fourth Military Medical University in Xi'an, China has extensively researched the application of brain electrical impedance technology in stroke and TBI, and published several important studies. Yang et al (2016-2017) extended the Dowrick et al rat studies and conducted a thorough characterizations of brain tissues spectra in-vivo and ex-vivo in rabbits [168,170]. Initially they studied the impedance spectra of healthy, ischaemic, and haemorrhagic brain tissue over the frequency range 10 Hz – 1 MHz. They measured tissue samples 15 minutes after incision in twenty-two rabbits, using a Solarton 1260 impedance/gain-phase analyser. They reported a 40% impedance change in is-

chaemic tissue. Clotted blood presented a higher impedance than that of fresh blood and remained flat at frequencies <10 KHz. They concluded that to discriminate between the two stroke types, the range 10 Hz – 100 KHz should be used. They also inferred that the imaginary part of the recorded signal has an important role in the ability to discriminate haemorrhagic from ischaemic stroke.

Thereafter this research group explored in-vivo animal stroke models, both haemorrhagic, ischaemic, and healthy controls. They measured the impedance spectra over the frequency range 10 Hz – 1 MHz in forty rabbits. Measurements were taken on a bare cortex after craniotomy using six electrodes, one injecting pair on the mid-sagittal plain and two recording pairs, one on each hemisphere. Significant differences ($p < 0.01$) were observed in the real part between the healthy control and the ICH groups, and between the healthy control and the ischaemic stroke groups across the whole frequency range. They also found a significant difference across the whole range in the rate of the impedance change between haemorrhagic and ischaemic stroke. Another important finding was that impedance increased after blood was injected even though blood, fresh or clotted is much more conductive than brain (see *section 1.2.3* for possible explanations).

Yang et al (2017) added a third thorough investigation of contact impedance spectra between 10 Hz – 1 MHz [166]. A ring of sixteen electrodes were applied to forty-seven healthy human volunteers. They found a rapid decrease in CI below 10 KHz. They also concluded that the imaginary part of the CI has a significant role in these frequencies, having a similar amplitude to the real CI component. CI was found to be smaller at the forehead than at other locations. They also investigated the effect of CI on current density beneath the electrodes and the influence of imbalance between CI of two recording electrodes. They found that CI imbalance could result in up to 0.3% measurement error at 10 Hz, and that the imbalance affect is reduced significantly as frequency increases.

The fourth study by Yang et al (2018) [167] aimed to find the optimal electrodes - conductive gel combination. Sixteen electrode – gel combinations were evaluated over time and frequency. The contact impedance of each combination was measured on the foreheads/scalp of ten healthy volunteers for one hour at frequencies from 100 Hz to 1 MHz employing the two-electrode strategy. The performance of each combination was evaluated in terms of the magnitude of contact impedance, and changes in contact impedance with time and frequency. A combination of silver/ silver chloride electrode and low viscosity conductive gel performed best with a relatively low mag-

nitude of contact impedance and superior performance with time and frequency over other combinations ($p < 0.05$).

A recent clinical study from the same group by Li et al from 2018 [100] examined the possibility of using EIT as a cerebral monitoring tool during Total Aortic Arch Replacement (TAAR). Using a ring of scalp electrodes, at 50 KHz, data frame was collected every 1 second, and a 2D image was reconstructed. Average reconstructed Resistivity Value (ARV) was calculated for the whole brain, and for each hemisphere separately, computing Asymmetry Resistivity Index (ARI) as the difference in ARV between the hemispheres. Maximal ARI (MARI) throughout the procedure was used to predict post-operative neurologic deterioration (ND). eight of the forty patients included in the study suffered from ND, and MARI as a sole predictor for ND had an Area Under the ROC Curve (AUC) of 0.86. ARV was found to be proportional to cerebral perfusion.

Another recent clinical study by Yang et al from 2019 [165] investigated the relationship between ICP and intracranial impedance changes during oedema dehydration procedure using mannitol in ICH patients. Using a ring of scalp electrodes, at 50 KHz, forty patients were administered mannitol and were monitored for three hours simultaneously with both EIT and an invasive ICP sensor. An image was reconstructed every minute and ARV was used in comparison with measured ICP. A strong negative correlation of $R^2 = 0.78$ was found, suggesting that EIT is a promising tool for the real-time and non-invasive monitoring and early detection of cerebral oedema.

Studies by Wang et al [159], Dai et al [41], and Cao et al [33] described earlier in the 'bioimpedance of brain lesions' section of this chapter, are also recent studies from the same group.

1.7.4 EI Spectroscopy and Brain Symmetry Studies

The literature in the field of bio-electrical impedance spectroscopy (bio-EIS) also deals with its applications to stroke and TBI. Important work was done in Sweden and in the United States (2015-2016) exploring the possibility of detecting and classifying strokes with symmetry analysis of EIS signals. Bonmassar et al (2010) established the idea of baseline left-right hemispherical symmetry in the healthy human head. They studied symmetry on four healthy volunteers by stimulating across the midsagittal plane with 0-50 KHz white noise at 500 μ A, and measured with two pairs of electrodes positioned symmetrically relative to the midline (frontal-temporal

left and right, temporal-occipital left and right). The CI values were all under 3 K Ω at DC, and they observed a very high symmetry in all measurement pair spectra. In addition, they simulated a haemorrhagic lesion on the right frontal lobe with a 3D head phantom and found a significant asymmetry in the frontal-temporal electrode pairs. On the side ipsilateral to the lesion, absolute impedance increased in the frontal-temporal left measurement and decreased in the left temporal-occipital measurement. No significant change was recorded in the right-side measurements [22].

Seoane et al (2015) studied the impedance spectra symmetry in ten acute stroke patients (four ICH, six IS, at Karolinska University Hospital, Sweden) and three healthy controls. They used a set-up where on each hemisphere there was a frontal-occipital injection pair (200 μ A, at 256 frequencies over 3-1000 KHz) and two measurement pairs (lateral: frontal-temporal pair and central: parietal-temporal pair) using a SFB7 bio-impedance spectrometer. Symmetry ratios were calculated side-to-side and central-lateral. In nine out of ten patients, at least one symmetry ratio was found significantly different from the control range, and six of ten presented with two or more significantly different ratios. Discrimination between haemorrhagic and ischaemic stroke cases was not possible [140].

Atefi et al (2016) continued that study with a cohort of six ICH patients (6-53 ml in volume) and ten healthy volunteers at the Massachusetts General Hospital, USA. They stimulated at 500 μ A with white noise of 0-50 KHz, and recorded with three electrodes on each hemisphere. The potential was measured between the three pairs, across the midsagittal line to calculate side-to-side symmetry. Using the pair with maximal potential difference in every participant, they found a significant difference between the ICH and healthy control groups. CI was measured at 100 Hz, 1 KHz, 10 KHz, and 100 KHz and all values were below 5 K Ω . The CI for patients was slightly higher than for the controls, but not significantly. They also studied the equipotential lines of a numerical detailed model of fifteen tissue types with similar electrode settings. This study clearly presented the side-to-side equipotential line across the head, which is straight and symmetric in a healthy model but becomes asymmetric when a lesion is introduced. They also found that asymmetry occurs close to the location of the lesion (see figure 1.23) [12].

An earlier study by Atefy et al (2013), investigated the possibility of using classification trees with EIS signal to detect brain injury. They considered 720 measurements from nine participants: three chronic ICH patients and six healthy volunteers. The electrode arrangement was the same as that used in the study by

Seoane et al [140] described above. They extracted three Cole parameters from the data representing asymmetry and applied then to a hierarchical classification tree with a Leave-One-Out cross tree validation. Results showed a 100% success in separating healthy controls from ICH patients [13].

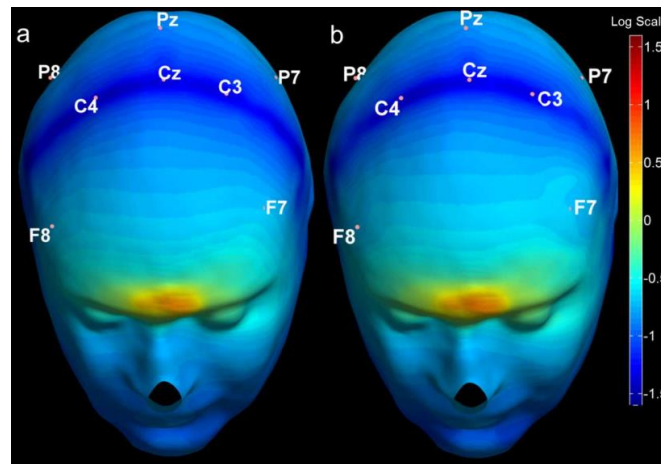


Figure 1-23: Atefi et al Symmetry Simulation Study [12]. Scalp potential distributions on the surface of the numerical head model. a) The healthy numerical head model and equipotential line distributions on the scalp with three pairs of electrodes located on the frontal (F7–F8), central (C3–C4), and parietal (P7–P8) areas of the scalp according to the 10–20 international EEG electrode placement system and symmetric relative to the midsagittal plane of the numerical head. The equipotential lines and potential gradients are symmetric relative to the midsagittal plane of the model and the three electrode pairs. (b) Numerical head model with a spherical hemorrhagic lesion 20 mm in radius in the frontal left hemisphere close to F7 electrode. The hemorrhagic lesion creates a different potential gradient at F7 compared to the healthy control and its counterpart on the right hemisphere, F8; however, the other two electrode pairs in a greater distance from the lesion remain symmetric.

An Israeli study by Cohen et al (2015) presented a simulation study with a realistic head model. Current injection was simulated between the nasion and inion, using sixteen measuring electrodes (eight pairs measuring left right asymmetry). They simulated both ischaemic and haemorrhagic damage, in five different locations and volumes between 0.5 and 50 ml. They found that the Asymmetry Index (AI) increased when haemorrhagic volume increased, but AI in some cases decreased when ischaemic volume increased. They also found that greatest asymmetry is present close to the damaged area [36].

An interesting approach combining asymmetry with EIT imaging (SEIT) was presented by Ma et al (2014) from the Xi'an EIT group. They used the asymmetry in the patient measurements and a clinical assessment of which side of the head the lesion is present. They then copied the measurements on the healthy side to the damaged hemisphere and thus created a “before” reference measurement. The difference between the actual measurement and the computed reference is then reconstructed. They validated the method with a simulated 2D head-shaped experimental set-up

using 1250 μA at 50 KHz, both for ischaemic and haemorrhagic models 1 cm in radius [106]. However, this study should be considered carefully as the UCL group tried unsuccessfully to approach the researchers in order to try repeat their findings.

A new interesting body of work carried out at the National University of Ireland Galway (NUIG) has recently been published. McDermott et al. (2018) [115] proposed a new EIT modality for use for stroke detection and classification. The proposed technique, Symmetry Difference EIT (SD-EIT), makes use of the inherent symmetry in the region being imaged (i.e. head and brain) and creates a set of two images and four metrics. It is reliant on an aggregate approach. The two outputted images are needed to confirm the results of each other, both visually and quantitatively by the metrics, to give a final result that a potential user would have confidence in. A first image is created as a difference between the clockwise and anti-clockwise measurement frame, and targets the question whether a brain injury is present or not. The second image is a time-difference image between a simulated measurement with no lesion present ('before') and one of the real measurements frame ('after'), and targets the question what type of lesion is it – ischaemic or haemorrhagic? One metric is created with the first image (Percentage symmetry) and three more with the second image (Centroid difference, F1 score, Mean intensity difference). This first study tested the new SD-EIT approach with simulated data and with measurements taken on a cylindrical tank filled with saline. Simulations included lesions in different locations and of several different volumes (2-30 ml) using a two-layers head model and a ring of sixteen electrodes. The saline filled tank model included similar variety of lesions types, volumes and locations. This work provided a proof of concept for SD-EIT evaluated on a variety of test cases.

This study illustrated cases where SD-EIT was successful together with cases where it was inconclusive. The more robust performance was seen for larger lesions, lesions near the exterior, lesions of higher conductivity contrast, and situations where there is a higher SNR. It also did well with cases where the simulated 'before' was well modelled in terms of anatomy and conductivity profile. However, this is still at an early stage, and more realistic cases will need to account for factors such as poor anatomical modelling, incorrect conductivity profiling, imperfect electrode placement, and differing and unknown electrode contact impedance. These uncertainties will cause measurements to deviate from the ideal. Issues which affect other modalities that attempt to image static scenes are then likely to be introduced. An absolute limitation of SD-EIT is that it can only be used in cases where the lesions are unilateral.

In addition, McDermott et al. (2018) [114] also investigated the possibility of using machine learning with EIT data frames for detecting ICH. In this study, data were simulated for healthy and ICH of different locations and volumes (5-60 ml) using a two-layered head model and a ring of sixteen electrodes. Similar data were recorded on a two-layer head phantom. Simulated data were fed to a linear Support Vector Machines (SVM) binary classifier, and the effect of ICH size and location, noise level (SNR 20-80 dB) and head geometry was investigated. Recorded data were initially fed to linear SVM and then also to non-linear classifiers (Radial Basis Function SVM and Neural Network). Results demonstrated the basic feasibility of taking such an approach to achieve high sensitivity classification with EIT data. Despite impressive sensitivity values approaching 100% in some scenarios, simulations demonstrated that noise level and the ability to classify data from different head shapes had significant impact on the results. Physical phantom data demonstrated the superiority of more advanced classifiers over linear SVM. In general, this study demonstrated effectively that EI-based machine learning is worth exploring, and that using it successfully with real data (partial, much lower SNR, and with highly varying geometries) will be very challenging.

1.8 The Aims of this Research Project

The rationale behind this research project was to explore the possibilities of the application of EIT brain injury monitoring to clinical practice. EIT could have an important role in three main applications of brain injury diagnosis. The first possible application is the ability to positively diagnose stroke in patients with a clinical presentation of the relevant symptoms, and to exclude stroke mimics. This has the potential to direct the patient far more quickly to the most suitable treatment facility. The second possible application would be to distinguish between ischaemic and haemorrhagic stroke, which will impact the immediate treatment given to a patient (e.g. tPA administration, urgent cranial pressure release, etc.). The third possible application is monitoring high risk patient populations for the development of delayed brain lesions.

The first two applications require instant diagnosis without a baseline measurement, for which multi-frequency or absolute EIT are relevant options. They also require prompt application of electrodes to the head. Both MF-EIT and fast electrode application are still under development [[15](#),[107](#),[169](#)] and therefore the initial focus was on monitoring for delayed/ secondary brain injury with TD- EIT. This will most likely be needed in a hospital environment following head trauma, first stroke, TIA, etc., and mounting 16-32 EEG-like electrodes while applying TD imaging algorithms is possible. With TD imaging [[91](#),[129](#),[159](#)], a haemorrhagic lesion is the most likely to be successfully imaged [[50](#)], and thus identification of an intracranial bleed is an appropriate initial target.

For TD imaging, the principal technical challenge is baseline BV drift. A significant effort was therefore invested in characterizing and investigating the source of such drift first. Then, a feasibility study was planned with the hope of successfully proceeding towards a new clinical pilot study. For the possibility of unsuccessful TD-EIT feasibility, a non-imaging EI based method (EIS) was developed to be explored in the clinical pilot study.

In summary, the questions this PhD aimed to explore were as follows:

- **Drift:** to determine the component elements of scalp measurement drift over more than 5 hours. What are its characteristics: amplitude, change with time, location, and frequency? What are its component elements? What causes the drift?
- **Feasibility:** to estimate the feasibility of imaging brain injury with TD-EIT, based on simulations as close as possible to real drift conditions. What are reasonable choices for modelled pathologies and drift? What, if any, pathologies can be expected to be imageable by EIT? What is the biophysical explanation for these findings?
- **Clinical:** to establish a high-quality stroke EIT dataset to advance stroke/TBI and EIT research and secondly to find evidence of any useful diagnostic information in stroke MF-EI. Could it be used to separate out stroke patients from a healthy population? Could it be used to differentiate ischaemic stroke patients and haemorrhagic stroke patients? Can it be used with a reduced number of electrodes set-up as a base for a future point-of care set-up?

1.9 Statement of Originality

The material presented in this thesis is my own work and has not been previously submitted for a degree in any University. The intellectual content of this thesis is the product of my own undertaking, yet research such as this is inherently interdisciplinary and collaborative. I have been privileged to be a member of the multidisciplinary UCL EIT group. Coming from neuroscience to the medical physics and biomedical engineering field, I have received technical assistance in relation to hardware, image reconstruction, good clinical practice and presentation style as duly acknowledged in the introduction of this thesis.

I was supported by Dr James Avery when assembling and operating early versions of the ScouseTom EIT system as reported in chapter 2. The resistor phantom, mechanical abrasion applicator, and head-shaped tank were designed and manufactured by him. I was advised by Dr Gustavo Sato dos Santos regarding preliminary data processing and statistical analysis. Tugba Doru assisted me with preliminary bench set-ups. I was assisted by Dr Markus Jehl on how to apply my idea of using his electrodes movement correction algorithm to reconstruct drift.

For the work described in chapter 3, I was advised by Dr Kirill Aristovich on image reconstructions and how to adopt his code for 0th Tikhonov reconstruction. The FEM mesh I used was segmented by Dr Markus Jehl. I was also advised by Dr Brett Packham on image quality quantifications.

I was assisted by the stroke research group at University College Hospital led by Renuka Erande to establish the necessary documents and ethic approval for the clinical study reported in chapter 4. They assisted in sourcing eligible patients and supported the procedure throughout. Eleanor Mackle and Dr Anna Witkowska-Wrobel assisted me with bedside data collection at the Hyper-Acute Stroke Unit. Dr James Avery provided technical support for data collection using the ScouseTom system, and Dr Tom Dowrick was responsible for the technical quality validation for the data which facilitated its publication and online availability.

I personally undertook all subsequent data collection, data processing and analysis, and image reconstruction.

2 Investigation of Boundary Voltage Drift

2.1 Introduction

In Electrical Impedance Tomography (EIT), a low amplitude alternating current is applied to the body under investigation using surface electrodes. These electrodes also measure the voltage. Measured boundary voltages (BV) are taken together with prior knowledge of the electrical properties of the relevant biological tissues to form a tomographic image of conductivity changes inside the body under investigation.

Time-Difference EIT (TD-EIT) for brain monitoring aims to detect pathological changes within the skull using changes in electrical impedance. These changes are reflected in electric potential changes outside the skull, and are detected by non-invasive electrodes placed on the scalp. Electrodes on the scalp for EIT and EEG recordings, are normally placed using a conductive gel/ paste to create a lower and more stable Contact Impedance (CI).

This application type needs the change in BV to only reflect impedance changes inside the skull to prove successful. Since real world medical applications are never as perfect as in simulation or laboratory experiments, successful EIT based brain imaging will require the dominant portion of the change in BV to reflect intracranial changes.

Research has established beyond doubt that BV changes in brain EIT contain significant changes which are not the result of intracranial changes, and are in fact *Noise* [25,27,91]. Most noise are fluctuating changes of certain frequencies, going up and down and back to baseline value, and so are likely to be cancelled out by averaging BV values in two different time points. However, one type of noise, clearly recorded in former studies is of linear-like drift in baseline BV. Unlike other noise, *Drift* is a change in baseline BV over time, so could cause an erroneous EIT image.

EIT studies have addressed BV drifts, suggesting that it is significant and distorts reconstructed EIT images [24,27,57]. Most studies to date have suggested that the main cause of drift is a gradual change in CI which in turn effects the current going into the head and BV over time. Each component of the electrode-gel-skin complex might contribute to the change in CI over time, and therefore might be the principle component causing BV drifts [23,112, 150,166,167]. Temperature changes around the electrode, electrode movement, or even BV baseline amplitude and measurement methods have been proposed as correlated factors. Detailed summaries of these studies can be found here in sections 1.7.1 and 1.7.2 in this thesis.

2.2 Rationale

This chapter focusses on the study of the spontaneous changes in BV recordings which are not the result of intracranial pathological changes in general (noises), with an emphasis on the BV Drift Phenomenon. While the existence of drift is not debatable, its characteristics have not been thoroughly studied and the mechanisms generating it are not yet fully understood.

The rationale behind this study was to methodically quantify the drift and noise in long term EIT measurement, as accurately as possible and then, to break it down into individual components that will allow the identification or elimination of possible correlating factors: hardware, CI change, electrode type, gel, skin, temperature, and movement.

To separate the different component, different models would be used in phantoms and human subjects, with each model highlighting a specific possible factor. Successful correlations might assist in the discovery of the mechanism behind drift, hopefully resulting in a way to eliminate or reduce it, clearing the way for successful TD-EIT using scalp electrodes.

2.3 Purpose

The main purpose of this study was to determine the component elements of scalp measurements drift over more than 5 hours. The first question was to determine the noise and drift characteristics. The characteristics described were magnitude, change with time, space (scalp location), and frequency. The second question asked what were the component elements of drift. Possible elements investigated were CI, electrode type, hardware system, gel dehydration, recording methodology, and temperature. An additional purpose was to test a drift elimination method based on an existing algorithm for electrode movement correction.

2.4 Experiment Design

This study was an empirical exploration. A varied series of experiments were carried out in the laboratory. BV was recorded in different conditions, and several variables were analysed to fulfil the aims and objectives of the study.

2.4.1 Recording Types

Recordings using healthy human volunteers were performed in two stages for two separate purposes. Preliminary recordings were made over several hours with different electrode types and hair conditions to determine the most compatible electrode type for long term measurements. A second round of recording was carried out using the selected electrode type after the first round, over longer periods on a larger number of volunteers.



Figure 2-1: Recordings in Healthy Volunteers.

Recording using a resistor phantom was made on a resistor phantom whose load and contact impedances were fixed. Recording was continuous at one fixed frequency and one current amplitude over several hours. This measured the drift of the system itself.

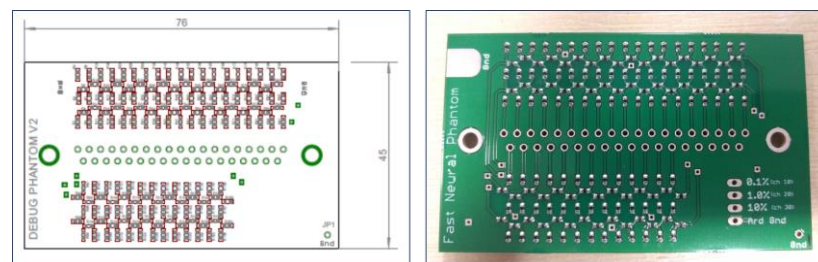


Figure 2-2: The UCL-Built Resistor Phantom. Left – technical sketch. Right – image of the actual phantom used in this study.

Recording using a head-shaped tank was used to measure the drift in a controlled three-dimensional environment where contact impedance is the same for all electrodes and fixed over time while the impedance between electrodes is proportional to the distances between the electrodes. The recording using the head-shaped tank, was continuous at one fixed frequency and one current amplitude, over several hours.

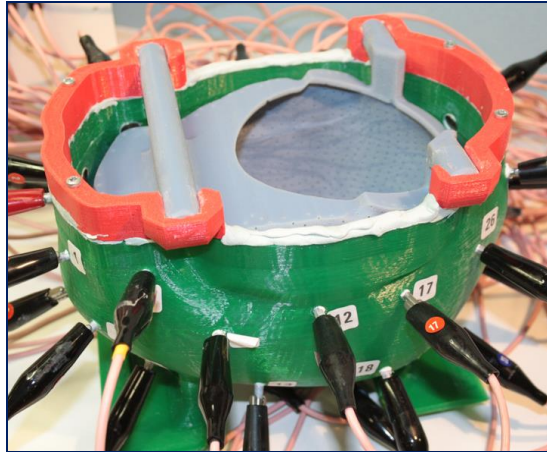


Figure 2-3: The UCL 3D Printed Head-shaped Tank.

Recordings using a marrow (giant zucchini) allowed some measurements that are not possible using human subjects, and permitted some experimental setups which are harder to try on human skin. In previous EIT studies, marrow skin was chosen to simulate human skin. It was compared with other fruits and post-mortem animal skin and was found to have the closest resistivity and the highest phase angle [150]. The preparation procedure for marrow was as in humans except that the abrasion of the skin was gently made by hand to ensure that the skin remained intact. Four separate types of recordings were made using marrow:

1. **Baseline Recording** – This was a continuous recording at one fixed frequency and one current amplitude, over several hours, to determine whether marrow basic drift characteristics are similar to those of human drift.
2. **Multi-frequency Recording** – This was continuous recording at three fixed frequencies and one current amplitude, over several hours, to investigate if and how drift changes with frequency. In this recording, each protocol line (current injection combination) which takes less than a second was performed in series for all 3 frequencies before moving to the next injection. This gave approximate multi-frequency drift recording over several hours.

3. **Dry vs. Wet Electrodes Recording** – This entailed continuous recording at one fixed frequency and one current amplitude, over several hours, to investigate the influence of the conductive gel on CI and drift. Half of the electrodes were applied as usual while the other half were applied without conductive gel between the electrode and the vegetable skin. To share the same skin properties, electrodes were divided in two while sharing the same specific marrow. To compensate for changes in skin properties in small areas, the type (wet-dry) of electrode in every ring was allocated randomly and then dry/ wet electrodes were evenly spaced (alternating dry/wet electrodes in each ring).
4. **System On-off Recording** – This was at one fixed frequency and one current amplitude, over several hours, to investigate if what was recorded as drift on the skin was in fact a combined effect of the system drift being amplified by the electrode-gel-skin complex. In this set-up, the system was on and recorded for 15 minutes every hour and then was on stand-by for the rest of the hour, in a repeated pattern.

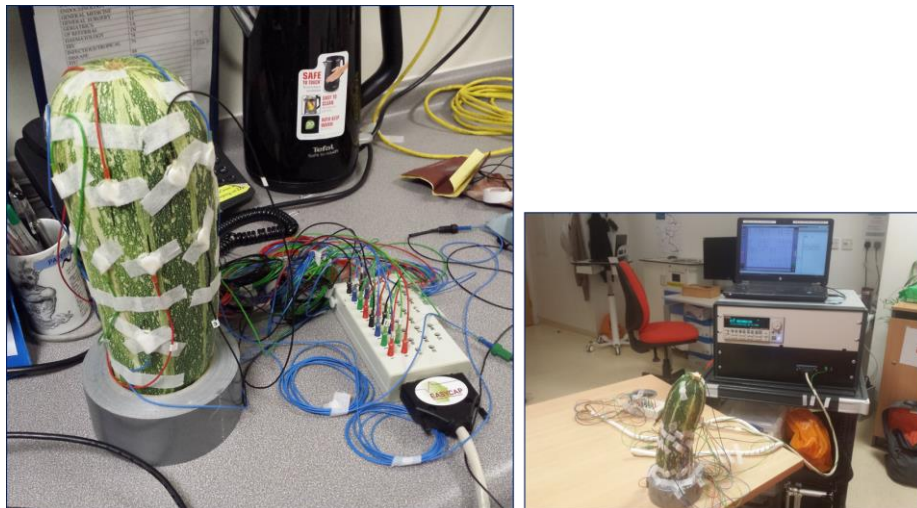


Figure 2-4: Marrow EIT Experiment Set-up.

2.4.2 Electrode Montage and Current Injection Protocols

Electrode montage for the human studies was based on the EEG 10-20 electrode system (figure 2.5). An earlier study published over a decade ago [150] indicated that different electrode types vary significantly in performance. A more recent study indicated a preferable combination of electrode and gel materials [167]. Here, three electrode types mentioned in the former study were used initially to determine the optimal setup for the more prolonged drift recordings in humans.

For the preliminary drift recordings in human subjects, the ‘Spiral16’ protocol [55] was used as it was the optimal known protocol at the time. For the second part of the recordings in human subjects and head-shaped tank, a new protocol designed for this experiment (the ‘DE16’ protocol) was used (see section 1.2.4 for details). For the recordings in marrow, electrodes were evenly placed in two parallel rings of eight electrodes, 10 cm apart. A reference electrode was attached to the distant tip of the vegetable (figure 2.4). The ‘Marrow DE16’ protocol was used for these experiments.

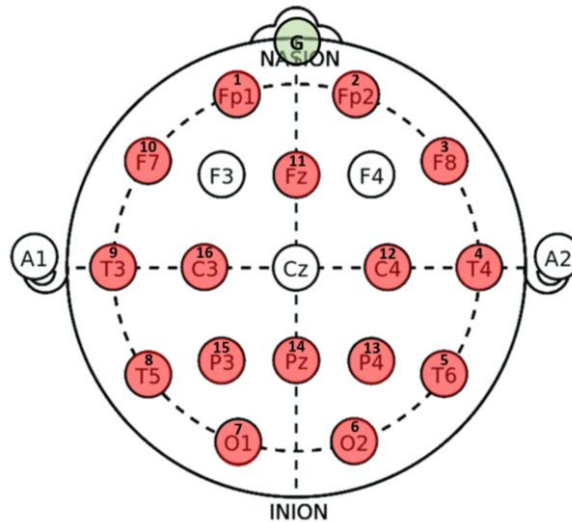


Figure 2-5: Electrode Montage Used in this Study, Based on the 10-20 Locations System. 16 injecting/ recording electrodes are marked in red (small number on top of the 10-20 mark represents electrode number for this study); the reference electrode is marked in green.

2.4.3 BV Processing

Differential voltage measurements methodologies ('COM' vs. 'ADJ') - The ScouseTom 2.5 system used in this study, takes differential measurements between each electrode and a common reference electrode (termed 'COM' measurements). In previous EIT studies [56,99,114], differential measurements were taken between two adjacent electrodes (termed 'ADJ' measurements). This was achieved here by subtracting two adjacent BV measurements. Since both methods have advantages and disadvantages, and might have different BV drift, both were used here for comparison in relation to drift.

Preliminary processing – A raw demodulated BV in μV was transformed to mV. Injecting combinations, where the injecting and recording electrode are the same, were excluded from the data due to exceptional high BV and drift.

Cleaning – Since the purpose of this study was to describe the nature of drift and noises over time, only data which exhibited a large artefact was removed. This was

done by removing data points where the difference from the previous data point was larger than 0.5 mV. These 'glitches' seemed to reflect poorly on the hardware quality rather than on the nature of this type of bio-signal, and while their presence could distort noise and drift figures, removing them left enough useful data. These artefacts were present predominantly in the first set of human recordings (where the hardware was not in its final version) but was still considered for below 0.4% of the data.

Quantifying noise/drift for the different bands – In this study, both terms '*Noise*' and '*Drift*' were used to describe signal changes not caused by a conductivity change in the brain. *Noise* was used to describe fluctuations around the baseline BV value, at different time bands. '*Drift*' however was used to describe changes diverging from the baseline BV, over time, and so essentially changing its average value over time.

For the comparison of electrode types, the type of noises existing in EIT data over hours had to be identified first. To find the main components in the signal, an FFT procedure was performed on the recorded time-series data. Dominant frequency bands were identified and then translated back into time bands. Inspection of the frequency domain suggested three main components should be further analysed: above 0.1 Hz – corresponding to '**fast changes**' in the signal occurring at up to 10 seconds time scale; 0.0015-0.015 Hz – corresponding to fluctuations in signal occurring within 1-10 minutes timescale ('**medium changes**'); and '**slow changes**' very close to DC corresponding to changes over more than one hour.

Dr James Avery from the UCL EIT laboratory designed a Butterworth filter for each of the three identified noise bands ('*fast*', '*medium*', and '*slow*'). Each of the data sets recorded for the purpose of electrode type comparison was filtered to leave only one band at a time (data were filtered twice, back and forth to filter the edges of the signal, and to avoid a phase shift in the filtered signal). Then, the standard deviation was taken to represent that noise band in a specific data channel, and the mean and standard deviation across all data channels of a specific dataset were calculated to represent that noise band in a specific dataset. This process was repeated for every dataset and every noise band.

In addition, linear fit over the whole timeframe (drift) was performed to determine whether the change in the signal over time could be characterised as linear. The R^2 parameter of the fit was used to estimate the linearity of the drift, and the slope was used to compute the linear drift of each data channel. The mean and standard deviation across all data channels of a specific dataset were then computed to represent

linear drift in a specific dataset. Since different recordings had different lengths, and drift is linear in nature, an **average hourly drift** was calculated for each dataset by dividing drift by the number of hours. This allowed comparison between different recordings. To track the change in drift with time, **hourly drift** was calculated as the linear fit over 60 minutes in a similar way to how it was calculated for the whole recording. This was calculated every 10 minutes, essentially with 50 minutes overlapping between consecutive measurements, enabling the change in drift with time to be tracked.

In summary, four main parameters were used to describe a dataset's noise and drift: '*average hourly drift*', '*slow changes noise*', '*medium changes noise*', and '*fast changes noise*'. 'Hourly drift' was used as an additional parameter to describe the stability of drift over time and its variability across channels.

'Best 90% quantification' – It was clearly visible in some datasets, that there were a few 'outliers' – channels with massive drift. The 10% of channels with the largest drift were removed before computing drift and noise parameters to enable effective comparison between the different recordings. In preliminary tests, the removal of 10% of the measurements impacted drift and noise significantly, while not impacting reconstruction quality. The term *best 90%* has been adopted to indicate where this has been done.

2.4.4 Additional Data Parameters

Estimated Contact Impedance (CI) – Contact impedance was computed at the beginning and end of each recording session for every electrode. It was estimated from the voltage measured on each injection electrode, at 2 KHz. In addition to CI checks before and after, an estimated CI was computed during the recording. For every injection cycle, Z was measured for every electrode by dividing measured voltage on the injecting electrode by the injected current. Estimated CI was taken as the mean Z value across different injections for the same electrode. The change in estimated Z was taken to be mainly due to change in CI. This was correlated with BV drift.

Phase Angle - In addition to BV which was recorded as the modulus, the Scouse-Tom 2.5 system recorded the phase angle of the signal in every injection – recording combination. The phase angle data were used to calculate the real (R) and imaginary (X) components. The real component was calculated as $R = BV * \cos(\text{Phase})$, and the imaginary component was calculated as $X = BV * \sin(\text{Phase})$. The two compo-

nents were analysed separately to investigate their percentages in the recorded BV drift.

Temperature – During the second phase of human data collection, recordings were made using human volunteers. A thermocouple (National Instruments, USB-TC01 with J-type tip) was taped to the headnet near the CZ position in order to record the temperature in the electrode area. The thermocouple was connected to a separate PC and had an accuracy of 0.1 Celsius and measured temperature every second. These data were used to investigate whether temperature changes near the electrodes correlated with BV drift.

2.4.5 Electrodes Movement Elimination (EME) by Reconstructing Changes in BV which are directly related to Electrode Movement

One possible explanation for the drift might have been slow tiny movements of the electrodes on the scalp over time. This possible mechanism was plausible since the electrodes were attached to the scalp with gel and a 1 mm movement in electrode location could result in an image artefact [91,89].

An algorithm for correcting electrode modelling errors in EIT was used to investigate this possibility [91]. The main purpose of using this algorithm was to calculate the recorded BV changes caused directly by electrode movement. This was achieved by computing the Jacobian matrix predicting voltage changes due to electrode boundary changes, originally shown by Dardé et al [45]. This Electrode Boundary Jacobian (EBJ) is used in TD-EIT reconstruction jointly with the traditional Jacobian matrix (J) and allows corrections for BV changes caused by changes in electrode location and shape. By using this technique, the BV changes caused by electrode movement could be computed by multiplying the reconstructed electrode movement with the EBJ, and then be deducted from the recorded signal. If this corrected signal was closer to a flat (less drifty) baseline, then the drift was proven to be originating from the electrode movements and could have been eliminated without eliminating BV changes caused by impedance changes inside the body.

2.5 Method

2.5.1 Electrode Types

Three electrode types were used in this study:

1. 9 mm radius conventional EEG silver-silver chloride **cup electrodes** (Ambu® Neuroline cup, Denmark, www.ambu.com) were applied with conductive EEG paste (Elefix, Nihon Kohden, Japan). These were applied by hand in pre-measured locations, secured with medical tape on top of each electrode, and a bandage wrapped over the whole head to hold it together throughout the recording and to secure optimal contact. Leads were approximately 1 meter in length.

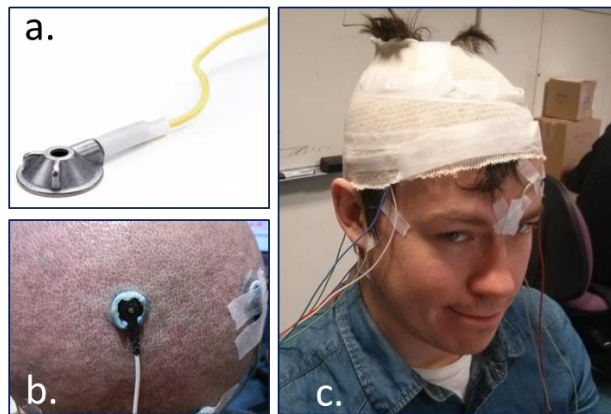


Figure 2-6: EEG Cup and Paste Electrodes. a) Single electrode (www.ambu.com) b) Single electrode as used in this study, on a bald head c) Set-up in this study.

2. Easy application silver-silver chloride electrodes cap (**EZ**) were applied using an elasticated nylon cap with holes and well-shaped adaptors. Ring shape electrodes, 12mm in radius (EasyCap®, Germany, www.easycap.de) were clipped onto the adaptors after skin abrasion, and conductive paste was injected through the holes, creating contact between the scalp and the electrode. The identical conductive paste to the previous electrode type was used with leads approximately 1 meter long. These electrodes were used in both human and marrow experiments.

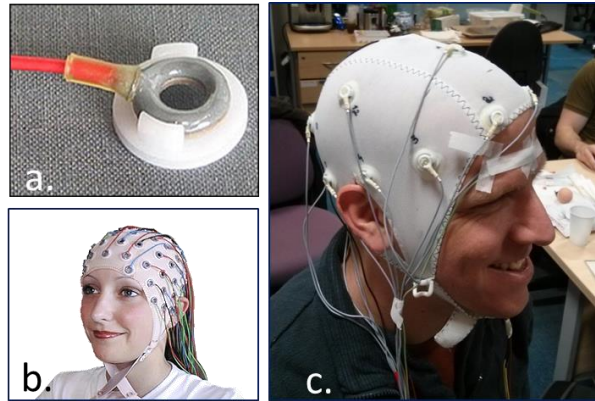


Figure 2-7: Easy to Apply Electrodes. a) Single electrode (www.easycap.de) b) Typical set-up (www.easycap.de) c) Set-up in this study.

3. Fast applying hydro-gel electrodes (**HD**) were applied using an elastic head-net with holes in pre-determined locations (EzeNet® headpiece, Hydro Dot Inc., USA). Cylindrical hydrogel electrodes of 9 mm in radius (HydroDot® biosensors) were inserted into the hole after skin abrasion, creating electrical contact with the scalp. Leads were approximately 1 meter long.



Figure 2-8: Hydro-Gel Electrodes. a) Hydro-gel bio-sensors (<http://hydrodot.wix.com>) b) Typical set-up (<http://hydrodot.wix.com>) c) Set-up in this study.

2.5.2 Data Collection

Recordings on a Resistor Phantom

A 32-channel resistor phantom was used to replicate the anticipated loads during EIT head measurements. The trans-impedances were approximately 100Ω and each channel had a contact resistance of $1 \text{ k}\Omega$. A hundred and sixty resistors were arranged in a two interconnected ring topology using 0.1% tolerance resistors (see

figure 2.2). Recording used sixteen channels of the phantom, applying the 'DE16' protocol, at 2 KHz and 100 μ A, for seven hours continuously.

Recordings on a Head-shaped Tank

Dr James Avery from the UCL-EIT group designed and manufactured the head-shaped tank for EIT measurements [16]. He used CT and MRI scans to produce the design for a realistic human head. He then printed this in 3D from non-conductive plastic. Thirty-two silver-silver chloride electrodes were moulded into the plastic in 10-20 EEG locations (figure 2.3). Electrode locations were identical to the sixteen locations used in human recordings. The tank was filled with 0.2 % saline with a conductivity of 0.4 S/m. There was no skull model inside it. Recordings were made for seven hours continuously using the 'DE16' protocol, at 2 KHz and 250 μ A.

Marrow Recordings

Marrows (the British term for a giant zucchini or the botanical name: *Cucurbita pepo* var. *Fastigata*,) used were typically 10-12 cm in diameter and ~40 cm in length. EZ electrodes and Elefix paste were used for recordings. The marrow skin was abraded manually, by gently swabbing it with abrasive gel commonly used in EEG labs (NuPrep, Weaver and company, USA, <https://www.weaverandcompany.com/>).

Baseline recording was made using the 'Marrow DE16' protocol, at 1.5 KHz and 140 μ A, for eight hours continuously.

Multi-frequency recording was made using the 'Marrow DE16', at 140 μ A and at 200, 1000, and 1500 Hz for six hours continuously.

Dry vs. wet electrodes recording was made using the 'Marrow DE16', at 1.5 KHz and 140 μ A, for seven hours continuously.

System on-off recording was made using the 'Marrow DE16', at 1.5 KHz and 140 μ A, for six hours continuously.

Healthy Human Recordings

Electrode locations were marked on the subject's scalp using the EasyCap® electrodes cap. Each location was uniformly abraded with NuPrep gel, prior to the electrodes being affixed to the scalp, using an abrading servo applicator [15] in order to decrease CI variability [23].

Data for Electrode Choice

Two healthy subjects consented to participate in this part of the study. Both were males, aged 27 (subject 1) and 35 (subject 2) respectively. Recordings were made

using the 'Spiral16' protocol, at 2 KHz and 250 μ A, for three and a half hours continuously while the subjects were sedentary and doing everyday work. For each of the three electrode types (Cup, EZ, HD) measurements were taken twice from subject 2, first with short hair, and then again after he had completely shaved his head, and once from subject 1 with short hair only. In total nine datasets were recorded for this section.

Data for Drift Analysis

Six healthy subjects aged between 23 and 31 consented to participate in this study. Three subjects were male with short or very short hair. Three were female with long straight hair. Recordings were made using the 'DE16' protocol and 'EZ' electrodes, at 2 KHz and 250 μ A, for six hours continuously while subjects were sitting and doing everyday work. A single break of ten minutes duration was taken when needed. The temperature was recorded near the CZ electrode area in addition to the BV recordings. Six datasets were recorded.

2.5.3 Data Processing and Statistical Analysis

Electrode Types Noise and Drift Comparison

Noise and drift were calculated for each of the nine datasets recorded over three and a half hours, and then compared. Noise was calculated for each of the three noise bands (*'fast'*, *'medium'*, and *'slow'*) in addition to the average hourly drift. The difference between estimated CI at the beginning of the recording and at the end of the recording was calculated for every dataset to quantify and compare electrode performance.

Noise and Drift Characteristics on Resistor Phantom and the Head-shaped Tank

For each of the recordings, noise in three bands (*'fast'*, *'medium'*, and *'slow'*), hourly drift and average hourly drift were calculated.

BV Noise and Drift Characteristics on Marrow

For the baseline recording, noise in three bands (*'fast'*, *'medium'*, and *'slow'*), hourly drift and average hourly drift were calculated. With the multi-frequency recording, hourly drift and average hourly drift were calculated for each of the three frequencies. In addition, hourly drift and average hourly drift were computed separately for the Real (R) and Imaginary (X) data components.

For the dry vs. wet electrodes recording, average hourly drift was calculated and compared in two separate ways: 1) Data were divided into two groups according to the recording electrode: wet recording electrode channels (N=214) and dry recording electrode channels (N=214). 2) Data were divided again into two groups according to the injecting electrodes: two wet electrodes (N= 101), and two dry electrodes (N=101). After testing the data for normal distribution, a *t-test* for independent samples was used to test statistical significance between the average hourly drift of the two groups separately. In addition, CI at the beginning of the recording and the change in contact impedance were compared between wet electrodes (N=8) and dry electrodes (N=8) using an independent samples *t-test*. For the On-Off recording, average hourly drift was calculated and compared with continuous recording at 1.5 KHz taken from the multi-frequency recording. After testing the data for normal distribution, a *t-test* for independent samples was used to test statistical significance between the average hourly drift of the two recordings (N=476).

Noise and Drift Characteristics in Humans

For each of the six datasets recorded over six hours, noise in three bands ('fast', 'medium', and 'slow'), hourly drift and average hourly drift were calculated. These were calculated using 'best 90%' of the data, initially for the data in its original 'COM' configuration, and then again for the same data in 'ADJ' configuration for comparison. The rest of the analysis was performed using only 'COM' configuration measurements.

Correlation between baseline BV (average voltage over the first five minutes of recording) and average hourly drift was calculated using Pearson's linear correlation coefficient (N= 428 channels per dataset).

The BV drift per measuring electrode was calculated to estimate the correlation between drift and electrode location. BV average hourly drifts measured (29-30 recordings per electrode) were grouped and averaged per electrode. This was completed for each of the 16 recording electrodes in each of the six recordings. Electrodes were segmented into four location groupings: front (electrodes 1,2,11), back (electrodes 6,7,14), right (electrodes 3,4,5), and left (electrodes 8,9,10). Two-way Analysis of Variance with repeated measures was then performed to assess significant difference ($\alpha = 0.05$) in BV drift variance of electrode locations (Front, Back, Right, Left) and between subjects. Where statistical difference was found ($p < \alpha$), a multiple t-test was performed to assess any significant difference between sub-groups.

The correlation between BV drift of electrodes and change in CI of electrodes was estimated using Pearson's linear correlation (N= 96, 6 subjects x 16 electrodes). Average hourly drift was grouped according to injecting electrode (56-76 recordings per electrode, as each measurement was attributed twice, to two injecting electrodes) and then averaged per electrode. The correlation between electrodes' BV drift and temperature change in their approximate area (electrodes 11,12,14,16), was similarly computed (N= 24, 6 subjects x 4 electrodes).

Results were expressed as Mean \pm 1 Standard Deviation

2.5.4 Drift Elimination Trial

Electrode Movement Elimination (EME) by reconstructing BV Changes related to Electrode Movement

In each of the six human recordings used in this chapter for quantifying the drift, recording over 6 hours included 1-2 bio-breaks of around ten minutes. Since these breaks were reflected in the data as ten minutes of no signal, it could have been reflected in this algorithm output. Hence, the three longest segments recorded without a break were chosen for this procedure. Segments of 3.6, 3.8, and 4.6 hours were taken from subject number 1, 3, and 5, respectively. The following algorithm steps were applied to each of these data segments:

1. Jacobian matrix (J) and electrodes Jacobian (EBJ) were computed from ΔBV data, using 2M elements Finite Element Model.
2. Conductivity changes ($\Delta\sigma$) and electrode movements (dx, dy) were reconstructed simultaneously using Tikhonov 0th order regularization algorithm.
3. BV change (drift) caused by electrode movements (ΔBV_{EB}) were computed by (dx, dy) x EBJ.
4. ΔBV_{EB} were deduced from recorded ΔBV to receive recorded BV without electrode movement related drift (ΔBV_{EME}).
5. ΔBV_{EME} was compared with ΔBV to identify the portion of drift that could be explained by electrode movement.

2.6 Results

2.6.1 BV Noise and Drift Comparison Between Electrode Types

Recorded boundary voltage amplitudes ranged between 0-10 mV (figure 2.9) For all nine datasets, more than 97% of the combinations had a significant correlation with the linear model (p value < 0.05). Average hourly drift was highest with HD electrodes and lowest with EZ electrodes. *Slow change noise* was between 10-25% and was lowest for the EZ electrodes in contrast with EEG and HD electrodes. *Medium* change noise was between 1-6% and was highest for the EEG electrodes and was similar for both the EZ and HD electrodes. *Fast change noise* was around 0.5-2.5% and was lowest for the HD electrodes in comparison with EZ and EEG electrodes. Table 2.1 below summarises average hourly drift and noise results.

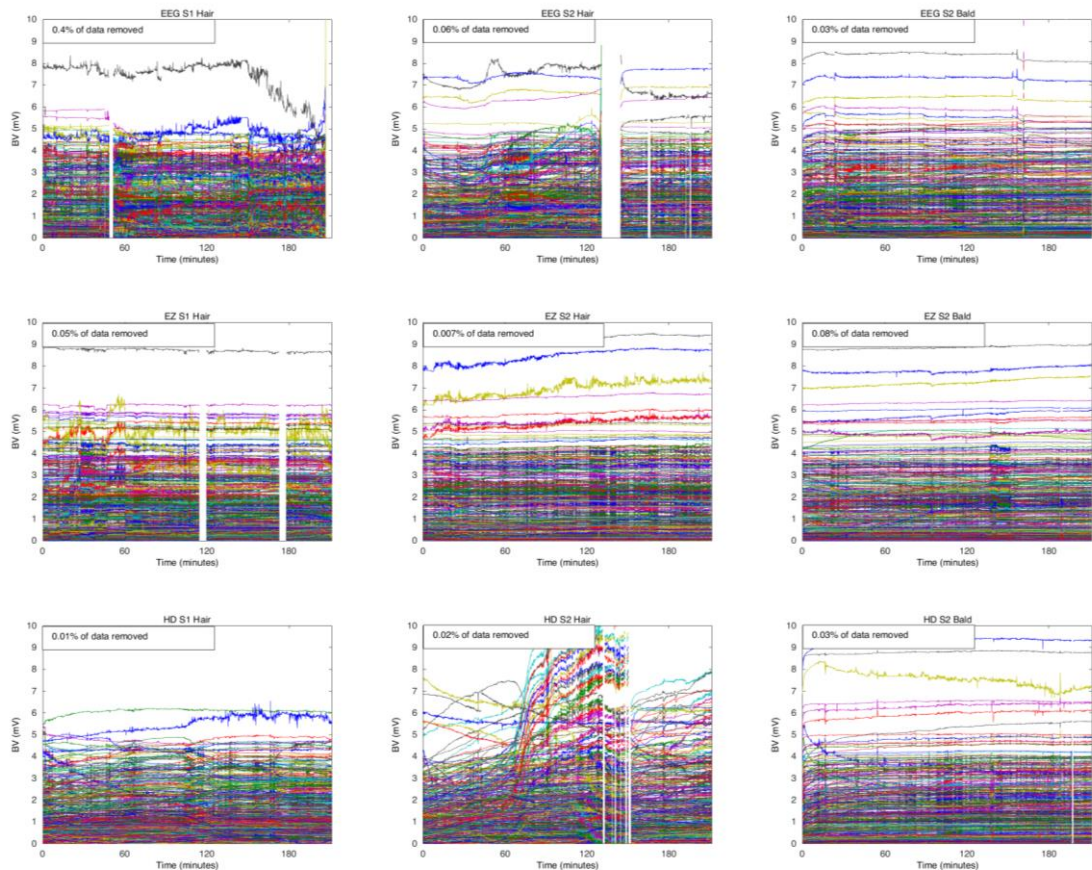


Figure 2-9: Raw BV (voltage- Y axis, over time- X axis). The proportion of data points removed in the data cleaning process are stated at the top left corner of each dataset.

	EEG			EZ			HD		
	S1	S2	S2b	S1	S2	S2b	S1	S2	S2b
Average Hourly Drift (%) - Mean \pm 1SD	30 \pm 95	32 \pm 89	18 \pm 110	21 \pm 110	8 \pm 23	20 \pm 100	27 \pm 73	52 \pm 174	19 \pm 68
Slow Changes (%) - Mean \pm 1SD	26 \pm 24	25 \pm 26	14 \pm 25	13 \pm 20	8 \pm 14	10 \pm 17	22 \pm 22	28 \pm 24	12 \pm 18
Medium Changes (%) - Mean \pm 1SD	6 \pm 7	3.6 \pm 4.2	6 \pm 33	3.1 \pm 5	1.6 \pm 3.6	2.4 \pm 11	1.5 \pm 2.4	3.2 \pm 3.3	1.7 \pm 3.4
Fast Changes (%) - Mean \pm 1SD	2.5 \pm 5	1.1 \pm 2.2	1.6 \pm 8	1.1 \pm 2.7	0.7 \pm 1.8	2.5 \pm 19	0.6 \pm 0.8	0.7 \pm 0.7	0.8 \pm 2.8

Table 2-1: Average Hourly Drift and Noise Results. Results are calculated for all electrode types for subject 1 (S1), subject 2 (S2), and subject 2 bald (S2b). All above units are percentage change from baseline (Mean \pm 1SD).

The mean of the absolute CI change for the EEG electrodes type was 533 ± 402 ohms for subject 1 (S1), 266 ± 210 for subject 2 (S2), and 91 ± 104 for subject 2 bald (S2 bald). For the EZ electrode type, CI change was 49 ± 45 , 84 ± 61 , and 45 ± 27 for S1, S2, and S2 bald respectively. For the HD electrode type it was 240 ± 210 , 376 ± 156 , and 274 ± 205 respectively. For detailed CI change per electrode see figure 2.10.

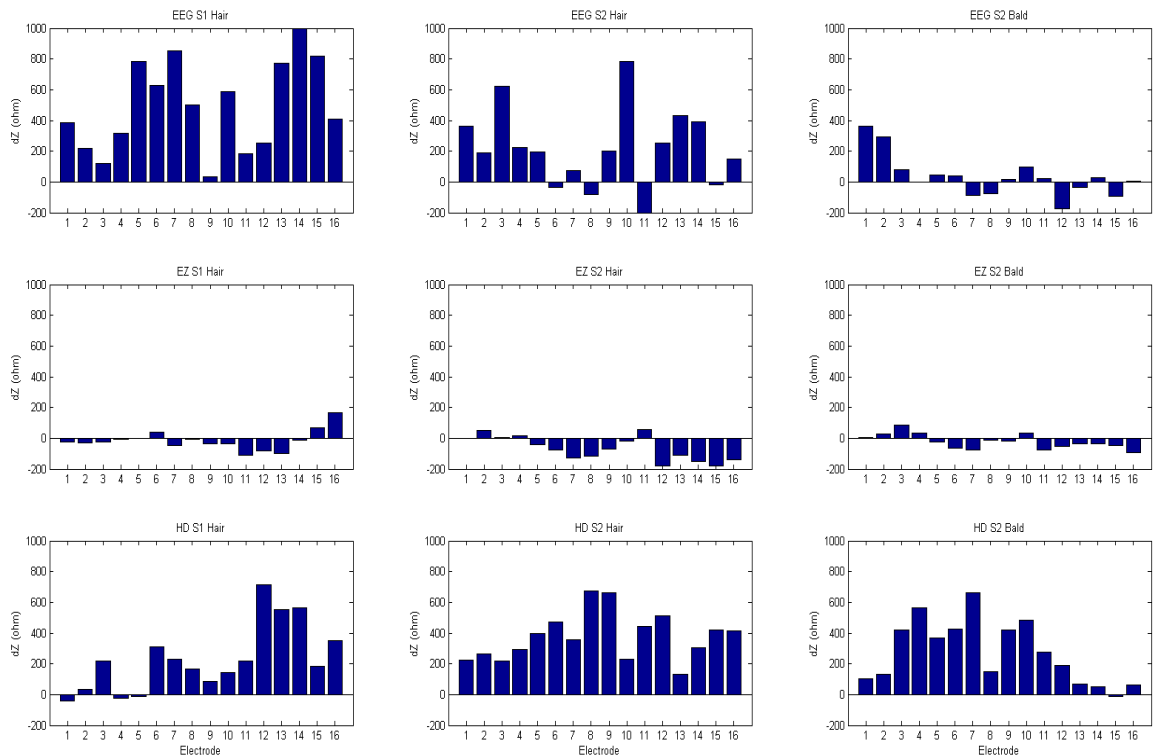


Figure 2-10: Contact Impedance Change. Each insert presents difference in contact impedance over 3.5 hours (ohms) of one dataset.

2.6.2 BV Noise and Drift Characteristics in Resistor Phantom

BV recorded on a resistor phantom had a baseline amplitude of 4.49 ± 4.99 mV. Average hourly drift was 0.06 ± 0.03 %/hour. Slow change noise was 0.2 ± 0.4 %, medium change noise was 0.3 ± 1.0 %, and fast change noise was 0.5 ± 1.8 %. CI change during the recording was 0.3 ± 0.02 %.

2.6.3 BV Noise and Drift Characteristics in Head-shaped Tank

BV recorded on a head-shaped tank had a baseline amplitude of 3.1 ± 2.5 mV. Average hourly drift was 0.2 ± 0.16 %/hour. Slow change noise was 0.47 ± 0.42 %, medium change noise was 0.17 ± 0.55 %, and fast change noise was 0.25 ± 1.0 %. CI change during the recording was 1.5 ± 1.2 %. These results are shown in detail comparing a human subject and a marrow in figure 2.11.

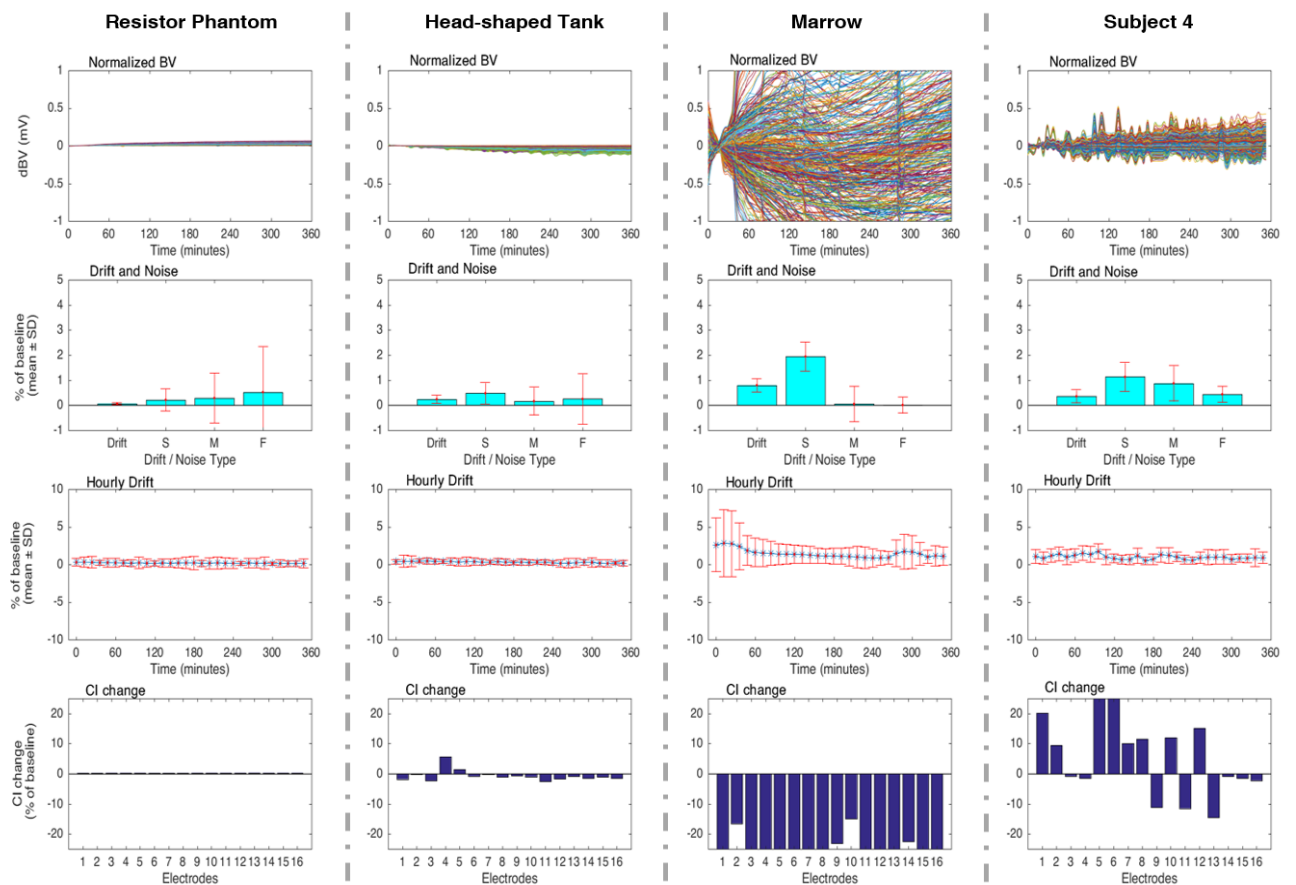


Figure 2-11: Recordings on Resistor Phantom and Head-shaped Tank. In this figure, results summary of measurements made on a resistor phantom and a head-shaped tank are presented alongside the same measurements made using a marrow and a human subject. From the upper row to the lower row: normalized BV over six hours, average hourly drift and three noise types (slow, medium, fast), hourly drift computed every 10 minutes, and CI change per electrode.

2.6.4 BV Noise and Drift Characteristics in Marrow

BV recorded on a marrow had a baseline amplitude of 25.4 ± 20.3 mV. Average hourly drift was 0.8 ± 0.72 %/hour. Slow change noise was $1.94 \pm 1.43\%$, medium change noise was $0.05 \pm 0.07\%$, and fast change noise was $0.01 \pm 0.01\%$ (see figure 2.11). CI change during the recording was $27.8 \pm 6.0\%$. When recording on marrow at three different frequencies, the modulus average hourly drift at 200 Hz was 0.716 ± 0.70 %/hour, 0.768 ± 0.72 %/hour at 1000 Hz, and 0.88 ± 0.88 %/hour at 1500 Hz. When the real and imaginary components were separated, the real component drift was very similar to the modulus (0.718 ± 0.70 , 0.773 ± 0.74 , and 0.88 ± 0.88 at 200 Hz, 1000 Hz, and 1500 Hz respectively). The drift of the imaginary component, however, presented a different trend and values (4.1 ± 3.5 , 4.11 ± 3.35 , and 3.97 ± 3.25 at 200 Hz, 1000 Hz, and 1500 Hz respectively, figure 2.12)

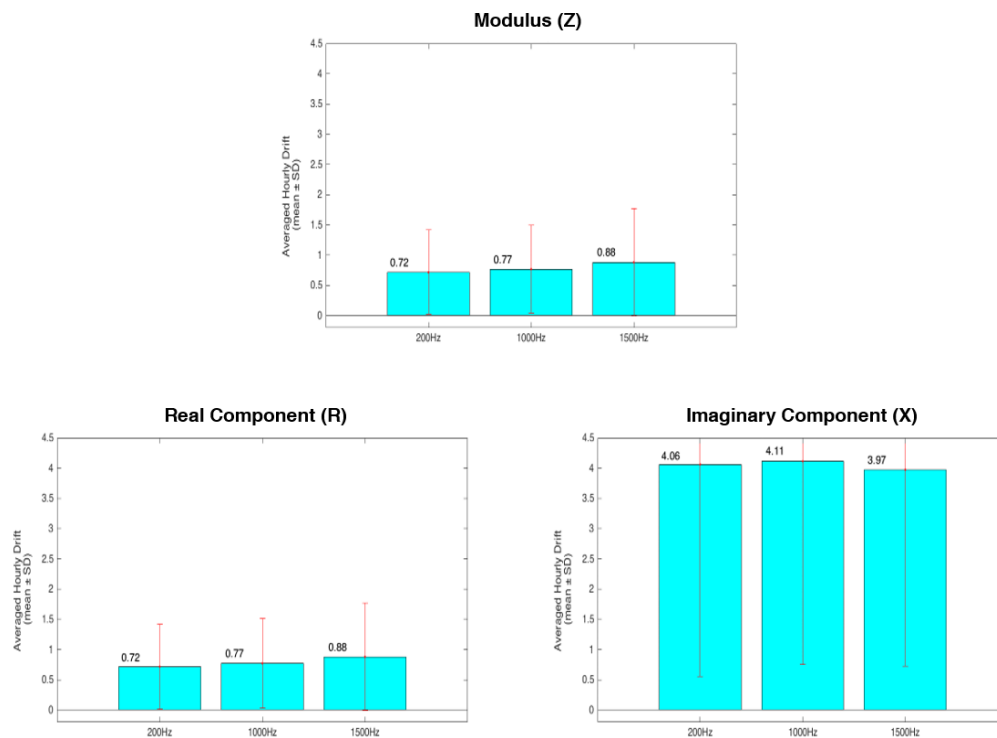


Figure 2-12: Drift over Frequencies. Average hourly drift recorded on a marrow at 200Hz, 1000Hz, and 1500Hz. Upper inset: the modulus impedance (Z), lower left: real component (R), and lower right: Imaginary component (X).

On a marrow, in wet channels, where both injecting electrodes had gel, baseline BV amplitude was 27.4 ± 19.9 mV. With these, average hourly drift was $1.39 \pm 1.16\%$. In dry channels, where both injecting electrodes had no gel on them, baseline BV amplitude 26.4 ± 19.1 mV. With these, average hourly drift was $1 \pm 0.7\%$. T-test showed a

significant difference between 'dry' and 'wet' channels average hourly drift ($p = 0.0073$).

When separating wet recording channels from dry recording channels according to the recording electrode, results changed. Baseline BV amplitude of wet channels was 26.6 ± 19.2 mV with average hourly drift of 1.24 ± 1.34 %. Baseline BV amplitude of dry channels was 26.6 ± 19.5 mV with average hourly drift of 1.14 ± 0.99 %. T-test showed no significant difference between 'dry' and 'wet' channels' average hourly drift ($p > 0.05$).

Looking at the CI of dry and wet electrodes, baseline CI of wet electrodes was $1,260 \pm 185$ Ohms in comparison with $2,372 \pm 393$ Ohms of dry electrodes. Over seven hours of recording, CI change of wet electrodes was 23.9 ± 30.0 % while CI change of dry electrodes was 113.9 ± 70.0 %. T-test showed significant difference ($p = 0.0139$), see figure 2.14.

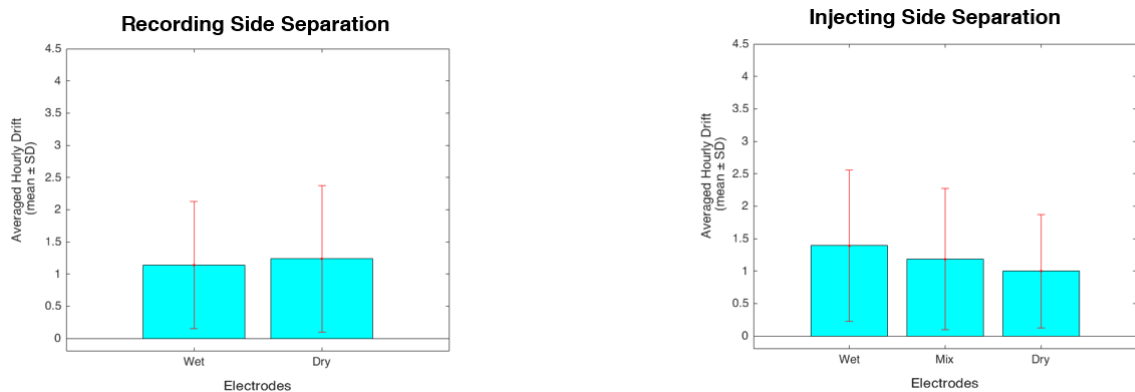


Figure 2-13: Drift in Wet vs. Dry Electrodes. Average hourly drift recorded on a marrow simultaneously with wet and dry electrodes. Left: channels wet-dry separation according to recording electrode. Right: wet-mix-dry separation according to injecting electrodes.

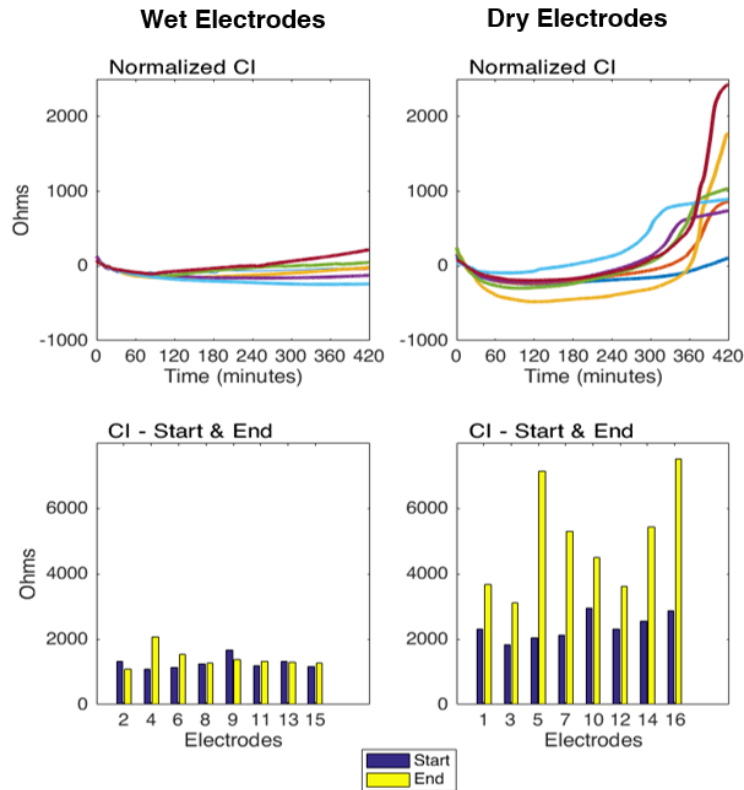


Figure 2-14: CI in Wet vs. Dry Electrodes. The upper row describes change in estimated CI over time per electrode (each line represents the estimated CI change in one electrode). The lower row describes CI at the beginning and at the end of the recording for each electrode.

When the system was recording intermittently on a marrow - 45 minutes off then 15 minutes on over six hours, BV baseline amplitude was 25.8 ± 18.15 mV. Average hourly drift was 0.82 ± 0.47 %/hour. Slow change noise was 2.17 ± 1.26 %, medium change noise was 0.17 ± 0.18 %, and fast change noise was 0.03 ± 0.03 %. Comparing average hourly drift with continuous recording on a marrow using a T-test, showed a significant difference ($N= 428$, $p < 0.01$), see figure 2.15. Looking at the CI of intermittent and continuous setting, baseline CI in On-Off setting was $2,042 \pm 424$ Ohms compared to $2,399 \pm 270$ Ohms in continuous setting. Over a six-hour recording, CI change in On-Off setting was 30.9 ± 8.0 % while CI change in continuous setting was 27.8 ± 6.0 %. T-test showed significant difference ($N= 16$, $p < 0.01$), see figure 2.16.

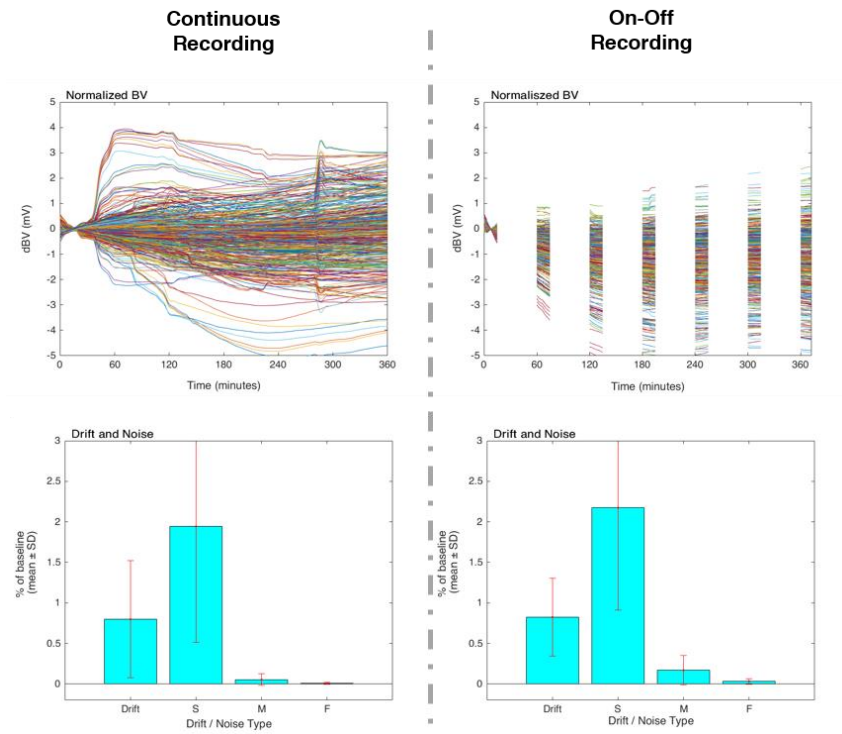


Figure 2-15: BV Drift and Noise in On-Off vs. Continuous Recordings. Upper row present change in BV over time (left – continuous recording, right – on-off recording). Lower row present average hourly drift and the three noise types of the two recording approaches.

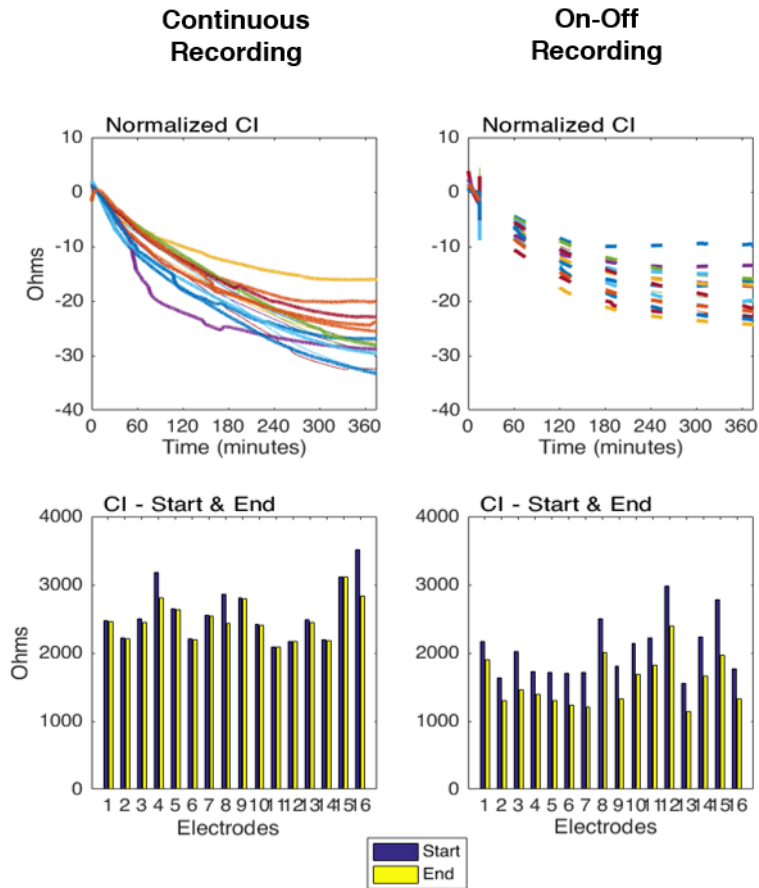


Figure 2-16: CI in On-Off vs. Continuous Recordings. The upper row describes change in estimated CI over time per electrode (each line describes the estimated CI change in one electrode). The lower row describes CI at the beginning and at the end of the recording for each electrode.

2.6.5 BV Noise and Drift Characteristics in Humans

The baseline amplitude of recorded BV was 5.4 ± 4.6 mV for the COM measurements, taking all 476 combinations in each of the six recordings into consideration. For the 90% of the combinations with the lowest percentage drift, average hourly drift was 0.41 ± 0.3 %/hour. Slow change noise was 1.3 ± 0.63 %, medium change noise was 0.75 ± 0.63 %, and fast change noise was 0.43 ± 0.62 % (figure 2-18).

The baseline amplitude of the recorded BV was 2.6 ± 1.7 mV for ADJ measurements, taking into consideration all 408 combinations in each of the six recordings. For the 90% of the combinations with the lowest percentage drift, average hourly drift was 0.5 ± 0.51 %/hour. Slow change noise was 1.7 ± 3.05 %, medium change noise was 0.75 ± 1.95 %, and fast change noise was 0.43 ± 1.53 % (figure 2-19).

The correlation between baseline amplitude and average hourly drift was found to be low in four out of six datasets ($p < 0.05$, $\rho = -0.18, 0.21, -0.3, -0.4$) and no correla-

tion was found in the remaining two datasets ($p > 0.05$, $\rho = 0.0007$, 0.01) ($N = 428$ per dataset). For further detail see figure 2.17.

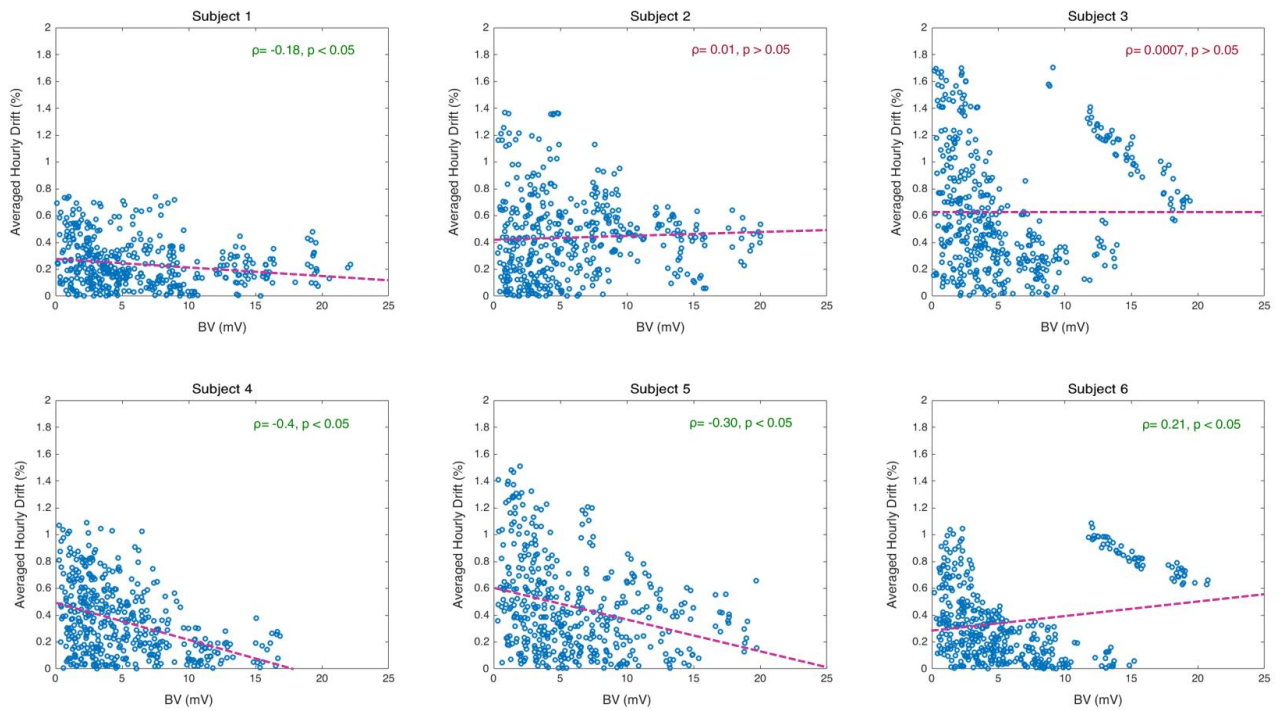


Figure 2-17: Baseline BV vs. Average Hourly Drift. In this figure, each data point represents a recorded channel in a specific subject ($N = 428$). The X axis is the mean BV averaged over the first 5 minutes, while Y axis represents average hourly drift. Correlation coefficient ρ between BV drift and CI change of an electrodes is presented on the top right corner of each dataset, alongside its p value. The linear trend per subject is presented in magenta.



Figure 2-18: Common Reference Measurements (Best 90% Combinations). Each column represents one of the six subjects. The upper row presents the change in recorded raw BV over time in milliVolts. The middle row summarises the average hourly drift and the noise (slow changes, middle band changes and high frequency noise) over the complete length of the recording, in percentage from baseline BV. Red error bars are $\pm 1SD$. The lower row describes hourly drift - change in linear drift over time, by calculating drift over the next 60 minutes. This is done repeatedly every 10 min. Blue asterisks represent the mean across combinations, red errors bars $\pm 1SD$.

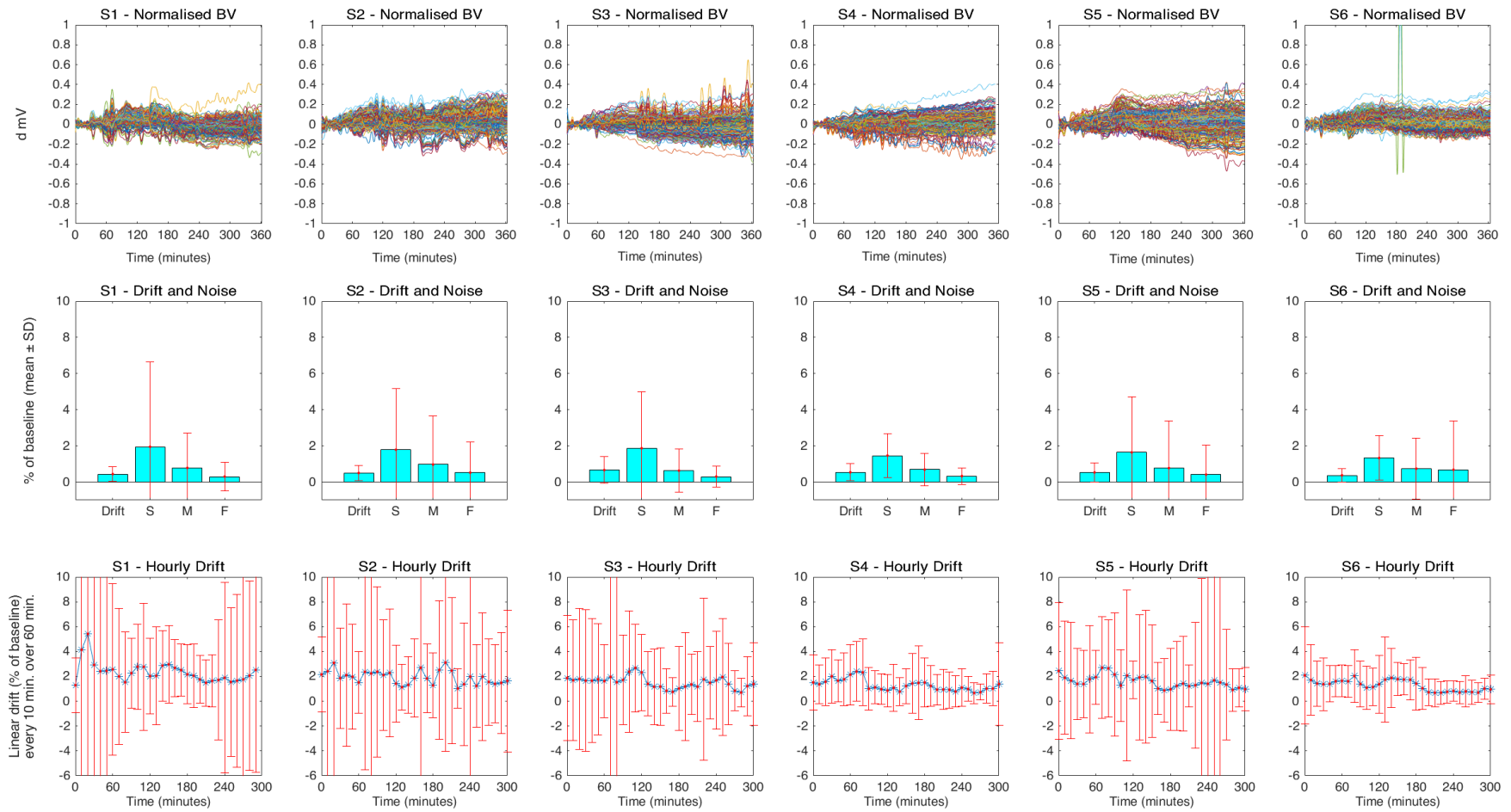


Figure 2-19: Adjacent Electrode Measurements (Best 90% of Combinations). As Figure 2-18.

Two-way analysis of variance showed a significant effect for average hourly drift in different electrode locations (F value = 2.2, $p = 5.5e-10$). Multiple t-tests showed that frontal average hourly drift was significantly higher than in the rest of the scalp (frontal-left $p = 0.0081$, frontal-right $p = 1.03e-4$, frontal-back $p = 8.6e-5$). No significant difference was found between the left and right sides of the head ($p = 0.55$). Average hourly drift was lowest in the posterior electrodes although not significantly different from the side electrodes (back-left $p = 0.52$, back-right $p = 1$), see figure 2.20.

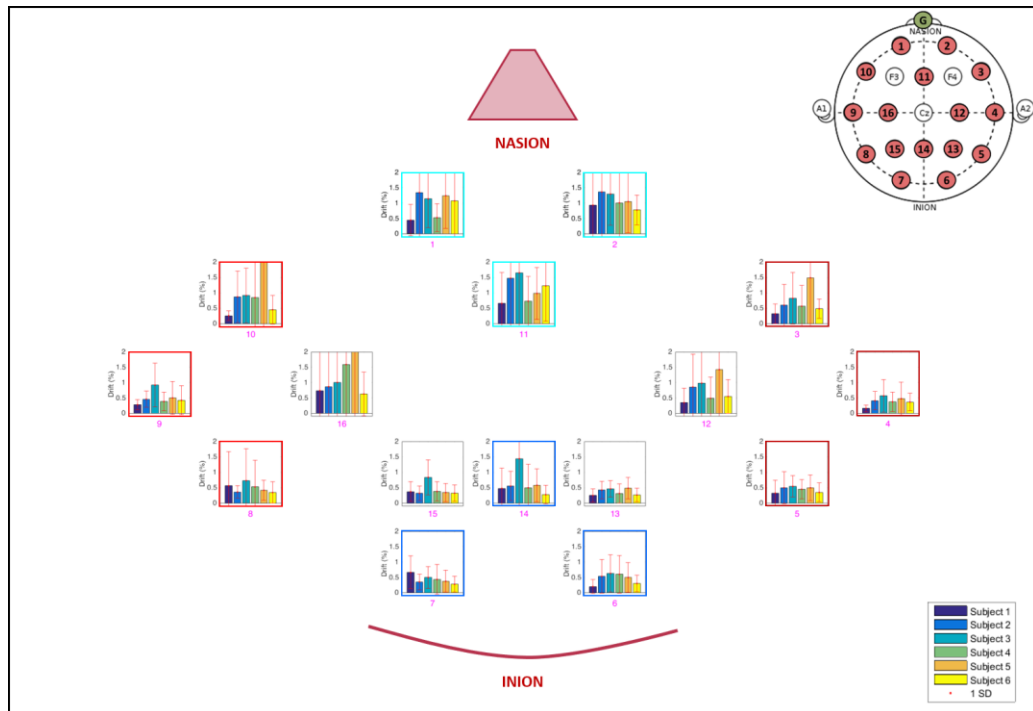


Figure 2-20: Spatial Distribution of the Drift on Human Scalp. Each location of the 16 in the above figure represents an electrode location on the subject's head relative to the Nasion and Inion fiducial points. Each location corresponds to the electrode in the 10-20 system. Within each location graph, each bar represents one subject's average hourly drift (in mV) for a specific electrode. Electrodes considered for ANOVA were divided to four groups: 'Front' electrodes (1,2,11) are marked in turquoise, 'Back' electrodes (6,7,14) in blue, 'Right' electrodes (3,4,5) in dark red, and 'Left' electrodes (8,9,10) in light red.

Taking into consideration all sixteen electrodes in the six healthy subjects ($N=96$), CI at the beginning of the recording was 785 ± 285 Ohms over all the recordings. CI change over time presented a linear trend and was confirmed with significant linear regression fittings (p value < 0.05) in more than 95% of the measurements. CI change was 1.9 ± 2.2 %/hour.

Correlation between CI change and average hourly drift was moderate to high in five out of six datasets and no correlation was found in the remaining dataset ($N = 16$ per dataset, see figure 2.21).

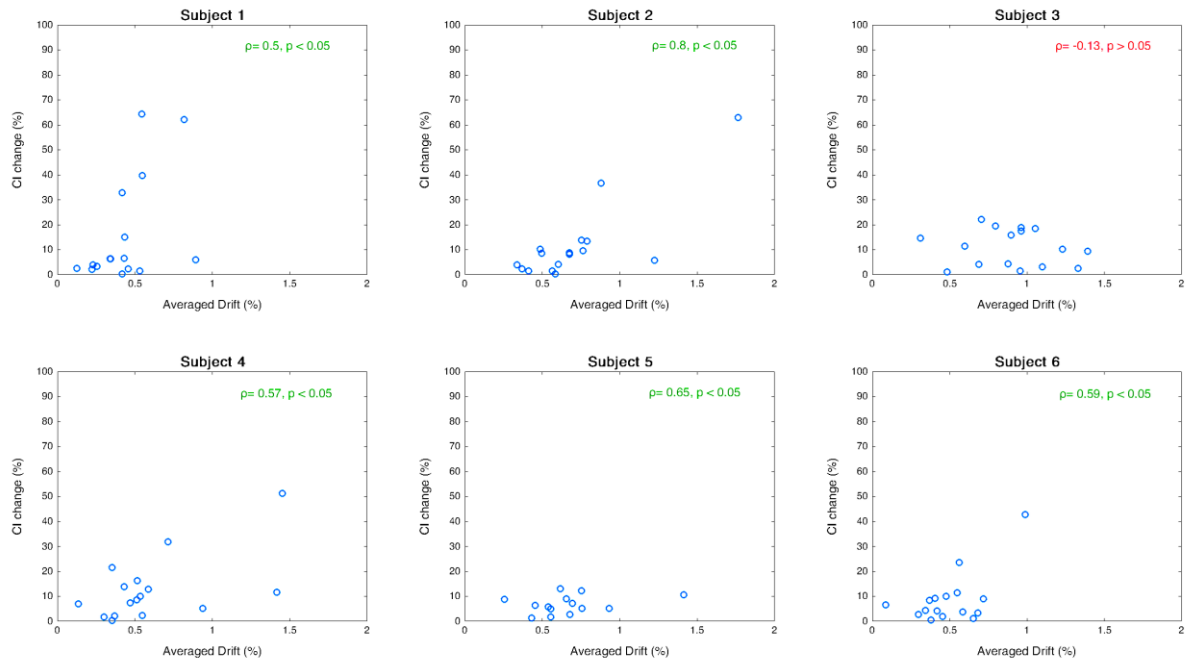


Figure 2-21: CI change vs. Average Hourly Drift. Each data point represents an electrode in a specific subject (N= 16). The X axis is the electrode's average hourly drift, while Y axis represents the electrode's CI change. Correlation coefficient ρ between BV drift and CI change of an electrode is presented on the top right corner of each dataset, alongside its p value.

In all six human subjects, baseline temperatures were between 26°C and 30°C and changed with a linear trend of 1°-5°C (see figure 2.22) which is between -10% and +19% of the baseline over six hours. The temperature decreased with time in three subjects but increased in the other three. No correlation was found between temperature change and drift in the surrounding electrodes (11,12,14, and 16).

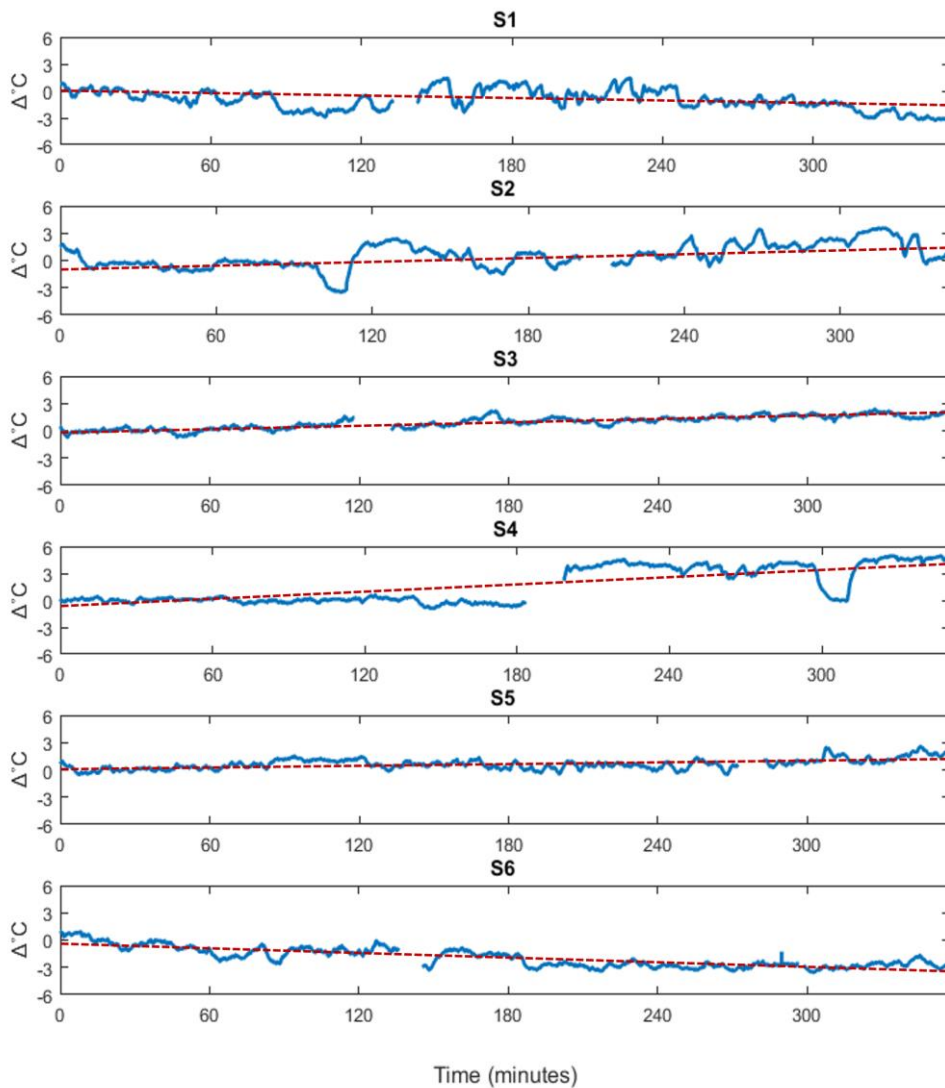


Figure 2-22: Temperature Change Near CZ Over the Course of six Hours EIT Recording. Each segment presents the temperature change in one subject (1-6), in Celsius. Linear trend is marked in red.

Comparing drift and noise before an EME procedure with drift and noise after an EME procedure, revealed that there is still a significant portion of drift and noise left in the signal. Moreover, results were inconsistent over the three datasets under investigation. With subject 5 data, average hourly drift measured was $3.03 \pm 2.15\%$ before EME, and decreased to $2.26 \pm 1.79\%$ after EME. With subject 3 data, average hourly drift was $1.15 \pm 0.79\%$ before, decreasing to $0.58 \pm 0.43\%$ after. With subject 1 data, as opposed to the first two, average hourly drift was $0.6 \pm 4.2\%$ before EME, but increased to $1.58 \pm 1.36\%$ after EME. Slow and Medium scale noise changes also presented mixed trends, similar to drift while high frequency noise grew stronger after the EME procedure in all three subjects (Figure 2.23).

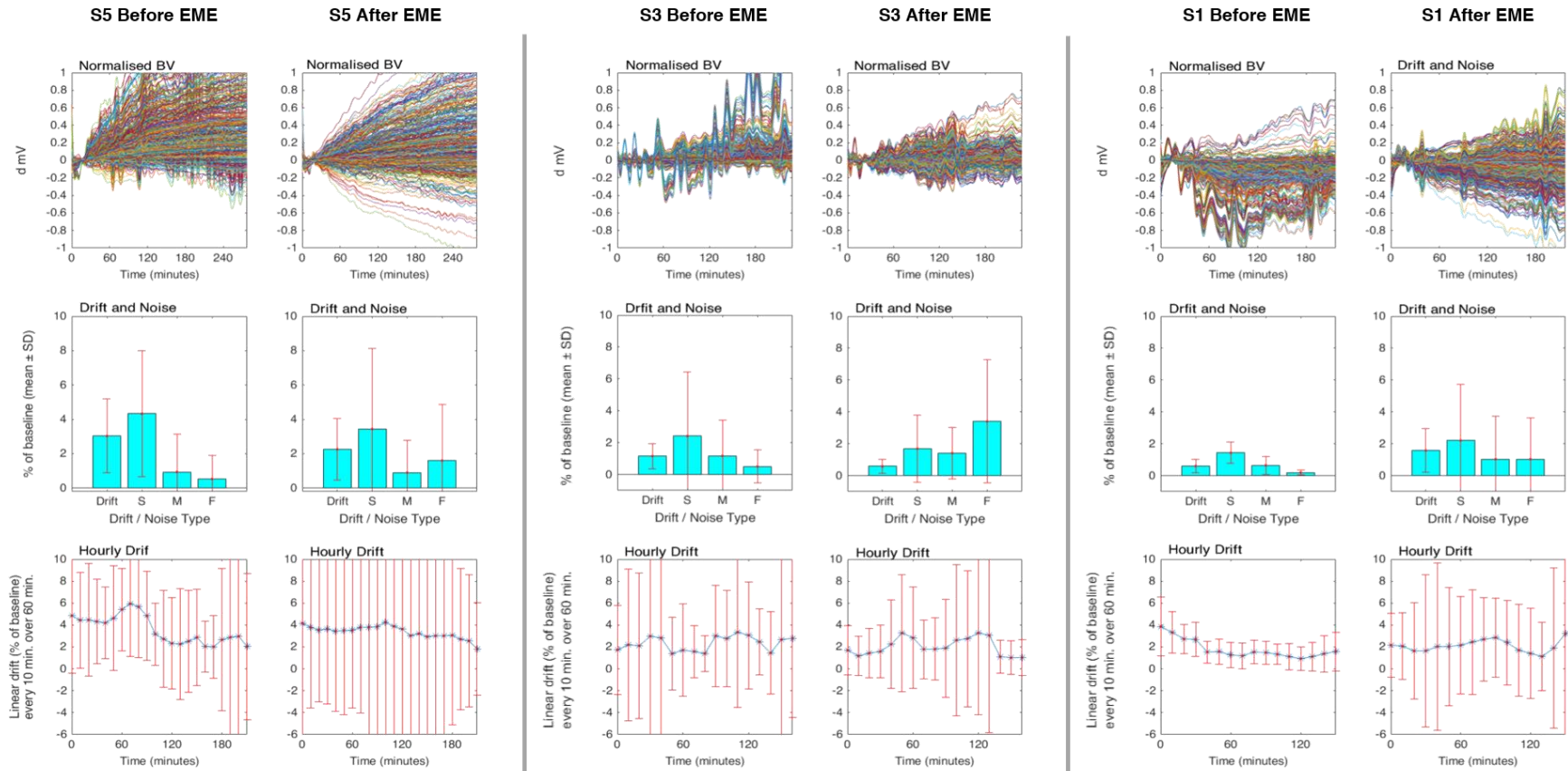


Figure 2-23: Drift and Noise Before and After EME Procedure. Each column contains three plots as in previous figures: Raw drift in time (upper), averaged hourly drift and noise characteristics (in %, middle) and hourly drift over time (in %, lower). The two left columns refer to subject 5 dataset before and after EME, the two middle columns refer to subject 3 dataset, and the two right columns refer to subject 1 dataset similarly.

2.7 Discussion

2.7.1 Summary of Results

Drift and Noise Characteristics in Human Long-term Recordings

The use of Easycap (EZ) electrodes resulted in lower drift and CI changes in comparison with the other two electrode types. This was consistent with recent findings by Yang et al [167]. Baseline amplitude was 5.4 ± 4.6 mV with EZ electrodes, in EIT measurements on human subjects with a common reference electrode (COM) over six hours. BV drift presented a clear and significant linear trend. Average hourly drift was 0.41 ± 0.3 %/hour. Slow change noise was 1.3 ± 0.63 %, medium change noise was 0.75 ± 0.63 %, and fast change noise was 0.43 ± 0.62 %.

Baseline amplitude was 2.6 ± 1.7 mV for measurements taken between adjacent electrodes (ADJ). Average hourly drift was 0.5 ± 0.51 %/hour. Slow noise change was 1.7 ± 3.05 %, medium change noise was 0.75 ± 1.95 %, and fast change noise was 0.43 ± 1.53 %. No clear correlation was found between BV baseline amplitude and drift.

Electrodes located in the front of the head suffered significantly larger drift than those on the sides in human subjects. Drift in electrodes located in the back was lowest. This was surprising considering Yang et al [166] found lower CI in frontal areas. Temperature near the crown during recordings changed gradually in a linear manner of 1.6-3.2%/hour but no correlation was found with drift in near-by electrodes. Eliminating the drift by reducing electrode movement related BV changes (EME) was neither consistent nor successful.

Drift in Resistor-phantom, Head-shaped tank, and Marrow Recordings

On a resistor phantom, average hourly drift was 0.06 ± 0.03 %/hour. On a saline filled head-shaped tank it was 0.2 ± 0.16 %/hour, while on a marrow it was 0.8 ± 0.72 %/hour. Average hourly drift slightly increased with frequency, going from 0.716 ± 0.70 at 200Hz, to 0.768 ± 0.72 at 1000 Hz, and 0.88 ± 0.88 %/hour at 1500 Hz. Separating the impedance into its real and imaginary components resulted in the real component demonstrating the same trend with a very close amplitude value, while the imaginary component showed different values and trends (4.1 ± 3.5 , 4.11 ± 3.35 , and 3.97 ± 3.25 at 200 Hz, 1000 Hz, and 1500 Hz respectively). When comparing drift in wet and dry electrodes, measurements where injections used wet electrodes resulted in a significantly higher drift than in measurements where injections used dry electrodes. On

the recording side, the trend was the reverse ($\text{Drift}_{\text{dry}} > \text{Drift}_{\text{wet}}$) although the effect was not significant. Average hourly drift on a marrow when the system was injecting 15 minutes and then resting for 45 minutes was 0.82 ± 0.47 %/hour, slightly higher (although statistically significant) than in a continuous recording (0.8 ± 0.72). CI change in the 'On-Off' recording was also higher than of the continuous recording ($p < 0.05$).

Contact Impedance Changes

CI in human subjects was 785 ± 285 Ohms at the beginning of the recordings and demonstrated linear change over time. Average hourly change was 1.9 ± 2.2 %/hour. A moderate to high correlation was found between CI change in an electrode to its related BV drift. On a marrow with dry and wet electrodes, baseline CI of wet electrodes was nearly half of the baseline CI of dry electrodes. Respectively, the CI change in wet electrodes was significantly lower than the CI change in dry electrodes.

2.7.2 Significance of Findings

The drift in BV measurements characterised in the study described in this thesis was much lower in comparison to those observed previously by Fabrizi *et al.* (2006), who described baseline BV changes of several percent over a period of minutes. Fabrizi *et al.* employed a set-up similar to our study, but with instrumentation that was at least ten years older and with different electrodes [57]. In 1996, Boone and Holder found that changes in skin impedance of about 2% were enough to inhibit imaging, while changes in BV of 10% over a few minutes were typical during EIT scalp measurements [23]. The findings of this study suggest that imaging brain injury might be possible and should be re-tested given the difference from earlier studies. In addition, these results should better inform future studies of brain monitoring using TD-EIT.

As this study demonstrates, the electrode type used for long term monitoring has a significant impact on BV drift in EIT. The presence of conductive gel also impacts significantly on drift. It is suspected of causing a larger drift although it is necessary for the safety and comfort of patients.

The proportion of drift in COM measurement was found to be lower than in ADJ measurements which make it possibly less prone to drift. However, while the proportion of ADJ drift is larger and varying more over time, the actual change in BV when measured in mV and not in %, is nearly half in ADJ measurements (0.021 ± 0.03 mV/hour for COM, 0.011 ± 0.01 mV/hour for ADJ).

Linear change in BV, continuously drifting away from its baseline values, is a clear threat to EIT imaging. However, when drawing conclusions from other types of noises carried by the brain EIT signal while recording over several hours, it is less obvious. Figure 2.24 is putting approximate numbers on drift and noise in four different mediums used in this study.

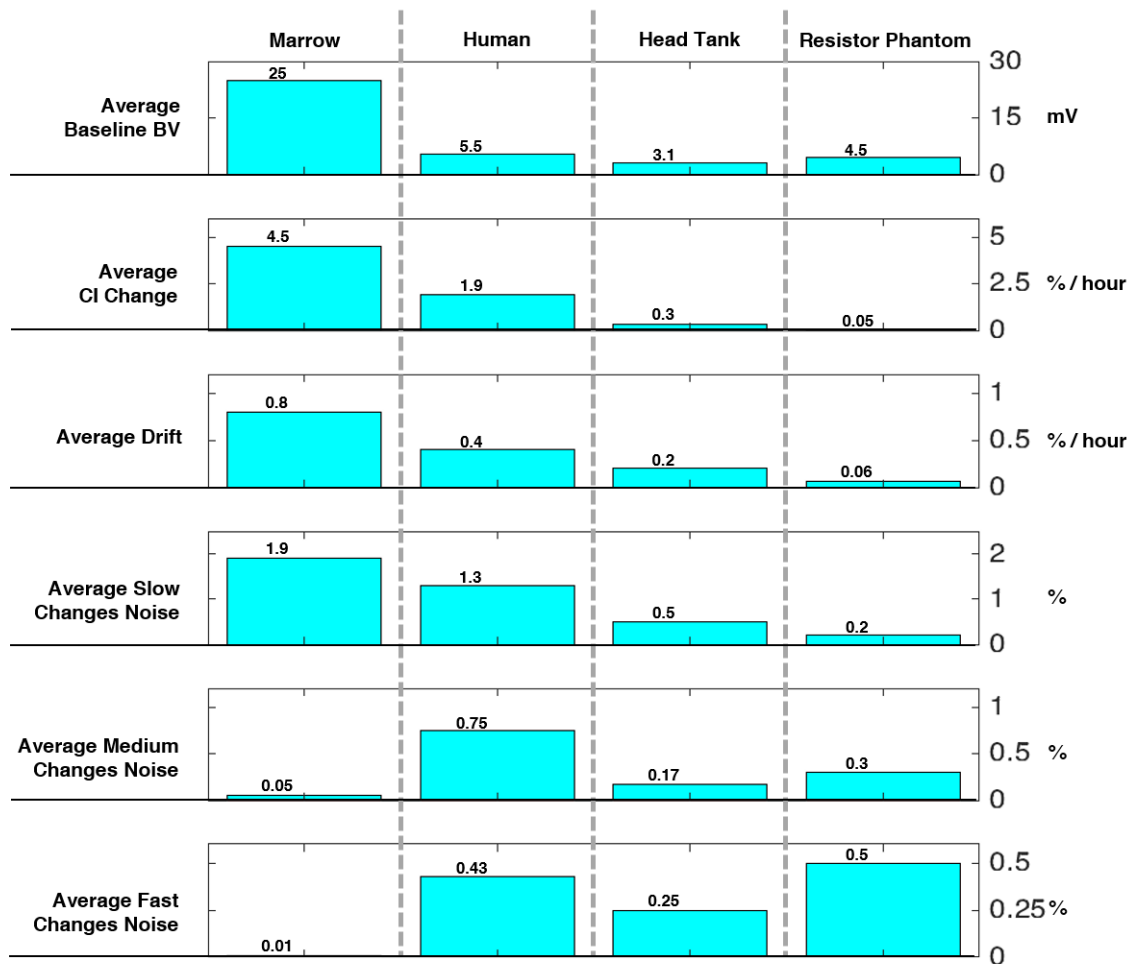


Figure 2-24: Drift and Noise Across Mediums.

Slow change noise presents similar patterns across different mediums as the pattern presented by average hourly drift. This might be explained if despite the difference in the method (the first one is by low pass filter, the latter is by linear fitting), they both measure the same phenomena of slow drift over time. Medium change and fast change noise present different patterns. Fast change noise, computed with a high pass filter, is highly likely to represent temporal system noise (difference between sequential measurements). This type of noise stays independent of the medium being recorded, and when calculated as the proportion of baseline amplitude is presenting a trend that is the direct reverse of the baseline amplitude.

Medium change noise, computed by a band pass filtering out fluctuation in a time scale of 1-10 minutes, could still be explained as changes caused by movements of the measured object. Largest movements are expected to show in living (and free to move) subjects, and minimal in still objects. The difference between human medium change and marrow medium changes fit well with this explanation. However, the difference between the marrow, resistor phantom and head-shaped tank do not. The recordings on marrows were made in a different type of building to where the recordings on resistor phantom and head-shaped tank were made. While marrows were recorded on the lower floor of the UCL Hospital building, a heavy and robust type building, the others were recorded in the UCL-EIT laboratory which is housed in an industrial style building with a floating floor, which is more susceptible to movement.

In this study, it was shown that drift is not correlated with BV baseline amplitude but is correlated with change in CI. Although shown in three different cases (human recordings, marrow wet-dry, and marrow continuous – ‘On-Off’), the trends were mixed, hence it is still unclear whether the change in CI is causing the drift, or whether a local impedance change in the skin causes both of them. While lower CI change of electrodes in the human study resulted in lower a BV drift, and lower average CI change in continuous recording on marrow resulted in a lower average drift compare with intermitted recording, the trend was opposite in the ‘dry-wet’ comparison. There, lower change in CI in the wet electrodes resulted in higher drift. This study needs to be repeated, in humans if possible, to clarify if this opposite trend was incidental.

It was also shown that the main effect of drift can be attributed to the injecting electrodes (see figure 2.25). When computing average drift per electrode according to injection electrodes, the difference in drift between electrodes of two significantly difference CI populations was significant. While doing similar comparison for recording electrodes, the difference in drift was not significant.

In addition, it was demonstrated that drift is larger in frontal areas compared to other areas on the scalp. However, the location of the reference measurement point was also located in the front, so this maybe is an indication of a drift spatial trend relative to the reference electrode rather than to the spatial location on the human scalp. With Yang et al [166] study finding CI to be lower in frontal electrodes, the location of the reference electrode was not clear, and CI estimation was performed with a different method.

Although system drift was found to be amplified by the hardware, this is not likely to be the explanation for the major portion of the drift (0.82 %/hour in continuous measurement vs 0.80 %/hour with intermitted recording).

All this information, now based on empirical evidence, should help future TD-EIT head-oriented data collections to be better informed, and hopefully more successful than previously.

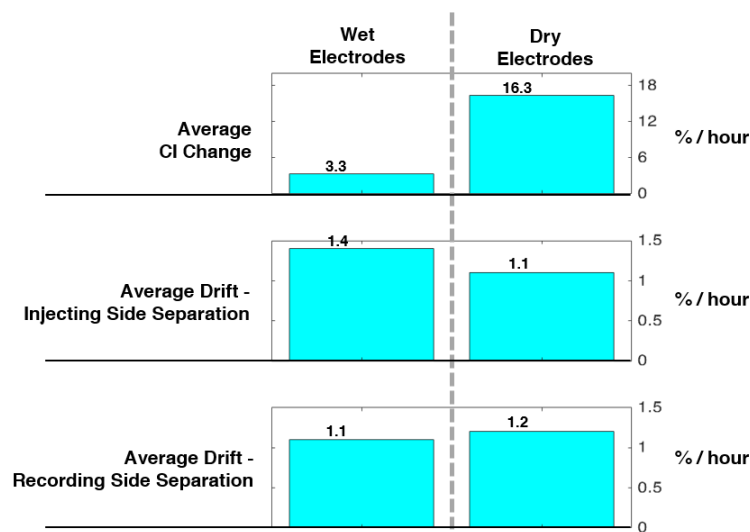


Figure 2-25: Drift in Injection and Recording Electrodes.

2.7.3 Study Limitations

The main limitation of this study is that it was limited to low frequency (below 2KHz), due to the available system's design. Although lower frequencies have been considered to be more suitable for brain injury detection [49,50], recent studies are showing that higher frequencies might also carry relevant information [168,170].

Another possible limitation is the size and diversity of the healthy control group. The group comprised six volunteers (three male, three female), with four of Caucasian ethnicity and 2 of Asian ethnicity. Indeed, a group of six might be considered as too small to be representative. However, EIT studies which investigated parameters such as contact impedance and SNR of different electrode types, used similar sized control groups with between four and ten volunteers [150,57,166]. Whilst having a larger and more diverse sample group would be desirable, making EIT recordings for

six continuous hours using healthy volunteers is no trivial task. This equally gender balanced group proved adequate and workable. The variance in scalp or other brain tissue characteristics has not been mentioned to date as being correlated with ethnicity, but has been correlated with age and pathological conditions [112,113]. Hence, while the findings of this study are valid, it would be beneficial to confirm them with more ethnically and age diverse sample groups.

In this investigation of drift and noise parameters, long measurements on a resistor phantom and head-shaped tank were taken mainly to establish reference figures for system drift and noise. Although these measurements served this purpose well, additional measurements such as temperature and movement recordings could add value. Measurements on marrows, which were in less orthodox set-ups (wet-dry, on-off, multi-frequency over time) yielded interesting information, and could prove beneficial with measurement repetition.

2.7.4 Conclusions and Future Work

The characteristics of BV drift are now well established. The principal cause appears to be changes in impedance across the scalp while electrodes are being applied. Further work is needed to model skin impedance changes across the scalp in a way that these changes could be separated from signal when internal brain impedance changes are incorporated. Another possibility is to develop statistical prediction models to compensate for measured BV changes based on electrode CI changes (see chapter 5).

3 Feasibility of Brain Injury Detection with TD-EIT

3.1 Introduction

TD-EIT has been investigated as a possible brain monitoring technology for almost three decades. Main Brain-EIT applications under consideration are epilepsy [57, 77, 157], fast neural activity [9, 10, 151], and brain injury including trauma and stroke [49, 129, 135].

In traumatic brain injury and stroke, identification and classification of the primary injury requires static imaging without baseline measurements and therefore could not be imaged with TD-EIT. However, it has been suggested that TD-EIT could monitor effectively other important aspects including early identification of both ischaemic and haemorrhagic primary injury in high-risk patients, and monitoring for a secondary injury after stroke and or TBI [33, 50, 54, 100].

The main technical barrier for successful imaging in brain TD-EIT is the drift in baseline BV recordings. Spontaneous slow changes in BV recordings over minutes and hours, could mask or even resemble to an evolving brain injury which occurs over the same time scale. Most studies attribute BV drift to changes in contact impedance (CI) [23, 112, 150, 166, 167]. Early studies found measured drift to be in the order of 5-10% per minute and to cause significant distortions in reconstructed images [23]. These findings have motivated EIT researchers to seek alternative options for dynamic imaging rather than traditional TD-EIT.

The first body of work in this thesis investigated the drift phenomena. BV drift in human subjects were found to be in the order of 0.5% per hour. Additional efforts to find the specific mechanism underlying this drift were only partially successful. However, the work suggested that the most probable source of the drift are impedance changes in the scalp tissue. Compensating for the drift by correcting for electrode movements was not successful, and other possible algorithms are still to be developed.

3.2 Rationale

The previous chapter of this thesis confirmed that drift is indeed significant, and might be still the dominant confounding factor in detecting brain injury with TD-EIT even if lower than expected. This feasibility study was carried out to better estimate the in-

fluence of real human drift on TD-EIT imaging of brain injury, considering the most updated drift figures, in a realistic configuration.

3.3 Purpose

The main purpose of the study presented here was to estimate the feasibility of imaging brain injury with TD-EIT, based on simulations as close as possible to real drift conditions.

To this end, three research questions were posed:

- What are reasonable choices for modelled pathologies and drift?
- What, if any, pathologies can be expected to be imageable by EIT?
- What is the biophysical explanation for these findings?

3.4 Experiment Design

The need to closely represent the complexity of EIT brain injury imaging was the driving force behind the design of this study. The study therefore required: a non-homogeneous background, lesions which evolve over time, and realistic drift in BV.

Computer simulations were used to model pathologies changing over time within a non-homogeneous background (complex brain tissues morphology). Real drift recordings from volunteers were used to represent realistic BV drift. Datasets of simulations together with real drift were sent for image reconstruction and quality evaluation.

Simulated Pathologies

The pool of simulated lesions was based on the literature review presented in chapter 1. Pathologies selected for simulation were representative of common real cases with testing factors most likely to influence imaging results: type of physiological change (ischaemia, haemorrhage), size (small, large), and location (centre, side, front, back).

Time Period

Since the development of a secondary or delayed lesion could occur at any point from minutes from the first or primary event to many hours later (see chapter 1) a time period had to be chosen for this study to correctly represent reality. I selected a time period of one hour after consultations with UCL Hospital Hyper Acute Stroke Unit (UCLH-HASU) physicians and after spending three months witnessing the treatment of hundreds of stroke patients (see chapter 4) including ones suffering from secondary injury. Secondary injury could develop, carrying significant clinical outcomes while symptoms were not yet evident to the medical staff over one hour.

Added Drift

One-hour segments from six hours of recordings of 6 healthy volunteers were used as drift samples in this study. Multiple samples were taken from each recording to permit the assessment of the effect of both between-subjects and within-subject drift variability on image reconstruction. Prior to the addition of real drift to simulated BV, checks were carried out to ensure that the two were in the same order of magnitude.

EIT Protocol

It was important to use the same EIT protocol throughout as it permitted the addition of the simulated BV with recorded BV drift. The DE-16 protocol (see chapter 1) was used for both simulation and real drift recordings in this study. The volunteers were three males with short or very short hair, and three women with straight hair. A sixteen-electrode montage was used, with current injection frequency of 2 KHz which is the maximum effective frequency of the ScouseTom 2.5 due to its limited sampling rate.

Data Cleaning

Data quality is important for successful EIT imaging, as demonstrated in earlier studies [50,57,129]. In this study a well validated method of data cleaning was adopted. Data channels with extremely low amplitude (< 0.1 mV) and data channels with high temporal noise (1 standard deviation divided by the mean) of over 1% were removed.

Image Quality Assessment

Images were reconstructed for every combination of simulated pathology added with real drift (576 images in total) using 0th order Tikhonov regularization, a well validated image reconstruction method which does not include prior assumptions regarding the expected changes in an image [103,154]. Every image was compared to an ideal reconstruction of the same pathology without the addition of any drift. An algorithm considering the location and volume of the reconstructed perturbation, as well as the amount of noise in the image was used for the comparison between two images (pure simulation vs. simulation + drift). This approach has been used in former EIT studies [56,129] and was adjusted for this study. Error indices resulting from the quality assessments of the images, were used to determine the feasibility of this application.

3.5 Method

3.5.1 Simulated Lesions

Modelled Pathologies

Sixteen different pathologies were simulated in this study. Two lesion sizes were simulated: small ~ 10 ml and large ~ 25 ml in volume. Four locations were simulated: centre (limbic region), side (temporal cortex), back (occipital cortex), and front (pre-frontal cortex). Each lesion was simulated once as a spherical ICH (blood replacing the volume of brain, 200-600% more conductive) and once as a spherical ischemic change (20% less conductive). Figure 3.1 illustrates the locations and volumes of simulated lesions.

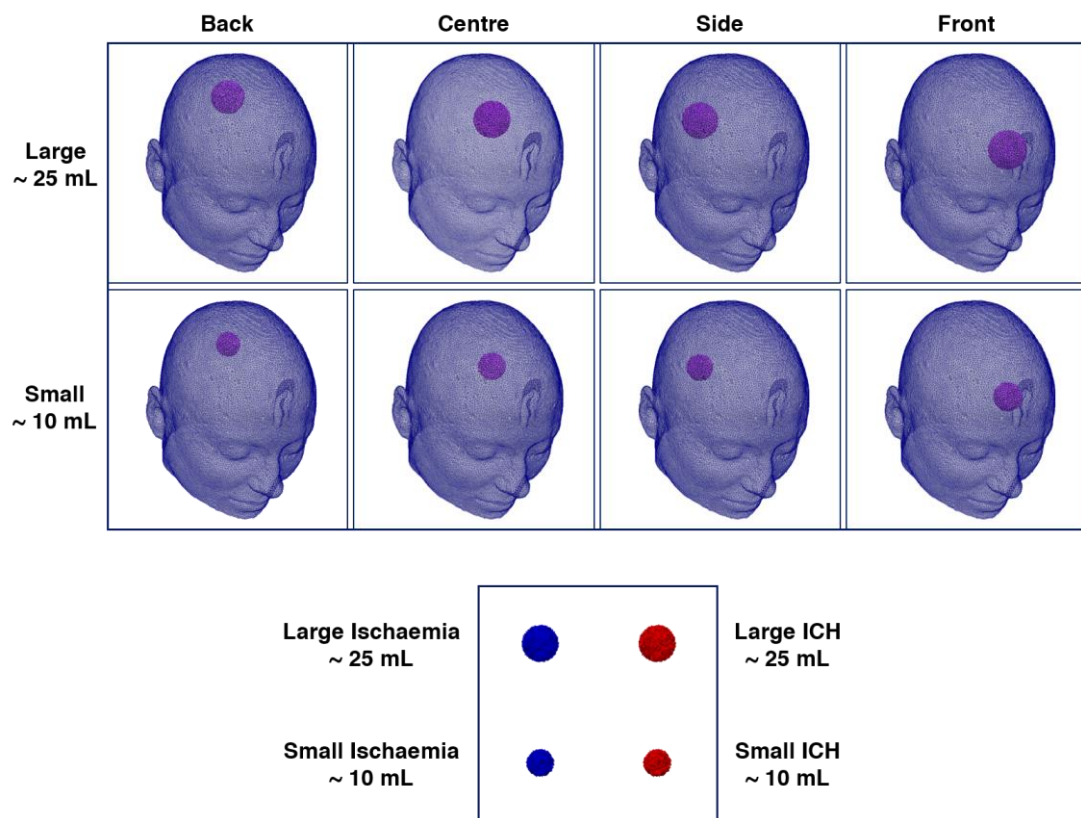


Figure 3.1: Simulated Pathologies. In this study, lesions of different volumes, locations, and types were simulated. Finite element models in the upper part of the figure present the locations (back, centre, side, and front) and volumes (small and large). Lower part of the figure demonstrates the type of change – ischaemic (negative conductivity change) is demonstrated in blue, while haemorrhagic change (positive conductivity change) is demonstrated in red.

Finite Element Mesh

A head mesh of 2 million elements was created, based on CT and MRI scans of a healthy (anonymous) subject received from London's National Hospital for Neurology and Neurosurgery (NHNN).

Segmentation of CT and MRI scans into seven different tissues (grey matter, white matter, Dura matter, scalp, skull, CSF, and air) was performed using Seg3D software (CIBC, Seg3D: Volumetric Image Segmentation and Visualization. Scientific Computing and Imaging Institute (SCI), <http://www.sci.utah.edu/cibc-software/seg3d.html>, 2014). The segmented image was then meshed using CGAL software (CGAL, Computational Geometry Algorithms Library, <http://www.cgal.org>). Dr Markus Jehl (UCL-EIT Laboratory) completed the segmentation and meshing.

The seven mesh layers corresponding to the different tissue types, were then assigned conductivity values (Siemens/meter): grey matter (0.3 s/m), white matter (0.15 s/m), Dura matter (0.44 s/m), skull (0.018 s/m), scalp (0.44 s/m), CSF (1.79 s/m), and air (0.001 s/m) [82]. A separate model for each of the 16 simulated lesions was created by assigning to the lesioned area appropriate conductivity changes (blood conductivity was set to 0.7 s/m, and ischaemia was set to be 20% less conductive [82]).

Forward Modelling

A sensitivity matrix (Jacobian) and expected BV for the mesh without any lesion (baseline) and for meshes of the 16 simulated cases were computed using the Super Solver package [83], a version of the EIDORS reconstruction software currently being used by most EIT research groups [5]. The injecting combinations, where the same electrode is used for injecting and recording, were excluded from the data due to exceptionally high BV, leaving 408 data channels in adjacent measurement (ADJ) format. Finally, the difference between the BV of each of the 16 simulated cases and the BV of the baseline image have created simulated ΔBV sets of 16 cases free of drift.

3.5.2 Real Drift Samples

EIT data secured from six healthy volunteers recorded for six straight hours was used for this. These are the same recordings described in detail in the previous chapter. Injecting combinations were excluded from the data leaving 408 data channels in adjacent measurement (ADJ) format. For each of the six recorded datasets, BV was averaged over five minutes every 60 minutes: $BV_{T=0\text{min}}$, $BV_{T=60\text{min}}$, $BV_{T=120\text{min}}$,

$BV_{T=180\text{min}}$, $BV_{T=240\text{min}}$, $BV_{T=300\text{min}}$, $BV_{T=360\text{min}}$. Six drifts were calculated to reflect 1 hour drift: $D_1 = BV_{T=60\text{min}} - BV_{T=0\text{min}}$, $D_2 = BV_{T=120\text{min}} - BV_{T=60\text{min}}$, ..., $D_6 = BV_{T=360\text{min}} - BV_{T=300\text{min}}$.

3.5.3 Data Cleaning

Real drift and simulated BV were checked to make sure that they were of the same order of magnitude. 95% or more of 408 recorded data channels were of the same order of magnitude as the simulated BV for all recorded datasets. Two data cleaning steps were then taken: simulated data channels with baseline BV lower than 0.1mV were removed as these are more susceptible to significant drift impact; Recorded data channels with temporal noise (1 standard deviation divided by the mean) of more than 1% were removed as these were suspected of being corrupt. These two cleaning steps had been evaluated and validated in previous brain EIT studies [56,57,129].

3.5.4 Combining Simulated and Recorded BV

Simulated BV were added to real drift samples, resulting in a total number of 576 test cases (16 simulated pathologies x 36 drift samples). Each test case had different numbers of data channels (mean \pm 1std was 252 ± 77 channels) since the cleaning process had eliminated data channels from both the simulated channels and recorded channels. Figure 3.2 illustrates the complete process of sampling real drift and adding it to simulated BV.

3.5.5 Image Reconstruction

Inverse solution computation resulted in a matrix of conductivity change ($\Delta\sigma$) for every element in the original head mesh (conductivity change image). This image was created using a 0th order Tikhonov regularisation algorithm utilising singular values decomposition (SVD) [152,9]. These conductivity changes were then translated into significance values for the change in every element, using a novel noise-based correction method [9]. This approach uses the inverted Jacobian matrix to compute the standard deviation of the estimated conductivity change in each element, utilising the temporal noise in the recorded BV. In the final images, conductivity changes were translated to significance expressed as z-scores. This converted the conductivity change image into a significance image. Images were then voxels with significance above half the maximum value, as in former EIT studies [49,60,77,78,129,133].

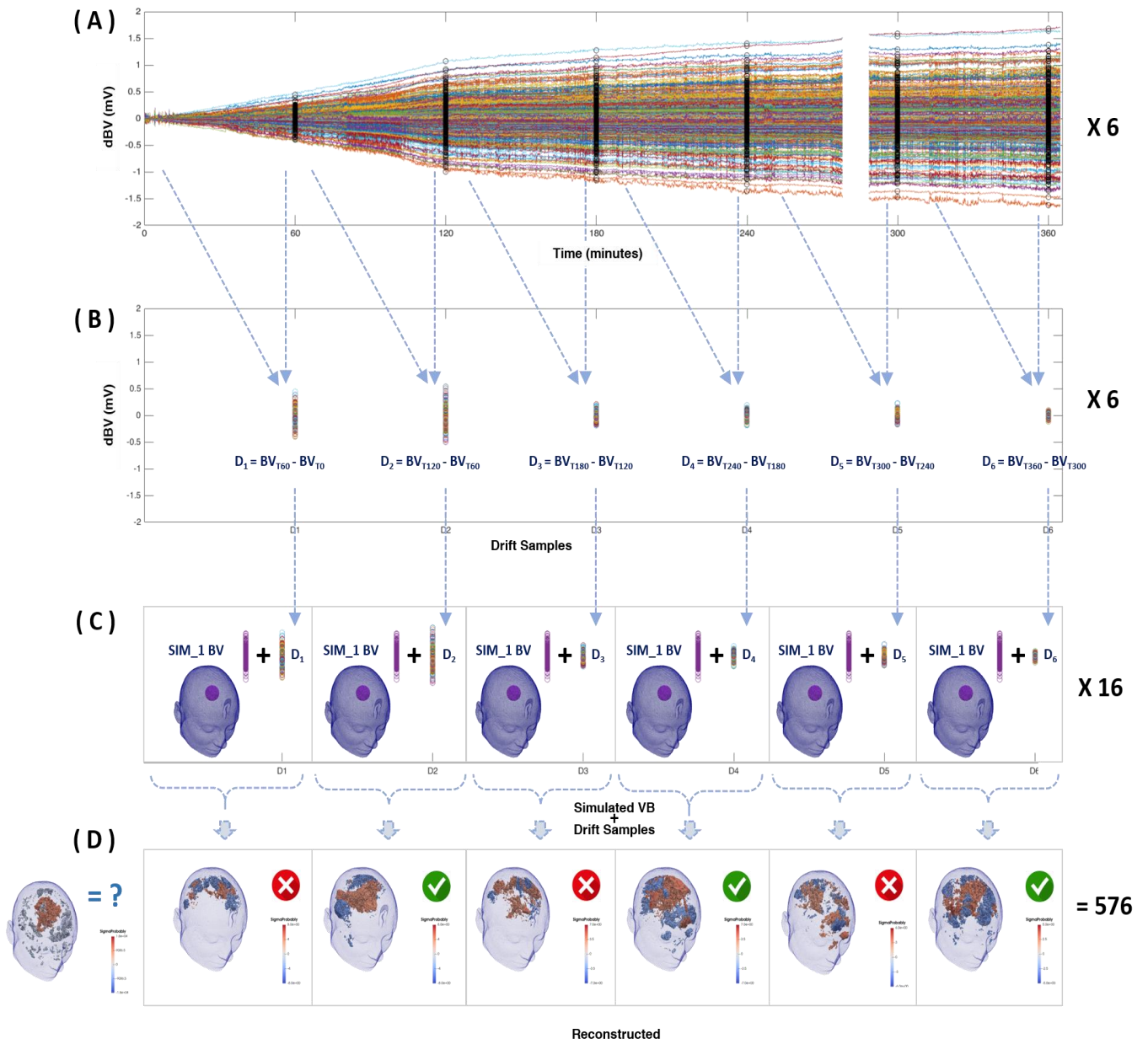


Figure 3.2: The Process of Adding Recorded Drift Samples to Simulated BV. This study contained four main stages which are demonstrated above: **A)** For each of the six recordings, averaged BV was sampled every 60 minutes. **B)** One-hour drifts were computed by taking the difference between two consecutive BV samples (six drift samples per recording). 36 drift samples were computed altogether. **C)** 16 simulated BV sets were added with each of the drift samples, accumulating to 576 different cases tested in this study. **D)** Tomographic image was reconstructed for each of the 576 cases and was evaluated as successful or unsuccessful.

3.5.6 Image Quality Assessment

Previous EIT studies have used four metrics to assess image quality in comparison with a reference ideal reconstructed image: localisation, shape, noise, and spectra [55,129]. A slightly modified approach was taken in this study to fulfil this study's specific objectives.

Image Quality Metrics

Reconstructed perturbation was defined as a group of connected mesh elements in the reconstructed image. The largest perturbation was assumed to be the reconstructed image while the rest of the perturbation was assumed to be artefacts. The metrics were defined as:

- Localisation error (weight 0.5) – the vector displacement of the centre of mass of the reconstructed image with respect to the centre of mass of its reconstructed ideal image, as a percentage of the head diameter.
- Image noise error (weight 0.4) - the standard deviation of all significant values not belonging to the reconstructed image expressed as a percentage of the mean of the reconstructed image significance values.
- Volume error (weight 0.1) – the difference in volumes between a reconstructed image and reconstructed ideal image, as a percentage of the ideal image volume.
- Artefacts factor – the proportion between the total volume of reconstructed artefacts and the volume of the reconstructed image.

The four metrics were combined into one value of *image error* by summing the three single errors (weighted according to importance) multiplied by the *artefacts factor*.

Successful / Unsuccessful Reconstruction Classification

Initially, a subset of 36 images were judged by the author to be successful or unsuccessful reconstructions. The judgment was made after comparing each of the constructed images (containing drift) to the reconstructed image of the same pathology without any added drift ("ideal reconstruction"). An Image was considered successfully reconstructed if:

- 1) The biggest reconstructed perturbation was of the right conductivity change (negative or positive).

- 2) The main perturbation was similar in volume ($\pm 50\%$ of the ideal reconstruction).
- 3) The location of the centre of the main reconstructed perturbation was similar to the ideal reconstruction (left/ right & front/ centre/ back).
- 4) The amount and size of the artefacts were reasonable, and where it is not reasonable to consider one of the artefacts as the primary lesion.

The same subset of images was then evaluated using the four metrics described above. Considering the image error given by the algorithm, a value separating successful (12/36) from the unsuccessful images (24/36) was set to 20.

Finally, all the reconstructed images were evaluated by the four metrics algorithm, and were labelled as successful if their image error was smaller or equal to 20, and unsuccessful otherwise. Images with an error image between 15 and 25 were then reviewed visually by the author. Of the 101 images reconsidered, 33 were reclassified (16 from successful to unsuccessful, 17 from unsuccessful to successful).

Paraview 5.0.1 (www.paraview.org) was used to visually inspect the images. For examples of successful/ unsuccessful reconstructions, see figure 3.3.

3.5.7 Reconstructions' Meta-Data

In addition to image quality assessment, two additional metrics were computed and collected for each image:

Number of Channels – The number of data channels remaining after applying data cleaning procedures, was recorded for each reconstructed image.

Signal to Noise Ratio (Signal to Drift Ratio) – The ratio between simulated BV and added real drift was calculated for every data channel proven to be valid for reconstruction. This ratio was averaged across all channels per image to represent Signal to Noise Ratio (Signal to Drift Ratio).

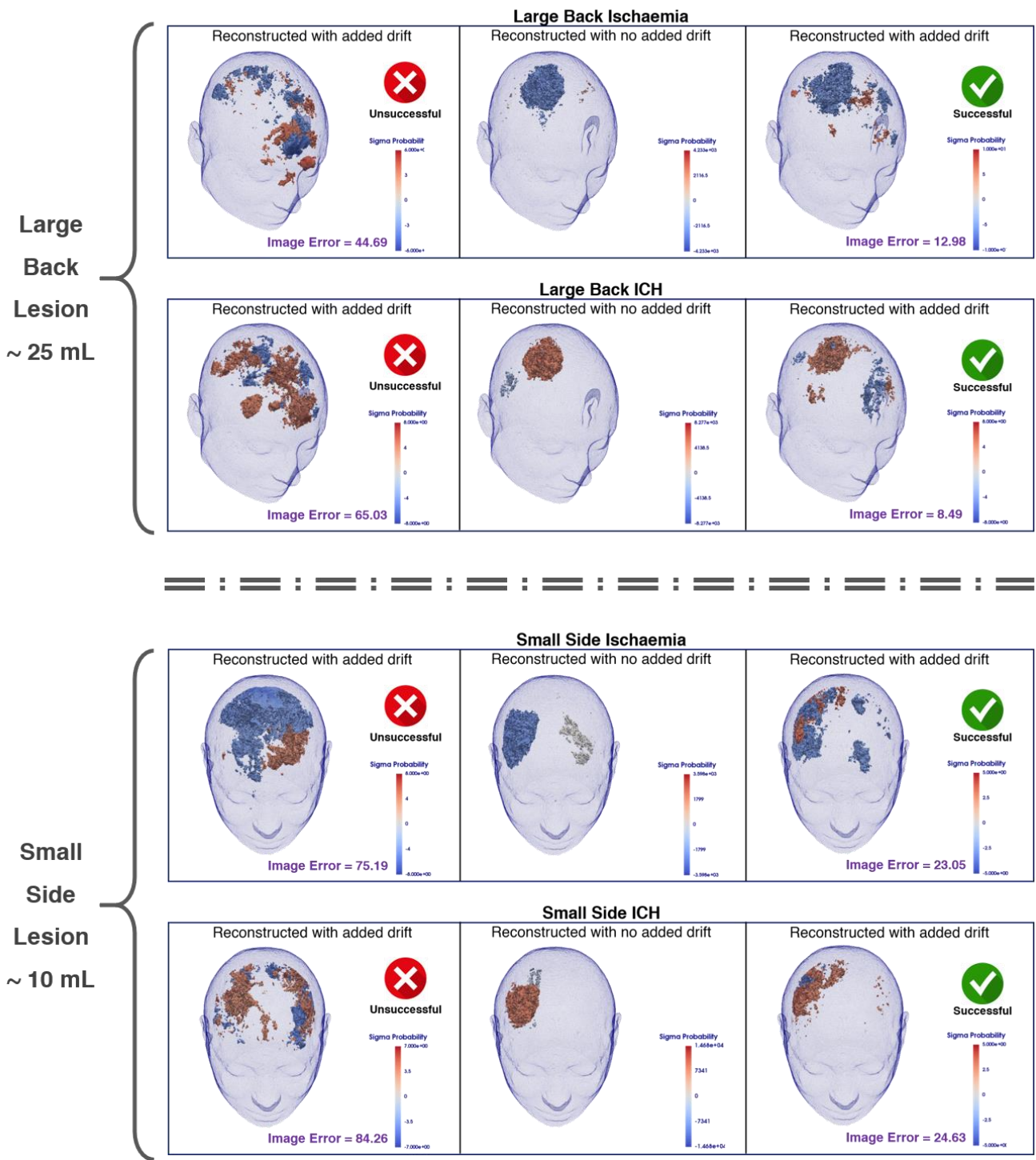


Figure 3.3: Successful and Unsuccessful Reconstruction Examples. Above figure demonstrates eight reconstruction examples evaluated by image error value. Upper examples are of large lesions (ischaemic and haemorrhagic) located on the back of the head. Lower examples are of small lesions (ischaemic and haemorrhagic) located on the side of the head. Middle images are ‘ideal’ images reconstructed without adding drift to simulated BV. Images on the right were evaluated by the algorithm as successful compared with ideal image (image error < 25) while images on the left were evaluated as unsuccessful images (image error > 25).

3.6 Results

Reconstructed images of 576 test cases were created and evaluated as successful or unsuccessful. 79 cases from the total set of 576 were evaluated as successful (~14%). Out of the 288 cases of simulated intracranial bleed (ICH), 64 were appraised as successful (~22%), while out of the 288 cases of simulated ischaemia, 15 were considered successful (~5%). The highest success rate was with reconstructing large volume ICH, 48 of 144, at 33%. The second highest success rate was for small volume ICH, 16 of 144, at 11%. Success rates of large and small volume ischaemic lesions were lower, 9/144 (6%) and 6/144 (4%) respectively. Success rates per lesion type and location were as follows:

For large ICH (~ 25 mL), developing over one hour, success rates were:

- For lesion located frontally: 10/36 (28%)
- For lesion located in the back: 16/36 (44%)
- For lesion located on the side: 11/36 (30%)
- For lesion located centrally: 11/36 (30%)

For small ICH (~ 10 mL), developing over one hour, success rates were:

- For lesion located frontally: 1/36 (3%)
- For lesion located in the back: 8/36 (22%)
- For lesion located on the side: 4/36 (11%)
- For lesion located centrally: 3/36 (8%)

For large Ischaemia (~ 25 mL), developing over one hour, success rates were:

- For lesion located frontally: 0/36 (0%)
- For lesion located in the back: 7/36 (19%)
- For lesion located on the side: 1/36 (3%)
- For lesion located centrally: 1/36 (3%)

For small Ischaemia (~ 10 mL), developing over one hour, success rates were:

- For lesion located frontally: 0/36 (0%)
- For lesion located in the back: 4/36 (11%)
- For lesion located on the side: 1/36 (3%)
- For lesion located centrally: 1/36 (3%)

Analysis of signal to drift ratio (SDR) was performed on the 288 reconstructed images of ICH cases, where success rates were high enough for both groups of

successful and unsuccessful images to be big enough for statistical analysis (64 and 224 respectively). SDR for the entire ICH images group (N=288) was 4.9 ± 14.7 (mean \pm 1 standard deviation). Separating the groups, SDR for the successful ICH images (N= 64) was 10.9 ± 28.1 , while SDR for the unsuccessful ICH images (N= 224) was 3.2 ± 6.3 . Minimum, maximum, and median SDR values of the successful images group were 0.13,137.0, and 2.35 respectively, while those of the unsuccessful group were 0.11, 52.6, and 1.63 respectively. A similar analysis of the number of data channels used by each reconstruction, was performed on the 288 reconstructed images of ICH cases. This time, no significant difference was found between the groups: averaged number of channels in successful reconstructions was 250.4 ± 74.6 (mean \pm 1 standard deviation) and 257.7 ± 86.6 in unsuccessful reconstructions. Figure 3.4 summarizes success rates results:

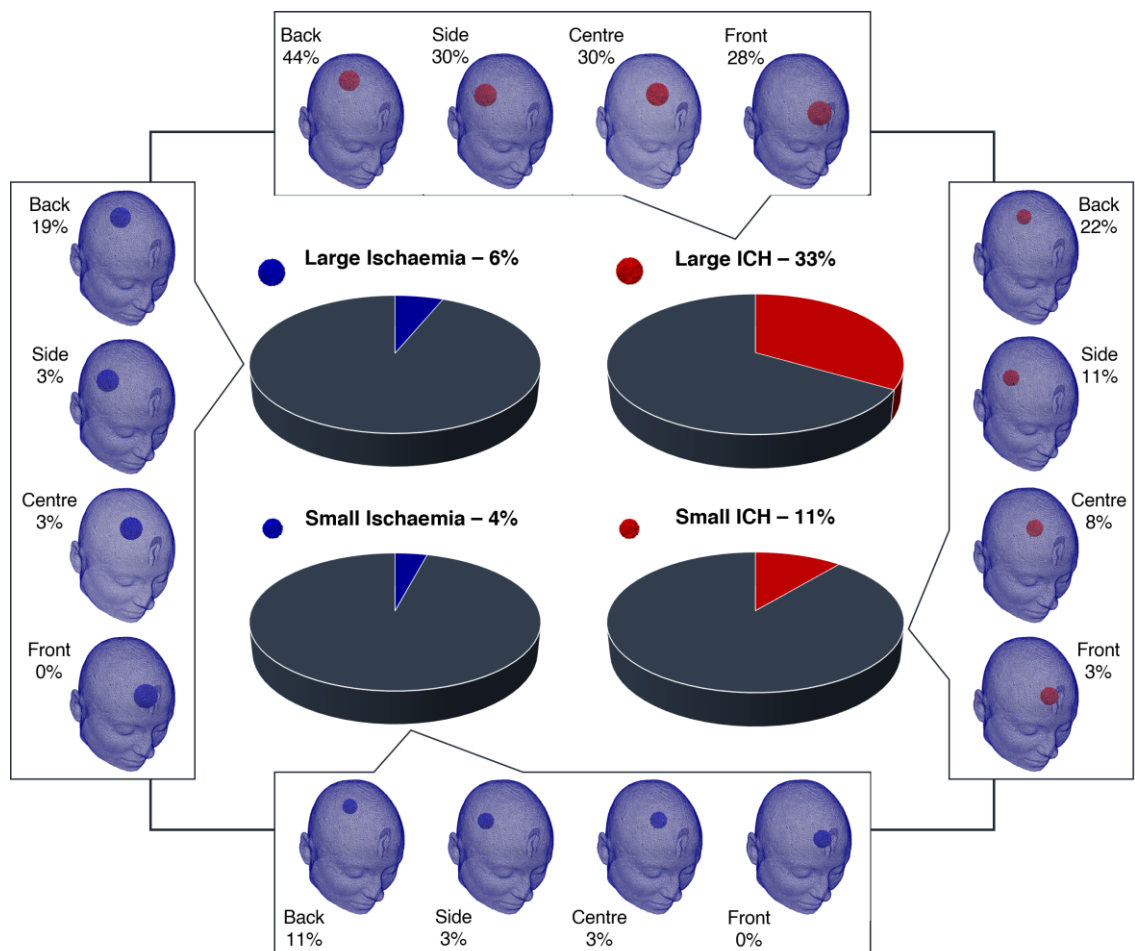


Figure 3.4: Successful Reconstruction Rates Summary. Pie charts summarize success per pathology volume/ type. Frames on the sides present success rate breakdown per location.

3.7 Discussion

3.7.1 Summary of Results

The highest success rate was 44% (back large ICH) of all sixteen simulated pathologies which was significantly higher than the next best success rate. Odds of successfully reconstructing ICH (22%) were much higher than successfully reconstructing Ischaemia (5%). Odds of successfully reconstructing a large volume lesion of 25 ml (20%) were higher than successfully reconstructing a small volume lesion of 10 ml (7.5%). The chances of correctly identifying a lesion located in the back of the head was significantly higher than in all other locations (24%). Success rates for lesions located on the side and centre of the head were 12% and 11% respectively. Identifying a lesion developing in the frontal lobe (7.5%) was the least likely to be found. This was true in all pathology types (ICH, Ischaemia, large, small).

3.7.2 Significance of Findings

According to published studies [[7](#),[20](#),[21](#),[131](#),[146](#)], conversations with clinicians, and personal observations drawn from spending significant time on a stroke ward, detecting small volume changes, in the order of 10mL or less, before it can be clinically observed and damage is irreversible (i.e. within an hour) proved essential. Since both ischaemic and haemorrhagic injuries are relevant both as a primary injury in patients at risk and as secondary injuries [[46](#),[62](#),[120](#)], both types were simulated. Larger lesions were simulated to test the feasibility of less preferable scenarios. Since drifts in baseline BV are the main obstacle to successful brain TD-EIT imaging, and these cannot currently be realistically simulated, it was decided to add real drift samples to simulations in this study.

Findings from this study suggest that none of the pathologies simulated can be expected to be successfully identified in real drift conditions. Small volume pathologies are highly unlikely to be detected, if BV drift is not eliminated efficiently. Detecting large volume pathologies is more feasible, although too low to be considered as an effective monitoring method.

The main reason for the failure to successfully image brain injury over a long period (an hour or more) are drifts in BV which exist in TD-EIT regardless of the changes in BV caused by developing pathologies inside the head. The change in conductivity in a certain volume of brain tissue becoming ischaemic, is far smaller than the change in conductivity of the same brain volume filled with fresh blood (see section

1.2.3). Since the change is far greater with ICH, the change in BV caused when ICH occurs is expected to be larger, hence is expected to be less prone to added noise (drift in our application). It therefore has a greater chance of being imaged successfully. This is consistent with the findings of this study. A smaller volume lesion will have a smaller conductivity change and therefore be less detectable than a higher volume lesion. This is also confirmed by this study's findings.

The effect of lesion location on the chances of being successfully imaged are not fully aligned with the expectation that changes occurring closer to the surface (scalp in our case) are more likely to succeed. It had been expected that pathologies developing in the centre of the head would be the least successfully reconstructed pathology [55,129]. However, these were more likely to be imaged than lesions located in the front of the head, and of similar likelihood to be imaged as lesions located on the side of the head. Possible explanations for these findings are spatial variability in skull conductivity, a different sensitivity of the protocol used in this study for different locations, and electrodes' coverage of different locations.

Skull conductivity changes significantly in different parts of the skull [15,113]. According to the most systematic study of skull conductivity available, made by Tang et al [148], at 1 KHz the frontal bone (0.0126 s/m) is more conductive than the parietal bone (0.0068 s/m) and much more conductive than temporal bone (0.0050 s/m). However, the most conductive areas are around the sagittal, lambdoid, and coronal sutures (0.0178 s/m). This, in theory, should make frontal lesions more likely to be imaged. However, the variability in skull conductivity was not reflected in the simulation part of this study (uniform conductivity of the skull was assigned, 0.018 s/m), and frontal simulations carried similar simulated BV to these of back located lesions. For example, a large ICH resulted in an average BV of 2.586 mV when located in the front, and 2.593 mV when located in the back.

Examination of spatial distribution of drift, as described in chapter 2 of this thesis, shows that the frontal area suffers higher drift compared with the sides and the back of the scalp, which was consistent with frontal area being the least probable location to be successfully imaged here. Electrode coverage, however, might have also varied in favour of central and dorsal parts of the brain. This could possibly result in lower sensitivity in frontal areas.

Hence, likely explanation for these findings is that cases of frontal reconstructions contained less data channels sensitive to the frontal areas with sufficiently low levels of drift.

3.7.3 Conclusions and Future Work

Currently, detecting brain injury with TD-EIT is not feasible as there is no efficient method to eliminate BV drift without corrupting BV changes caused by intracranial conductivity changes. Drift, although found to be lower than expected in experiments described in chapter 2, still limits the possibilities for the application of TD-EIT to brain injury monitoring. Recommendations for future work are laid out in chapter 5.

4 EIT Clinical Study at UCL Hospital Hyper Acute Stroke Unit (HASU)

4.1 Introduction

The original intention behind this PhD research work was to advance the applicability of TD-EIT as a brain monitoring technology. Whilst the work described in chapter 2 found that the drift in baseline BV is much smaller than expected, separating this from actual pathological conductivity changes is still a challenge. The feasibility study described in chapter 3 confirmed that using TD-EIT monitoring for brain injury with realistic drift present is currently unachievable. Despite these disheartening conclusions, the last project, a clinical pilot study to investigate the clinical information hoarded in MF-EIT data, and its possible applications to brain monitoring and to the main challenges in stroke care was carried out.

Two of the most important challenges in the care and management of strokes is to positively confirm an occurrence and to diagnose whether it is a haemorrhagic or ischaemic stroke as early as possible, to enable the appropriate treatment to be started as soon as possible [120]. CT/ MRI imaging and angiography are currently necessary to determine which cases are suitable for thrombolysis and thrombectomy. It is estimated that delays in admission to stroke centres, and to obtaining a CT or MRI scan mean that treatment rates in eligible patients can be as low as between 4% and 10% [154]. This increases the importance of early differentiation between ischaemic and haemorrhagic strokes, to ensure patients are placed on the correct diagnostic pathway. Thus, there is a clear clinical need for new methods to rapidly diagnose strokes and to distinguish haemorrhagic from ischaemic strokes, without waiting for hospital admission and a CT or MRI scan. EIT has the potential to provide an inexpensive portable unit for use in ambulances or GP surgeries which would revolutionise thrombolytic management of strokes by providing cost-effective imaging at the point of contact.

As described in section 1.2.3, contrast in the electrical impedance of ‘healthy’ brain tissue, blood and ischaemic brain tissue ($\Omega_{\text{blood}} < \Omega_{\text{brain}} < \Omega_{\text{ischaemia}}$) has been shown experimentally, and it is these spectral differences which EIT attempts to exploit [49, 50, 168, 170]. In rats [49], when comparing in vivo impedance measurements of normal brain, ischaemic brain and blood, the ratio between values at 20 Hz and at

1500 Hz, of healthy brain is about 1.25. The same comparison for ischaemic brain results in a ratio of about 1.15, while blood's ratio will be approximately 1.05 (figure 4.1). Yang et al [170] found similar trends in ex-vivo measurements of ischaemic and haemorrhagic rabbits' brain tissues.

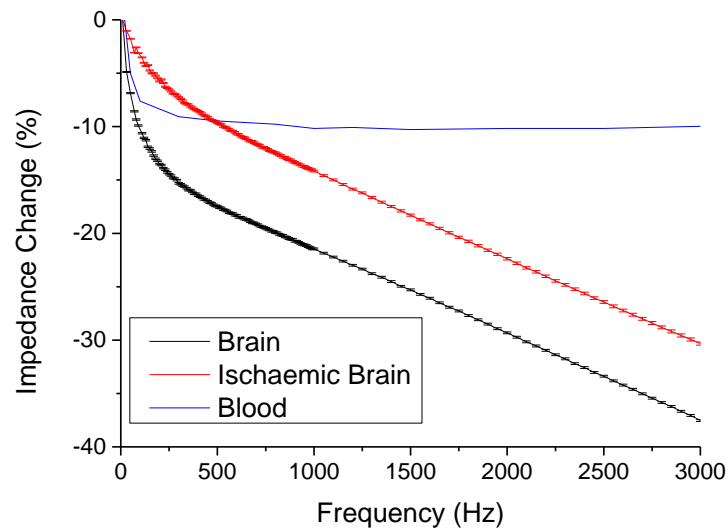


Figure 4-1: Rat's Brain Impedance Spectra (from Dowrick *et. al.* [49]). Mean values, calculated using all measurements, are shown. The error bars, corresponding to the standard error, are shown for blood, healthy and ischaemic brain data.

In humans, spectral patterns of normal brain, ischaemic brain, and blood, as described by Horesh et al [82] and McCann et al [113], are similar to the pattern in animals described above. However, slightly larger ratios are reflected, and the conductivity ratio between 20 Hz and 1500 Hz of ischaemia is the largest ($R_{\text{blood}} < R_{\text{normal}} < R_{\text{ischaemic}}$, where R is the ratio between impedance at lower frequency and impedance at higher frequency). Blood conductivity remains flat over the frequency range of 0-2 KHz, while healthy and ischaemic brain tissues' conductivity increases with frequency (see figure 4.2).

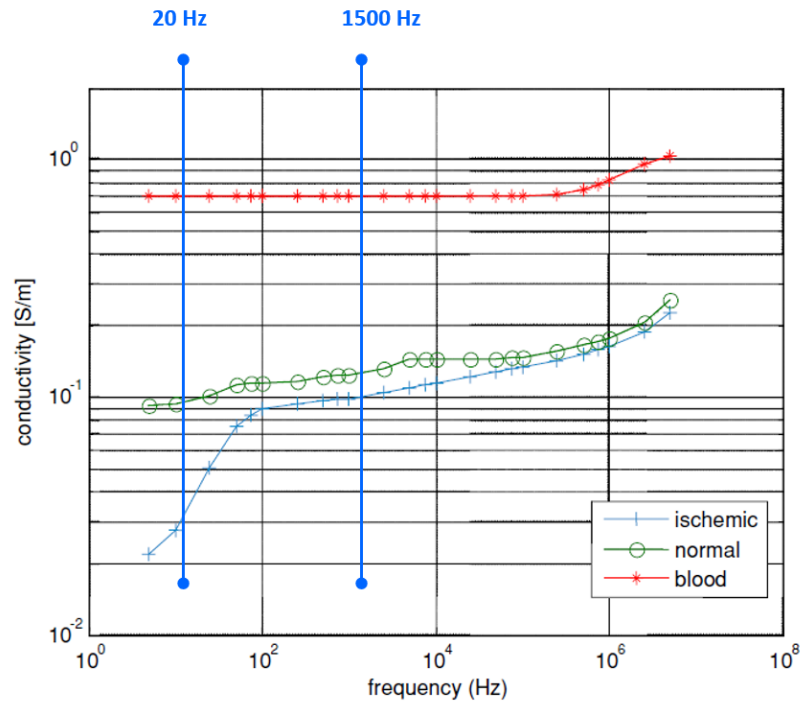


Figure 4-2: Human Conductivity Spectra (adapted from Romsauerova *et al* [135], based on Horesh *et al* [82]). Representative human conductivity values across frequencies.

According to this, the impedance spectra of a measurement sensitive to ischaemic, haemorrhagic, and healthy brain tissue is expected to look like this:

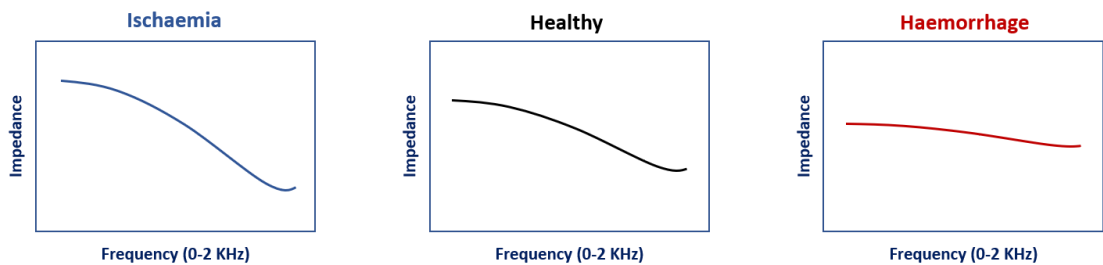


Figure 4-3: Schematic Impedance Spectral Patterns.

According to this, a larger percentage of the measurements of a haemorrhagic stroke patient will show the flatter pattern on the right, while a larger proportion of the measurements of an ischaemic stroke patient will demonstrate the steeper pattern on the left.

However, the picture is not so simple as the dominant pathology is reflected differently once it is measured on the scalp while the skull is intact. Recent findings suggest that when the cranium is intact, impedance changes of ischaemic and haemorrhagic strokes become similar, as the overall impedance inside the head increases [41,168]. This is explained as being the result of secondary ischaemic

changes in the brain as a result of increased intracranial pressure, or alternatively due to healthy brain tissue being pushed aside replacing volumes of CSF, a much more conductive material than brain tissue.

Following the same two guiding ideas that spectra measurements proportions represent the proportions of the tissue spectra measured, and that physiological changes within a closed skull turns haemorrhagic changes into ischaemic, it should be expected that a smaller ischaemic change will impact a smaller proportion of the measurements. It should similarly be expected that a smaller haemorrhagic change will in turn cause less surrounding ischaemic penumbra. This will cause smaller amounts of brain tissue replacing CSF spaces, so impacting a smaller proportion of the measurements to reflect ischaemia.

EIT is an imaging method. However, MF-EIT nonlinear reconstruction methods are still in their infancy and have significant limitations. Whilst these algorithms have been demonstrated in simulation and in phantoms, they have not to date been successfully translated into animal or human studies, largely due to increased sensitivity to errors in modelling electrode shape and position, and systematic errors in the impedance spectra of the tissues [27,91,107,108,129]. The added complexity of 3D data, realistic noisy environments, and processing resources make its application in real life highly unlikely now. Most of the current significant studies in the field of Electrical Impedance based methods for brain injury, were using the data without imaging, to extract relevant information, mostly indices and metrics related to symmetry between hemispheres [12,13,33,36,41,114,115,140]. Some studies that do apply imaging, are using reconstructions in 2D, to use the average reconstructed impedance value as the data being analysed later for clinical findings, rather than analysing the images themselves [100,165].

Progress has been made in some aspects of brain EIT research including algorithms, data processing, hardware, and clinical findings in animals. A component as important as all the others mentioned is human data, which is almost completely unavailable. The absence of available high-quality human data against this background, leads to the need to collect such data using the latest research techniques.

The full dataset acquired in this study was published and is now available online at: Goren, N. *et al.* (2018), 'Multi-frequency electrical impedance tomography and neuroimaging data in stroke patients' [69].

4.2 Rationale

The clinical scenario of stroke diagnosis dictates that data must be collected at a single point in time without a reference or 'pre-stroke' image. Data are therefore needed to be collected at a single point in time and must utilise changes occurring over frequency. The development of sufficiently robust MF-EIT algorithms requires high-quality MF-EIT human data. The rationale behind this clinical study was both to establish the first available high-quality MF-EIT dataset for future studies worldwide, and to investigate the possibility of MF-EIS for stroke diagnosis.

4.3 Purpose

This study was designed to achieve the following goals: to establish a high-quality stroke EIT dataset to advance stroke/TBI and EIT research and secondly to find evidence of any useful diagnostic information in stroke MF-EI. It was important to learn whether MF-EIT data could be used to separate out stroke patients from a healthy population, and whether lesion size determines this. Another key was to discover if MF-EIT data could be used for differentiating ischaemic stroke patients and haemorrhagic stroke patients. It was also imperative to see if similar observations using a reduced electrode set-up could be used as a basis for a future point-of-care set-up.

4.4 Experiment Design

This study was designed as a clinical pilot study. As such, it contained two endeavours: data collection, and data analysis. As described above, instantaneous imaging with absolute or MF-EIT is still premature, and TD-EIT is still not feasible due to BV drift (chapters 2-3).

Data collection focused on recording a variety of lesion types (ischaemic/ haemorrhagic, different sizes and locations), as fresh as possible, in a clinical environment. It was important to collect this data alongside clinical imagery (MRI/CT) to be able to compare clinical findings. Data from healthy controls was collected in addition.

Data were collected in seventeen frequencies between 5 Hz and 2 kHz. This frequency range spans both the operating band width of the ScouseTom system, the best available HW system for human recordings, and the region where the tissue conductivities demonstrate the largest differences [17,135]. A current injection pattern was chosen to maximise the overall magnitude of the voltages recorded, and the number of independent measurements ('OP32', see section 1.2.4). Current amplitude at each frequency was set to the maximum permitted under the guidelines set out in IEC 60601-1 [88].

In order to reduce the total data collection time (needed in a clinical setup), while still affording redundancy, the number of current injection periods applied was reduced at lower frequencies. A full spectrum recording with all measurements collected at all frequencies was collected for a total of three frames over the course of 20 minutes. A second reduced spectrum recording was collected at three frequencies, 200 Hz, 1.2 KHz and 2 KHz, for a total of 60 frames collected over 25 minutes. This increased number of frames improves the accuracy of the measurements through an increased number of averages as well as giving a clearer picture of the noise present in the measurements, enabling the quality of the collected data to be characterised. Signal to Noise Ratio (SNR) is an important factor in determining the performance of both TD and MF EIT methods. In simulation, MF images have been successfully reconstructed with an SNR of 30 dB [173], and with noise equivalent to 44 to 48 dB [4]. However, these MF-EIT algorithms are particularly sensitive to spectral errors, or systematic errors across frequencies. Therefore, the most important characteristic of the EIT system is that the SNR and amplitude is frequency invariant and was therefore a focus of previous work [17]. Data collection took around 45 minutes per patient (excluding preparations and cleaning).

In some patients there was a higher probability that the pathology would evolve over time, such as Haemorrhagic transformations in a large territory infarct after thrombolysis, or ICH which tend to develop secondary expansions. In these cases, it was routine on the ward to perform a further CT or MRI scan within 24 hours of admission as part of the HASU monitoring protocol. In these instances, the EIT recording session was also repeated as close to 24 hours after the previous recording as was feasible, giving both a new full spectrum (17 frequencies) and reduced spectrum (3 frequencies) dataset. It is thus possible to correlate the changes in EIT data with the radiology reports. This second recording session was also repeated for every healthy volunteer, to characterise the variation arising from the reapplication of the electrodes aside from any physiological changes.

Current was injected between a pair of electrodes while voltages were measured at all electrodes in parallel, relative to a common reference electrode ('COM') in line with common practice and as present in the Scouse Tom system used in this study.

Impedance symmetry between the hemispheres was also investigated. Any comparison between left and right hemispheres, could be influenced by the location of the reference electrode relative to the sagittal midline. To make data less prone to this influence, measurements were taken between two adjacent electrodes ('ADJ'). This was achieved by subtracting two adjacent measurements originally taken as 'COM' (figure 4.4).

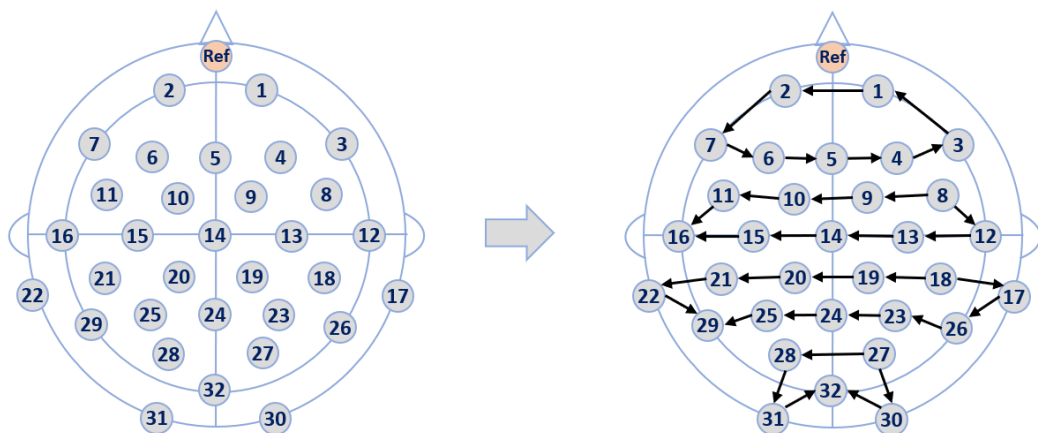


Figure 4-4: COM to ADJ. On the left, original 'COM' set-up – each measurement is made between an electrode (1-32, in grey) to a common reference electrode (orange). On the right, Measurements are made between adjacent electrodes ('ADJ') as the difference of two 'COM' measurements.

The general approach of this study was to look at measurement sets as data sampled from different populations and to separate these populations by analysing the mean and variance of the different samples. The data considered in this study contains a few possible dimensions which might shed light in a different way on the

questions under investigation. While TD-EIT data usually tracks conductivity changes over time using a single frequency, MF-EIT data present in this study contains information embedded in the frequency spectrum. Each data frame contains hundreds of measurements, but not all the measurements carry the same amount of information. Some measurements are more sensitive than others to internal impedance changes. When analysing groups of measurements, a more sensitive subset of the measurements could potentially emphasize differences between groups otherwise blurred by a complete data frame. Finally, while one option is to look at measurements taken from all parts of the scalp as one dataset, another option is to use the symmetrical nature of the human head. This perspective looks at the differences between the two otherwise symmetrical sets of measurements recorded on the left and right hemispheres.

A More Sensitive Data Subset – A more sensitive data subset was created to refine the tests in cases where the complete dataset does not yield a significant result. For this purpose, a Jacobian matrix (J) was utilised to create data subsets containing the measurements which are the most sensitive to conductivity changes inside the head. Each line in this matrix holds sensitivity values for a specific measurement, per element in the Finite Element Model (FEM). These values were summed to calculate a single sensitivity value for a specific measurement ($Sens_i = \sum_k (\sqrt{|J_{i,k}|^2})$, where i is a measurement and k is an element in the FEM). The graph of sorted sensitivities (figure 4.5) presented an exponential change, hence the top ~ 10% were selected to represent a more sensitive subset of data. Similar method for creating a more sensitive dataset was used in previous EIT study [135].

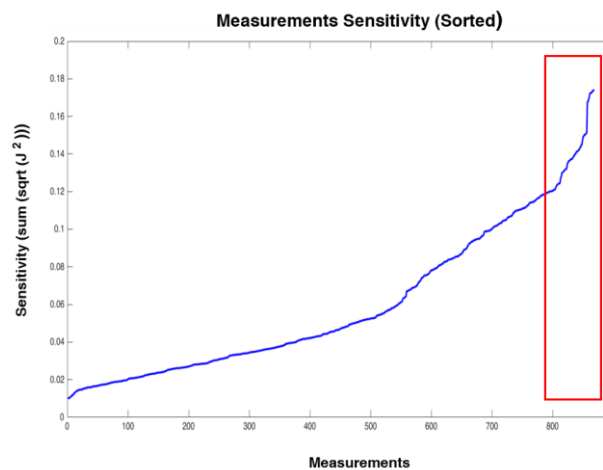


Figure 4-5: Measurements' Sensitivity. In blue – sensitivity values of a full set of 868 measurements, sorted by sensitivity computed using Jacobian rows, and presenting an exponential trend. In red frame, the 10% most sensitive measurements.

Left-Right Symmetry Measurements – The head and brain are symmetric structures; all anatomical features are distributed approximately symmetrically either side of the midline. Accordingly, previous studies had shown that inner-hemispheric BVs vary similarly across both hemispheres in healthy subjects [22]. When a brain lesion is unilateral, brain conductivity is likely to change on just one side of the brain, which in turn is expected to yield a left-right measurement asymmetry [12,22]. To test for L-R asymmetry, data were divided into two sets of measurements, recorded on the right and left sides of the head. All measurements involving midline electrodes or measurements crossing the midline were excluded, leaving ten measuring pairs per hemisphere (figure 4.6). For example, measuring between electrodes 1-3 on the right hemisphere is a mirror of 2-7 on the left hemisphere, as 18-17 and 21-22.

To ensure current injections for this analysis were symmetric, the twenty-eight of the thirty-one injections which had a symmetric pair were included. For example, injection between electrodes 7 and 30 is symmetric with injection between 3 and 31. Injection between 5 and 32 was also included in this analysis as it is purely on the midline. two injections (1-24 and 14-31) were excluded for not having a symmetric pair (figure 4.6).

L-R symmetry data, therefore, included pairs of measurements where both the two injecting electrodes, and the two measuring electrodes were symmetrical, and the absolute value between the two measurements was considered.

Spectral Ratio Measurements – The ratio between BV measured at low and high frequencies was computed to exploit the difference in conductivity change over frequencies of different tissues, while reducing data dimensionality to enable simple comparisons between datasets. This technique was used previously in stroke EIT [135], and was termed here as Spectral Ratio (SR) measurements. SR, therefore, represents the information hidden in a single EIT measurement taken at a single point in time across several frequencies, using a single unit-less number. Variations in SR values are supposed to represent variations in the proportions of the different tissue types (brain, blood, ischaemia) in the area under investigation.

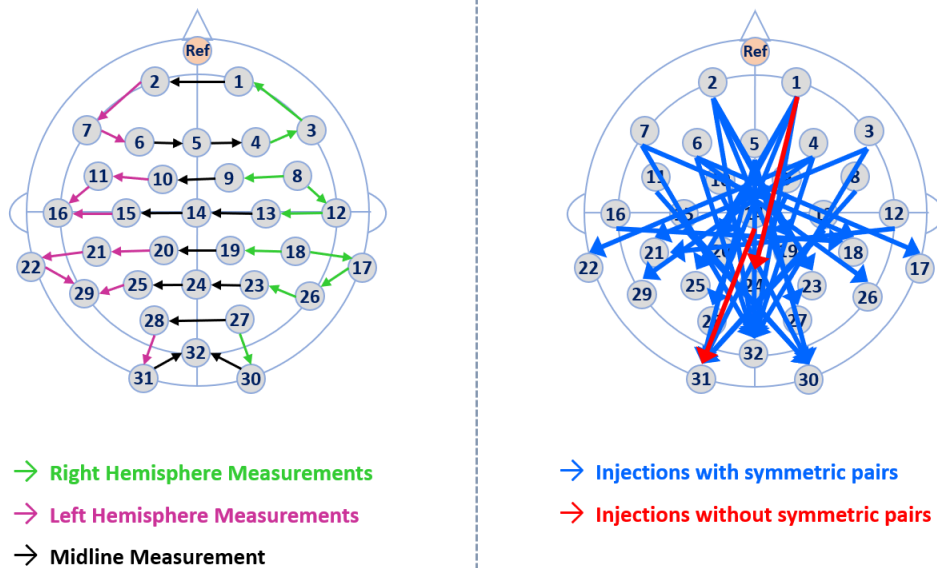


Figure 4-6: Measurements and Injections Symmetry. On the left – Measurements considered for L-R symmetry datasets. L-R symmetry is calculated as the difference between green (right) and purple (left) measurement pairs. On the right – all 31 current injections injection of the OP32 protocol used in this study. 29 were considered for L-R symmetry analysis (blue). 2 were excluded for not having a symmetrical pair (red).

Practical ‘Dry’ Location Subset – One of the considerations for this study was whether there was a possibility to make diagnostic observations using a drastically reduced number of electrodes, placed in hairless locations for quick, easy application similar to those made with a full electrode montage. Such a reduced montage would be the basis for any future point-of-care EIT/EIS application for stroke/ TBI diagnosis. A data subset containing injections and measurements made with electrodes located around the head close to the hairline was created for this purpose. This specific dataset was created only in cases where both the full dataset and its more sensitive subset demonstrated the ability to separate between controls and patients. It contains thirteen injecting pairs, and seven measuring pairs on each hemisphere, resulting in twenty-eight pairs of measurements (figure 4.7).

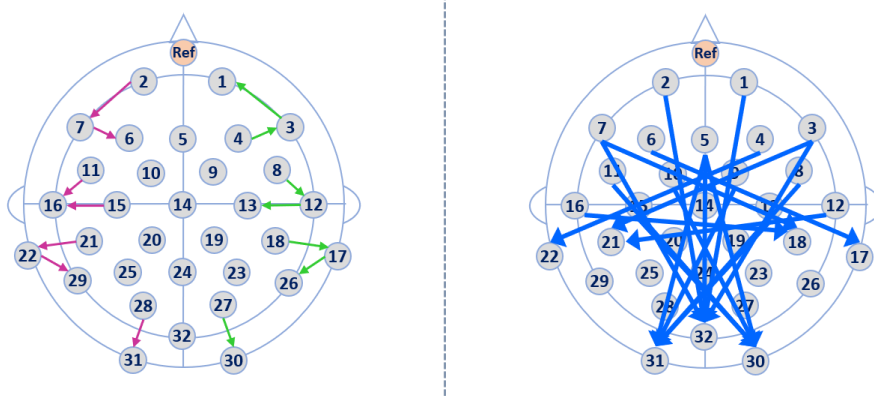


Figure 4-7. ‘Dry’ Locations Set-Up. Injections (right, in blue) and measurements (left, in green and purple) considered for the ‘Dry electrodes’ data subset for being close to the hairline.

4.5 Method

4.5.1 Data Collection

4.5.1.1 Participants

All experiments were performed at the UCLH HASU and were approved by the University College London Research Ethics Committee, the London - Harrow Research Ethics Committee (REC favorable opinion reference number:15/LO/0092) and NHS/HSC R&D (IRAS ID:168765). Patients were selected using the following criteria:

Inclusion criteria:

- Adult patient, of at least 18 years of age, with no upper age limit.
- Clinical diagnosis of cortical ischaemic stroke or lobar intracerebral haemorrhage (ICH).
- The stroke has an axial diameter >1.5 cm on CT/MRI, OR the patient has a National Institutes of Health Stroke Scale (NIHSS) score ≥ 5 .
- Able to undergo the EIT assessment within 7 days of onset.

Exclusion criteria:

- Expected to require critical transfer or intervention, Intensive Therapy Unit (ITU) admission or to be transferred out of the HASU for any other reasons.
- Unlikely to tolerate the procedure (e.g. agitation on admission), or an extremely high likelihood of death within 48 hours of stroke onset.
- Additional medical illness (such as Epilepsy, skin problems, head or face metal implants) or technical aspects (such as no available bed on HASU) that interfere with EIT assessments.

Potential participants were first identified by the UCL stroke research team and then discussions with the suitable patient were initiated. If they were willing to participate, written consent was obtained. Where the patient lacked the capacity to give consent, assent was given by a family member. Experiments were also performed on healthy subjects after obtaining written consent.

Twenty-six stroke patients (eight female, eighteen male, age 70.2 ± 17.6 years) and ten healthy volunteers (four female, six male, age 28.4 ± 7.4 years) were recruit-

ed for this study. Thirty datasets have been collected in patients, and twenty additional datasets have been collected in ten healthy volunteers.

4.5.1.2 EIT Data Collection

The EIT system used in this study (the ScouseTom 2.5, figure 1.4) was developed at UCL [17] and uses a Keithley 6221 Current Source (Keithley Instruments, Cleveland, Ohio, USA), BioSemi EEG Recorder (Biosemi, Amsterdam, The Netherlands), EasyCap EEG electrodes (EasyCap, Germany) and custom circuit boards for current routing and system control.

Voltages were recorded on a total of 32 electrodes arranged in the configuration used in previous stroke EIT studies which includes 21 locations from the EEG 10–20 standard and 11 additional electrodes [151]. For these experiments, the locations were updated to match the nearest equivalents in either the 10-10 or 10-5 extensions [35,125]. The reference electrode was placed on the forehead at position NFpz, above the Nasion fiducial point, as detailed in figure 4.8. The Biosemi Active Two system implements a driven right leg circuit, which required an additional electrode, which was placed on the forehead 20 mm closer to the right temple at position NFp2.

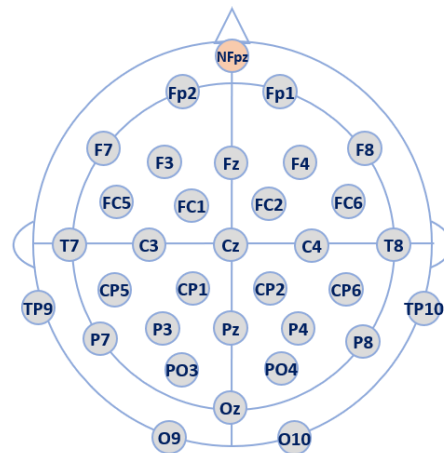


Figure 4-8: Electrodes Montage. Layout of electrodes locations used in this study (32 measuring electrodes (grey) + reference (orange)).

Prior to data collection, each electrode site was cleaned with surgical spirit, abraded using Nuprep gel (Weaver and Co., USA) and Elefix conductive paste (Nihon Kohden, Japan) was used to affix the electrodes. To ensure the quality of the electrode contact at each site, the contact impedance was estimated at 1 KHz and the electrode site was abraded until all electrode sites met a $< 3 \text{ K}\Omega$ criteria used in previous EIT stroke studies [135].



Figure 4-9: Images of the Clinical Set-up at UCLH HASU. Top left – applying electrodes to a bed-sitting patient. Top right – The UCL ScouseTom 2.5 EIT system in its hospital version, fully stacked for bedside data collection. Bottom-left – Running the ScouseTom near a patients’ bed. Bottom right – full running set-up on a chair-sitting patient at UCLH HASU.

The OP32 protocol yielded a total of 992 measurements per data frame. Measurements were taken using seventeen frequencies between 5 Hz and 2 KHz (table 4.2), with the current amplitude at each frequency set to the maximum allowed under the guidelines set out in IEC 60601-1 [88]. A full spectrum recording with all 992 voltage measurements collected at all 17 frequencies (for a total of 16,864) was collected for a total of three frames over the course of 20 minutes.

4.5.1.3 Technical Validation of the EIT Data

The normalisation for the gain of the BioSemi EEG system during data processing was validated in resistor phantom measurements, where the deviation from the expected values was 0.07%. A reciprocity error of 0.42%, comparable to state-of-the-art EIT systems further demonstrated the accuracy of the ScouseTom [136,160]. Equally important is the frequency invariance of the demodulation. As the collection time and injection periods changed across frequency (table 4.2), it was not possible to use the same filter design in each case. The filter selection was validated by demodulating a simulated signal matching the expected amplitude, DC offset, frequency, phase and time, and comparing the results with the true value. The maximum amplitude and

phase error were 0.001% and 0.0017% respectively at 10 Hz, and less than $10^{-5}\%$ for 100 Hz and above.

The quality of the electrode contact was verified using two different methods before data collection. It was also continuously monitored throughout recording. First the electrode “offset”, i.e. the voltage at DC on each channel, as displayed through the BioSemi software was maintained at a level below 50 mV. This was necessary to measure the quality of electrode contact, and to prevent clipping of the EIT voltages. Second, the contact impedance was estimated from the voltage on each electrode when used to inject current at 1 KHz, and the electrode application process was repeated until a value of 3 K Ω or less was obtained. To verify that there were no significant changes in contact impedance during recording, this estimate was repeated prior to electrode removal. For further validation the contact impedance was also estimated at each of the 17 carrier frequencies from the data.

The quality of the final data, figure 4.10, showed no significant changes of SNR across frequency for both subject and patient’ data, $P = 0.16$ and $P = 0.52$ (one-way ANOVA) respectively. Increased artefacts from patient movement resulted in a mean 5 dB drop in SNR in patients compared to subjects, however this change was not significant at any frequency ($P \geq 0.54$). The $<1\%$ noise in these measurements was less than that applied in a successful simulation study [107], less than half than that observed in the most directly comparable clinical recordings [135], and within the range found using an order of magnitude greater current amplitude at 50 kHz [162]. Therefore, this dataset meets the requirements for imaging and statistical analysis both in terms of SNR and frequency invariance.

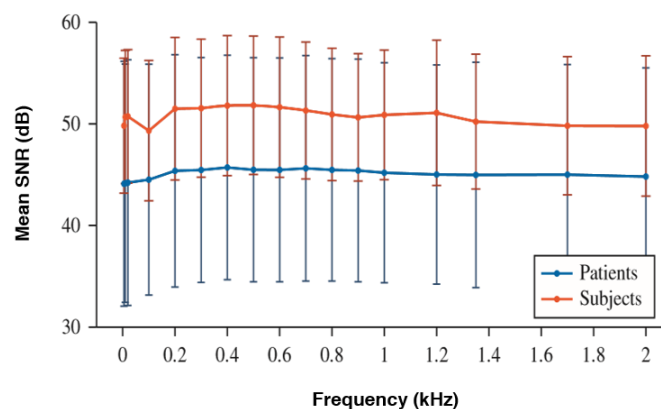


Figure 4-10: Signal to Noise Ratio Across Frequency (mean \pm standard deviation) [69]. There were no significant differences in SNR across frequency in both patient ($N = 18$, $n = 24$) and subject ($N = 10$, $n = 20$) recordings.

4.5.1.4 Additional Clinical Data Collection

As part of the clinical diagnostic procedure in the HASU, each patient underwent an MRI and/or CT scan (DICOM format). All data were anonymised by removing any identifying data from the DICOM file, using DICOM Cleaner. The scans and their clinical interpretations by the ward radiologists were used to classify different lesions by type, size, and location. All relevant clinical data (former lesions, co-morbidities, etc.) were assembled with medical records, and concentrated in a Case Record Form (CRF) for future analysis in accordance with Good Clinical Practice (GCP) requirements. Only data specifically relevant to this study were extracted from these forms, and subsequently anonymised according to UK data service guidance.

4.5.1.5 Applicable Data Subset

Of the twenty-six patients who consented to participate in this study, data were recorded from eighteen patients. Four patients dropped out of the study before starting the data collection procedure (changed their mind, was discharged from the ward, or did not actually meet the inclusion criteria). Two patients were found not to be suffering from acute stroke (TIA, old lesion), and in another two cases data collection had to be stopped due to a required medical procedure. This resulted in a non-continuous list shown in table 4.1.

The eighteen qualified patients included five females and thirteen male of average age 72.4 ± 14.2 years. Healthy volunteers stayed unchanged (four female, six male, age 28.4 ± 7.4 years). In six of the qualified patients, and in all ten healthy subjects, data were recorded twice. Only one recording (the first for each patient) was considered for use in the following analysis to avoid the possibility that part of the samples were taken from the same patient. **Eventually, this resulted in a dataset reflecting two sample groups: 18 patients and 10 healthy controls.**

The patients' group was (N= 18) further labelled according to the type of stroke (ischaemic or haemorrhagic) and the size of the lesion (big or small). Ischaemic strokes were labelled as big in cases where the radiology report stated that there was a large territory acute infarct (6) and small if otherwise (4). After consulting a senior neuroradiologist, haemorrhagic strokes (ICH) were labelled as big (4) if scans presented with an axial diameter $> 30\text{mm}$ and were labelled small otherwise (4). Table 4.1 below summarises the numbering and labelling of all the data considered here for further analysis. Figure 4.11 presents thumbnail size images of patients' lesions.

DATA TAG	SEX	AGE	STROKE - EIT INTERVAL	SCANS AVAILABLE (Time from Stroke)	CATEGORY & MAIN RADIOLOGICAL FINDINGS
P1	F	72	24 hours	CT (12> hours) MRI (24 hours)	SMALL IS - Subacute infarct in left precentral gyrus and superior frontal gyrus (left MCA territory). Suspected infarct in left insula. Two mature small infarcts in left cerebellum.
P3	M	71	27 hours	CT (12> hours) MRI (24 hours)	BIG ICH - Acute ICH centered onto left paracentral lobule, with surrounding oedema. Imaging suggests presence of an underlying lesion containing older blood product.
P4	F	77	18 hours	CT (2 hours)	BIG IS - Acute right MCA large territory infarct involving basal ganglia, insula, areas in temporal and frontal lobes.
P5	M	72	32 hours	CT (2 hours) MRI (24> hours)	SMALL ICH - Small acute ICH on lateral side of the left Thalamus. Mild surrounding oedema, no midline shift.
P6	M	41	36 hours	CT (24 hours) MRI (24 hours)	SMALL ICH - ICH in right occipital lobe measuring approximately 2.3cm x 1.5 cm, with vasogenic oedema.
P9	M	85	2-3 days	CT (2> days) MRI (3> days)	BIG IS - Acute right MCA infarct involving anterior temporal lobe and insular cortex.
P11	M	87	15 hours	CT (12> hours)	BIG ICH - Massive acute ICH involving most of the right frontal lobe, operculum, and postcentral gyrus. Significant midline shift. Previous multiple ICHs.
P12	M	79	8 hours	CT (12> hours)	SMALL IS - Small acute infarct in the left medial occipital lobe
P15	M	52	3 days	CT (12> hours) MRI (2 days)	BIG IS - Left parieto-occipital lobe acute/ subacute infarct. Multiple deep white matter lacunes. Microhaemorrhages scattered throughout the cerebrum and cerebellum
P16	M	84	48 hours	CT (5 hours) MRI (24 hours)	SMALL IS - Right central gyrus and left posterior frontal lobe acute/ subacute infarct.
P17	M	56	21 hours	CT (2> hours) MRI (4 days)	SMALL ICH - Acute ICH in right thalamus and striato-capsular area approximately 2.5 X 1.9 in size. Scattered microhaemorrhages in midbrain and cerebellum.
P18	M	80	3 days	CT (5 hours) MRI (48 hours)	SMALL IS - Acute infarct in left premotor cortex.
P19	M	71	15 hours	CT (3> hours) CT (20 hours)	BIG IS - Acute large territory right MCA infarct, involving frontal, temporal, and parietal lobes, insula and basal ganglia.
P20	M	86	3 days	MRI (2> days) CT (8 months before)	SMALL ICH - Acute left occipital ICH, and a few peripheral microhaemorrhages.
P23	M	48	> 2 days	CT (2> days) MRI (3> days)	BIG ICH - Large acute/ subacute right frontal ICH, with multiple microhaemorrhages scattered in both hemispheres.
P24	M	79	27 hours	CT (2 hours) MRI (24 hours)	BIG ICH - Right acute lenticulostrate ICH, 3cm in AP diameter.
P25	F	75	12hours	CT (1 hour)	BIG IS - Large acute left MCA infarct involving parietal and frontal lobe. Small parietal haemorrhagic transformation is visible in second CT.
P26	F	89	3-5 days	CT (1-3 days)	BIG IS - Large acute/ subacute right MCA infarct. 3mm midline shift.
S1	M	31	N/A	N/A	Healthy - volunteer
S2	M	29	N/A	N/A	Healthy - volunteer
S3	F	30	N/A	N/A	Healthy - volunteer
S4	M	43	N/A	N/A	Healthy - volunteer
S5	F	24	N/A	N/A	Healthy - volunteer
S6	M	25	N/A	N/A	Healthy - volunteer
S7	M	21	N/A	N/A	Healthy - volunteer
S8	F	23	N/A	N/A	Healthy - volunteer
S9	F	20	N/A	N/A	Healthy - volunteer
S10	M	38	N/A	N/A	Healthy - volunteer

Table 4-1: Patients' and Subjects' Information.

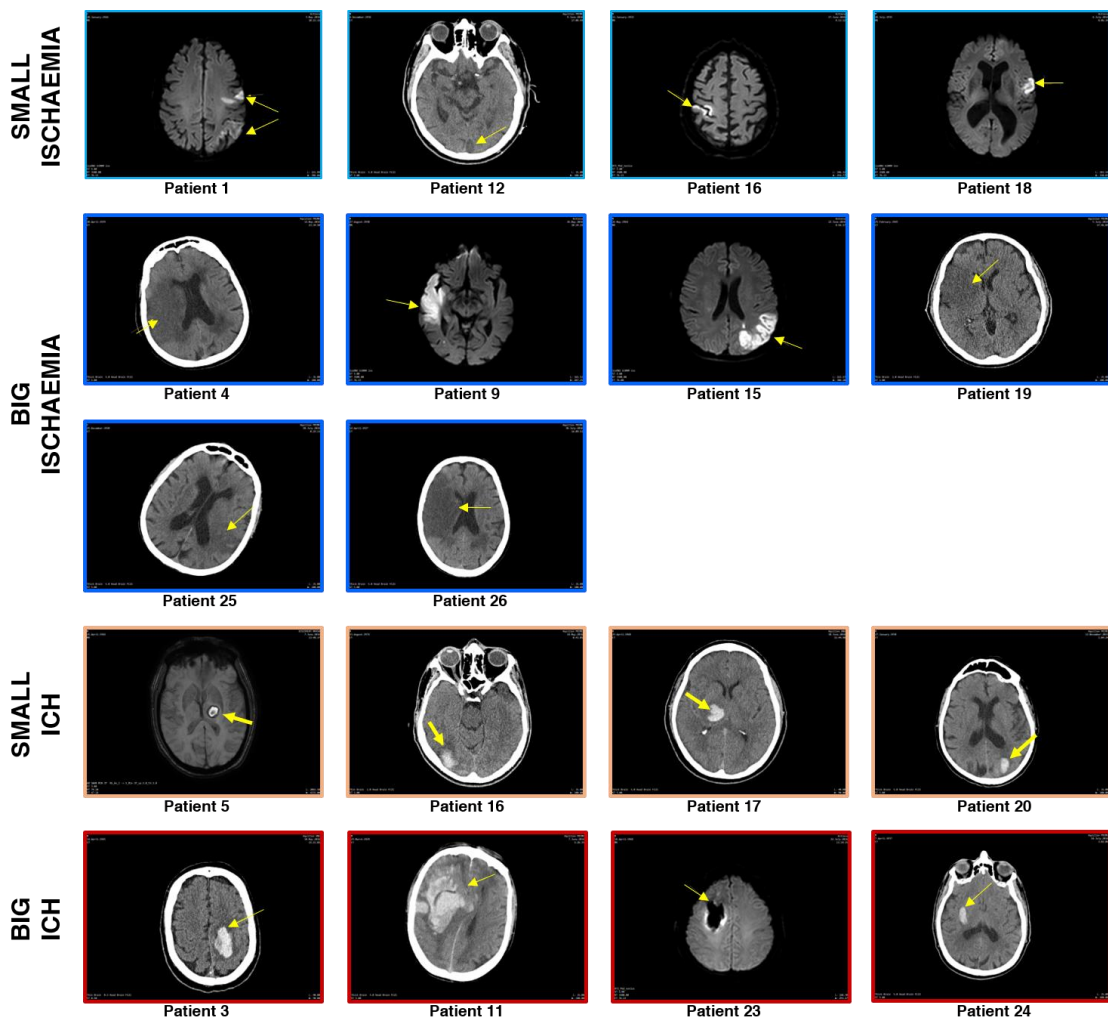


Figure 4-11: Patients' Scans. Small ischaemia (n=4, turquoise frame), Big ischaemia (n=6, blue frame), Small ICH (n=4, orange frame), and big ICH (n=4, red frame). Yellow arrow is pointing to the lesion location for easier identification.

4.5.2 Data Processing

The gain of the BioSemi has a known frequency dependence, resulting from the anti-aliasing filter with the -3dB point at 3 KHz. To account for these changes across frequency, demodulated values were multiplied by an appropriate scaling factor [17]. Similarly, as the injected current amplitude was different across frequency (table 4.2), the results were normalised to maximum current amplitude at 2 KHz. The real component of the voltages was then extracted from the magnitude phase angle as mainly resistive changes were expected within the frequency range [107,135]. Finally, the values from all three collected frames were averaged together, and the final dataset was presented in mV. Data rejection was performed to remove measurements contaminated by artefacts arising from patient movement or faulty electrode contact.

Reference values were calculated from ten datasets in healthy volunteers, and any subsequent value which differed by more than ± 20 mV was removed. To maintain data dimension consistency, removed values were replaced with NaN values.

FREQ. (Hz)	AMP. (μ A)	INJECTION CYCLES	INJECTION TIME (mS)
5	45	32	6,400
10	45	32	3,200
20	45	32	1,600
100	45	32	320
200	90	64	320
300	90	64	213
400	90	64	160
500	90	64	128
600	90	64	107
700	140	64	91
800	140	64	76
900	140	64	71
1000	140	64	64
1200	160	128	107
1350	190	128	95
1700	235	128	75
2000	280	128	64

Table 4-2: Current Injections Properties.

The original data frame contained 992 measurements when taken with a common reference (COM). Adjacent differential data (ADJ) was computed by taking the difference between two adjacent measurements in a pre-set pattern from the original data, (figure 4.4). From the 992 ADJ measurements per frame, a total of 868 were carried through for further analysis after measurements on injection channels were excluded.

Three additional steps which had been used in previous similar studies, were taken to clean the data for statistical analysis [56,57,129]. Very low amplitude data points (< 1 mV) were removed to avoid miniscule changes resulting in high ratios across frequencies. Outlying data points (> 3 STD) to which some statistical tests are sensitive were removed. Finally, channels where the first two steps resulted in the removal of more than 30% of the data across subjects, were completely removed from the dataset.

4.5.3 Datasets for Statistical Analysis:

After processing, four data types were created:

1. Standing BV – amplitude of measured BV at one specific frequency (100, 1000, and 1700 Hz). These contained 654/ 624/ 597 measurements, respectively, per subject/ patient.
2. Symmetry BV – the absolute difference between each right hemisphere BV measurement and its left hemisphere pair, at one specific frequency (100, 1000, and 1700 Hz). These contained 173/ 165/ 153 measurements, respectively, per subject/ patient.
3. Spectral Ratio (SR) – using MF data, each measurement was represented as the ratio between the averaged BV of the 4 lowest frequencies (5-100 Hz) and the averaged BV of the 4 highest frequencies (1000-1700 Hz). This contained 618 measurements per subject/ patient.
4. Symmetry SR – the difference between each right hemisphere SR and its left hemisphere pair. This contained 165 measurements per subject/ patient.

For each of these four types, a subset of the ~ 10% most sensitive measurements, or dry electrode measurements were created in addition.

5. Standing BV Most Sensitive (at 100, 1000, and 1700 Hz) - these contained 71/ 69/ 68 measurements, respectively, per subject/ patient.
6. Symmetry BV Most Sensitive (at 100, 1000, and 1700 Hz) - these contained 23/ 23/ 22 measurements, respectively, per subject/ patient.
7. SR Most Sensitive - this contained 68 measurements per subject/ patient.
8. Symmetry SR Most Sensitive - this contained 23 measurements per subject/ patient.
9. Symmetry SR Dry Locations - This contained 28 measurements per subject/ patient.

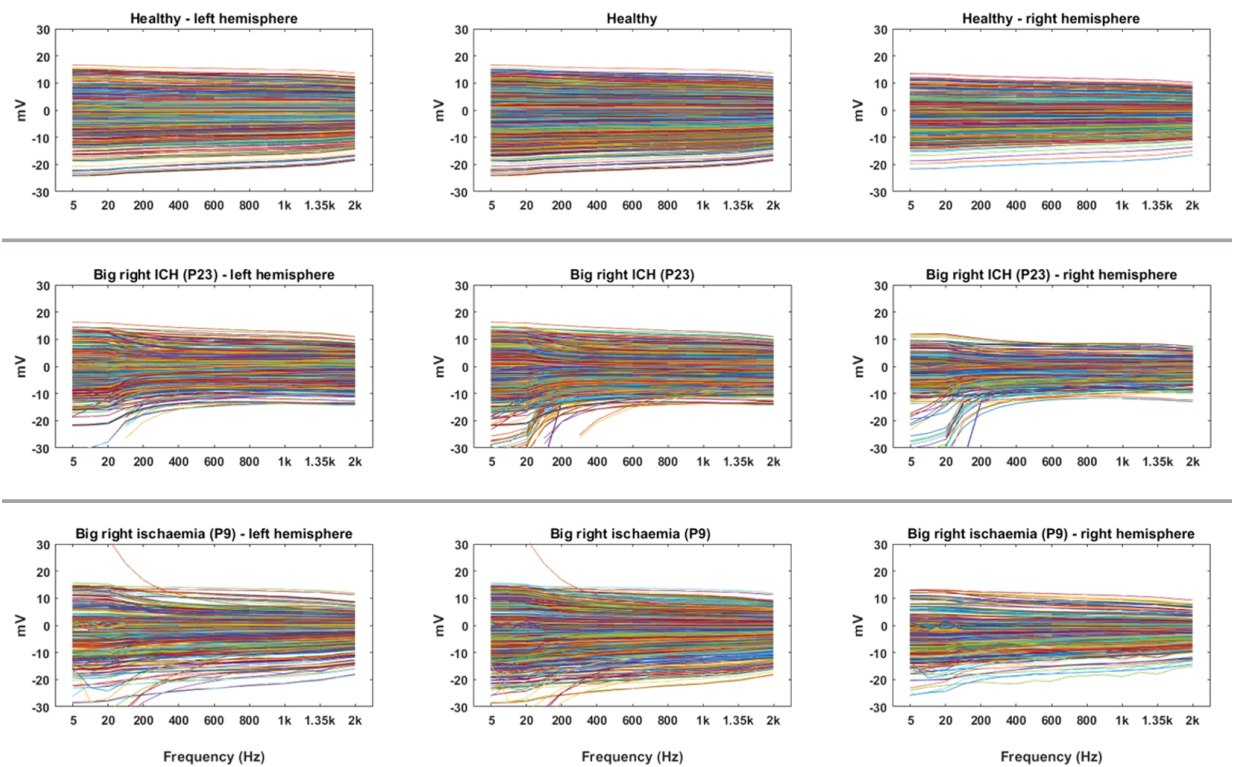


Figure 4-12: Raw MF data Examples from Patients and Healthy Subjects. Examples of raw MF data from healthy subjects, big ICH patients and big IS patients are used for left-right comparison. The middle column displays the complete recorded dataset. On the right of each central column data, right hemisphere measurements are displayed. On the left of each central column data, left hemisphere measurements are displayed. In all subplots X axis are recorded frequencies and Y is recorded BV.

4.5.4 Statistical Analysis

Each dataset described above was used separately to test for significant statistical difference between subjects and patients, and for differences between patients' subgroups according to stroke type (Ischaemia, ICH) and size (Big, Small). Factorial Analysis of Variance (ANOVA) with repeated measures ($\alpha = 0.05$) was used to test for any difference between subjects and patients, and to test for any differences between patients' subgroups.

4.6 Results

4.6.1 Standing BV

At 100 Hz, standing BV amplitude of patients ($n=11,772$) was 4.24 ± 2.71 mV, while BV amplitude of healthy subjects ($n=6,540$) was 4.47 ± 2.83 mV. No statistically significant difference was found between the groups ($F(1,26)= 0.07$, $p= 0.79$). When taking the most sensitive sub dataset ($n_{\text{patients}}= 1,278$, $n_{\text{subjects}}= 710$), standing BV amplitude was 6.44 ± 2.93 mV and 6.70 ± 3.09 mV respectively, also showing no significant statistical difference ($F(1,26)= 4.15$, $p= 0.052$).

At 1000 Hz, standing BV amplitude of patients ($n=11,232$) and healthy subjects ($n=6,240$) was 3.68 ± 2.31 mV and 4.05 ± 2.53 mV, respectively, showed no significant difference when all measurements were incorporated ($F(1,26)= 0.93$, $p= 0.34$). However, when using only the most sensitive measurements ($n_{\text{patients}}= 1,242$, $n_{\text{subjects}}= 690$), average amplitude increased to 5.62 ± 2.59 mV and 6.11 ± 2.79 mV respectively, with significant statistical difference between stroke patients and healthy subjects ($F(1,26)= 4.96$, $p= 0.035$). Using the most sensitive measurements, no significant difference was found between lesion types (ischaemic or haemorrhagic, $F(1,14)= 2.65$, $p= 0.12$) and lesion sizes (big or small, $F(1,14)= 0.0001$, $p= 0.99$).

Similarly, at 1700 Hz when including all measurements ($n_{\text{patients}}= 10,746$, $n_{\text{subjects}}= 5,970$) there was no significant difference between standing BV amplitude of patients and healthy subjects (3.42 ± 2.11 mV and 3.77 ± 2.33 mV, respectively, $F(1,26)= 2.54$, $p= 0.12$). But again, when including only the most sensitive measurements ($n_{\text{patients}}= 1,224$, $n_{\text{subjects}}= 680$), average amplitude increased to 5.25 ± 2.39 mV and 5.73 ± 2.60 mV, with significant statistical difference allowing stroke patients to be distinguished from healthy subjects ($F(1,26)= 5.84$, $p= 0.023$). No significant difference was found between lesion types (ischaemic or haemorrhagic, $F(1,14)= 2.80$, $p= 0.12$) and lesion sizes (big or small, $F(1,14)= 0.01$, $p= 0.91$) using the most sensitive measurements.

4.6.2 BV Left-Right Symmetry

At 100 Hz, BV difference between left and right hemispheres of patients ($n=3,114$) was 0.59 ± 0.78 mV, while BV difference of healthy subjects ($n=1,730$) was 0.42 ± 0.39 mV. No significant difference was found between the groups ($F(1,26)= 2.95$, $p= 0.10$). When using the sensitive sub dataset ($n_{\text{patients}}= 414$, $n_{\text{subjects}}= 230$), BV difference

was 0.89 ± 0.80 mV and 0.69 ± 0.55 mV respectively, also showing no significant difference ($F(1,26) = 2.35$, $p = 0.14$).

At 1000 Hz, BV left-right difference of patients ($n=2,970$) and healthy subjects ($n=1,650$) was 0.60 ± 0.60 mV and 0.44 ± 0.43 mV, respectively, when all measurements were included. A statistically significant difference was found ($F(1,26) = 8.51$, $p = 0.007$). However, no significant difference was found between lesion types (ischaemic or haemorrhagic, $F(1,14) = 0.23$, $p = 0.63$) and lesion sizes (big or small, $F(1,14) = 1.52$, $p = 0.24$) when all measurements were included. When using only the most sensitive measurements ($n_{\text{patients}} = 414$, $n_{\text{subjects}} = 230$), average left-right difference increased to 0.96 ± 0.85 mV and 0.71 ± 0.6 mV respectively, and yet no significant statistical difference was found ($F(1,26) = 3.17$, $p = 0.086$).

Similarly, at 1700 Hz, BV left-right difference of patients ($n=2,754$) and healthy subjects ($n=1,530$) was 0.59 ± 0.60 mV and 0.45 ± 0.45 mV, respectively, when all measurements were included. There was a statistically significant difference ($F(1,26) = 5.11$, $p = 0.032$). But again, no significant difference was found between lesion types (ischaemic or haemorrhagic, $F(1,14) = 0.40$, $p = 0.54$) and lesion sizes (big or small, $F(1,14) = 0.57$, $p = 0.47$) when all measurements were included. When using only the most sensitive measurements ($n_{\text{patients}} = 396$, $n_{\text{subjects}} = 220$), average left-right difference increased to 0.93 ± 0.85 mV and 0.71 ± 0.63 mV respectively, still with no significant statistical difference ($F(1,26) = 2.43$, $p = 0.13$).

	Healthy \leftrightarrow Patients Separation
Standing BV @ 100 Hz – All Measurements	✗
Standing BV @ 100 Hz – Most Sensitive Meas.	✗
Standing BV @ 1000 Hz – All Measurements	✗
Standing BV @ 1000 Hz – Most Sensitive Meas.	✓
Standing BV @ 1700 Hz – All Measurements	✗
Standing BV @ 1700 Hz – Most Sensitive Meas.	✓
Symmetry BV @ 100 Hz – All Measurements	✗
Symmetry BV @ 100 Hz – Most Sensitive Meas.	✗
Symmetry BV @ 1000 Hz – All Measurements	✓
Symmetry BV @ 1000 Hz – Most Sensitive Meas.	✗
Symmetry BV @ 1700 Hz – All Measurements	✓
Symmetry BV @ 1700 Hz – Most Sensitive Meas.	✗
Standing SR – All Measurements	✗
Standing SR – Most Sensitive Meas.	✗
Symmetry SR – All Measurements	✓
Symmetry SR – Most Sensitive Measurements	✓
Symmetry SR – Dry Locations Measurements	✓

Table 4-3: Patients - Healthy Subjects Separation. Datasets where separation between healthy subjects and stroke patients could be achieved are marked in green.

4.6.3 Spectral Ratio (SR)

Computing all measurements, the SR of patients (n= 17,304) was 1.33 ± 0.36 and SR of healthy subjects (n= 6,180) was 1.23 ± 0.18 . The statistical effect was not significant ($F(1,26)= 3.2$, $p= 0.085$). When reducing the number of measurements to the most sensitive only, SR of patients (n= 1,224) and healthy subjects (n= 680) remained similar with 1.29 ± 0.29 and 1.20 ± 0.17 , respectively. Again no significant difference between the groups was found ($F(1,26)= 1.3$, $p= 0.26$).

4.6.4 Spectral Ratio Symmetry

Moving to the difference in SR between left and right hemispheres, patients' measurements (n= 4,620) presented an average of 0.25 ± 0.30 , while healthy subjects (n= 1,650) showed an average of 0.11 ± 0.14 . This difference was significant ($F(1,26)= 13.82$, $p < 0.001$) so patient and subject groups could be distinguished. However, no significant difference was found between lesion types (ischaemic or haemorrhagic, $F(1,14)= 0.14$, $p= 0.72$) and lesion sizes (big or small, $F(1,14)= 0.92$, $p= 0.35$). Similarly, when using only the most sensitive measurements, the average difference between left and right SR was 0.20 ± 0.24 for patients (n=324), while 0.08 ± 0.11 for healthy subjects (n= 180). The difference between patients and subjects stayed significant ($F(1,26)= 9.37$, $p= 0.005$). However, even with the most sensitive measurements, no significant difference was found between lesion types ($F(1,14)= 0.045$, $p= 0.83$) and lesion size ($F(1,14)= 0.006$, $p= 0.94$).

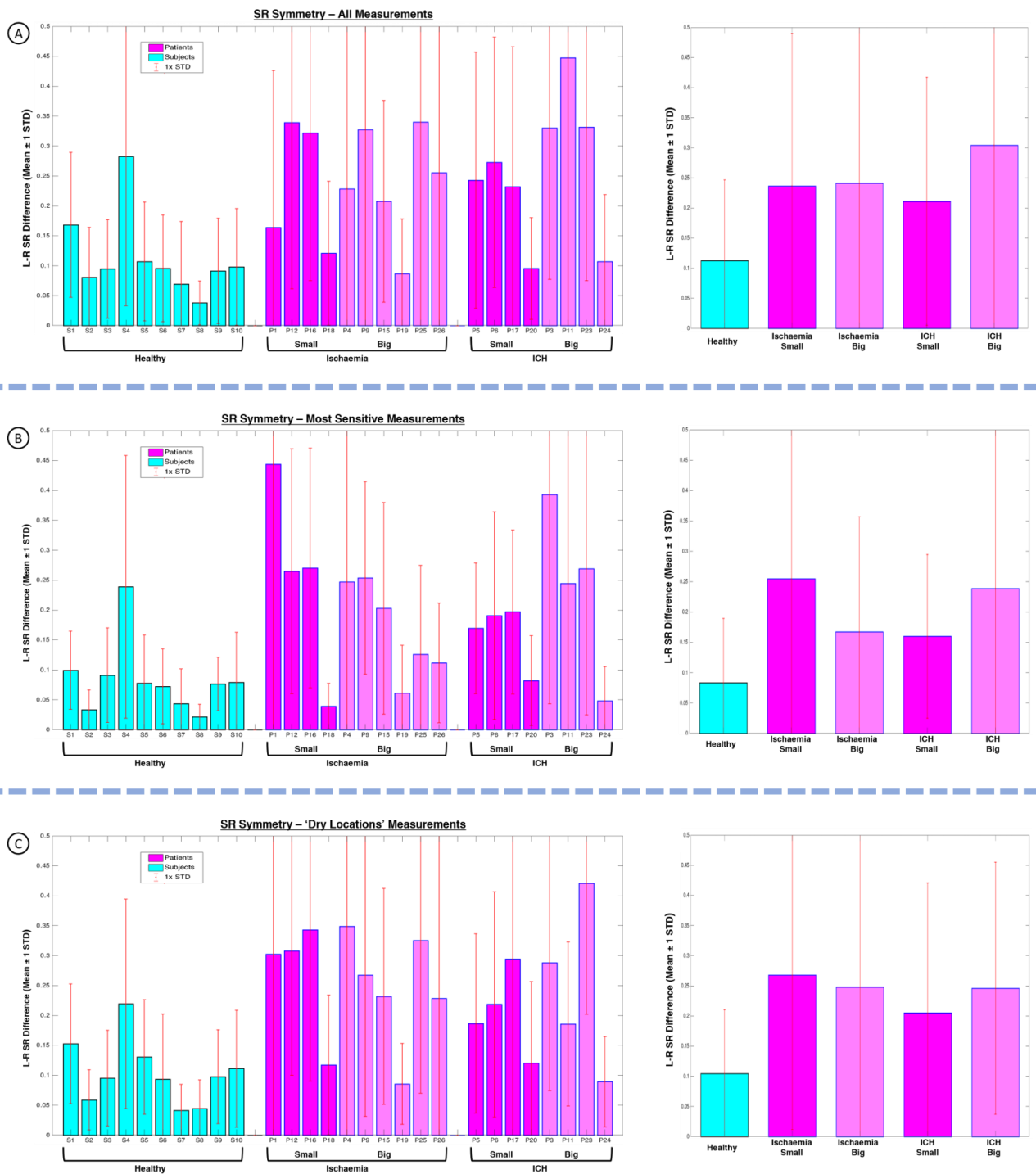
4.6.5 Spectral Ratio Symmetry with Dry Electrode Locations Only

Eventually, when taking left-right SR differences of measurements from 'dry electrodes' locations, patients had an average difference of 0.24 ± 0.25 compared with 0.1 ± 0.11 for healthy subjects. The statistical difference was significant ($F(1,26)= 17.1$, $p < 0.003$). As in all other cases, no significant difference was evident between lesion types ($F(1,14)= 0.042$, $p= 0.53$) and lesion size ($F(1,14)= 0.044$, $p= 0.83$).

	Healthy vs. Patients	Healthy vs. Ischaemia	Healthy vs. ICH	Healthy vs. Big	Healthy vs. Small	Ischaemia vs. ICH	Big vs. Small
Symmetry SR - All Measurements	✓	✓	✓	✓	✓	✗	✗
Symmetry SR - Most Sensitive Measurements	✓	✓	✓	✓	✓	✗	✗
Symmetry SR - Dry Locations Measurements	✓	✓	✓	✓	✓	✗	✗

Table 4-4: Symmetry SR Results Summary. The ability to distinguish between data groups using SR symmetry measurements is marked in green when successful and in red where unsuccessful.

For patients and subjects SR-symmetry data summary, see figure 4-13.



4-13: SR Symmetry Data Summary. Where: (A) Is all measurements (B) 'most sensitive' data subset, and (C) 'dry locations' data subset. Patients' data are marked in purple and subjects' in turquoise. Left column spreads average SR symmetry measurements per patient/ subject, while right column groups these measurements per lesion subtype (healthy, ischaemia – small and big, ICH – small and big).

4.7 Discussion

4.7.1 Summary of Results

4.7.1.1 The UCL Stroke-EIT Dataset

A rich, varied, high quality and well documented human stroke EIT dataset – the first of its kind – has been created and is now publicly available. The computed SNR for these data is ~ 45dB on average, which is double the size of its equivalent SNR in the last stroke EIT clinical pilot [135]. It contains 44 recordings: 24 of acute stroke patients and 20 of healthy volunteers. Data were recorded simultaneously with 32 scalp electrodes at seventeen frequencies between 5 Hz and 2 KHz.

4.7.1.2 Identifying Stroke Patients Using EI Data

BV of stroke patients was about 3.4 mV on average, and controls was about 3.7 mV on average (at 1700 Hz and 235 μ A). BV of healthy volunteers in chapter 2 was about 2.6 mV in average with similar conditions (at 2000 Hz and 250 μ A). While of the same order of magnitude, difference could be the result of the differences in electrode montage and injection protocol. At 1700 Hz, BV left-right difference of patients and controls was about 0.6mV and 0.45 mV, respectively. Distinguishing between subjects and patients was possible using standing BV across the whole head at 1000 Hz and at 1700 Hz, but not at 100Hz. This was achieved using the more sensitive data subsets. Similarly, subjects-patients separation was possible at the same frequencies using L-R BV difference. Surprisingly, this was achieved using all measurements, but was not possible using the more sensitive subset. No subjects-patients separation was possible at 100 Hz.

Average SR in sensitive measurements of patients was about 1.29 and about 1.2 in healthy volunteers. Average SR in sensitive measurements of ICH patients was about 1.28 (1.3 for big ICH and 1.27 for small ICH), and 1.29 for ischaemic patients (1.23 for big ischaemia and 1.37 for small ischaemia). Average SR in sensitive measurements of big lesions patients was about 1.26, and 1.32 for small lesions. Using SR data, separating subjects from patients was not possible when considering measurements from across the whole head, even with the more sensitive subset.

Average SR L-R symmetry of patients was above 0.2, while SR L-R symmetry of healthy volunteers was below 0.1 (less than half of the patients'). Patients–subjects' separation was possible using the full measurements set, the more sensitive subset,

and the 'dry locations' subset. Separation between subjects and patients, using SR L-R symmetry was also possible when considering each patients subgroup (ischaemia, haemorrhage, big or small) separately in comparison with the healthy subjects' group. The ability to distinguish between ischaemic and haemorrhagic stroke, and between small and big lesions could not be achieved.

4.7.2 Significance of Findings

In this study, four different data types were separately analysed to achieve the ability to identify stroke patients (patients–subjects' separation) and to distinguish between stroke types and lesion sizes: standing BV, L-R BV difference, SR, and SR L-R symmetry.

The ability to separate patients from subjects using standing BV was somewhat unexpected as the variability in BV measurements was expected to be high in both groups due to different geometries [90], skin parameters [23,112,166], hair, electrodes allocations, etc. However, these might be the results of difference in CI and SNR between the two groups which was better in subjects compare with of patients even if not significant [69]. The ability to separate patients from subjects using BV L-R difference supports the findings of Bonmassar [22], Seoane [140], and Atefi et al [12,13] which manage to achieve patients–subjects' separation in studies with smaller less diverse cohort. These studies also could not distinguish between ICH and ischaemia.

Measured SR matched the expectation of higher ratio in patients than healthy subjects (~ 1.3 vs. ~1.2). As recent studies suggest, when the skull is intact, impedance measured on the scalp is showing an increase in intracranial impedance for both ischaemic and haemorrhagic lesions [41,170]. This is suspected due to increase in ICP and brain tissue replacing VSF volumes, and might be the explanation for similar average SR for ICH and ischaemia here, both higher than the healthy controls. An unexpected result in both types of lesions was that small lesions exhibit higher average SR than big lesions. Although not fitting the expected trend, a possible explanation for this was that while large lesions impact large portion of the measurements, smaller lesions impact a smaller subset of the measurements but to a larger extent. When sampling the most sensitive 10% of the measurements of each lesion, smaller lesions remain with higher average SR. Indeed, when considering all measurements, average SR for small lesions is about 1.32 while average SR of big lesions

is about 1.37. In any case, patients-subjects separation was not possible using SR data.

Looking at the average BV spectra of the different lesion groups (figure 4.14) it is evident that small lesions of both types is closer in shape to healthy control. Big lesions of both types have a steeper shape, closer in shape to the ‘typical’ spectra shape of ischaemic brain. The spectra of ICH, small or big, is not presenting the expected ‘typical’ flatter spectra shape of blood, but instead similar to ischaemia.

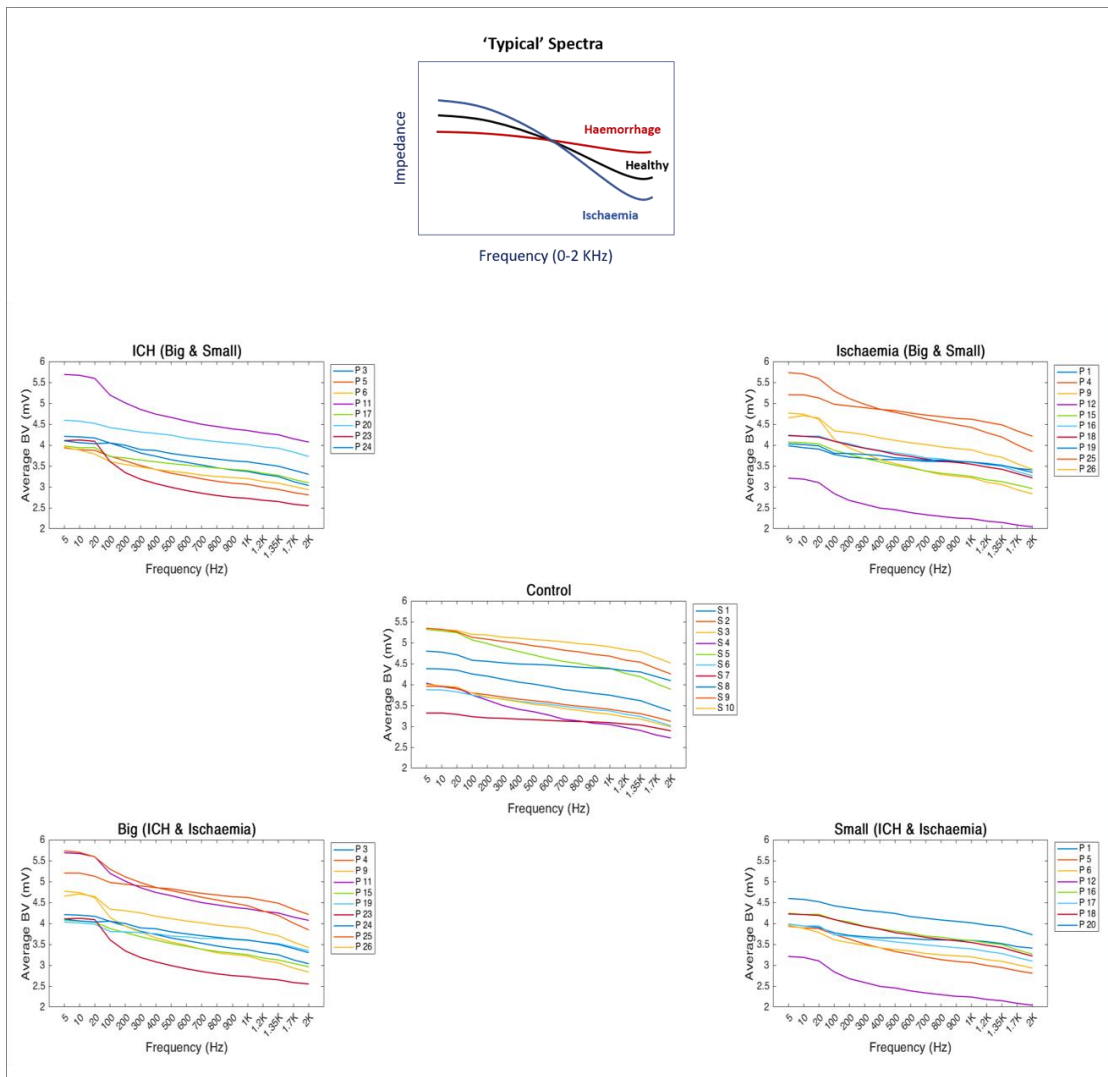


Figure 4.14: Average Spectra of Patients and Healthy Subjects. Each subplot presents a group of subjects/ patients grouped according to lesion type or size. Each line represents the average BV spectra across all measurements of a specific subject/ patient.

The first and last stroke-related EIT clinical pilot at UCLH was conducted in 2006 and included seven patients. Its results showed that it was impossible to observe any reproducible changes in raw data, sensitive channels or images between three patient groups (arteriovenous malformations, brain tumours, and chronic stroke) [135].

However, this study investigated this possibility in a much higher frequency band of 16 – 64 KHz, using less advanced hardware, a different injecting protocol, and was imaging oriented. SR in that study was computed as the ratio between BV amplitude at 64 KHz and 16 KHz.

Out of the four data types, SR L-R symmetry was found to be the most robust method to achieve patient-volunteer separation. The differences between patients and subjects with this data type were the most profound and the separation was possible using both the full set of measurements and the more sensitive subset. Being a method comparing data from the same patient (left and right hemispheres) is making it less prone to a basic limitation of this study, which is the difference in average age of subjects and patients. The SR L-R symmetry is in fact a novel fusion of two existing approaches, left-right symmetry which is now widely investigated [[12,13,22,36,106,115,140](#)], and spectroscopy of bioimpedance reduced to SR [[135](#)]. This fusion has resulted in a positive outcome as to the possibility of eventually verifying stroke or focal structural TBI in pre-hospital settings. This ability to verify a small stroke of any type is important for this method to become trusted in clinical settings. In addition to being a useful option for preliminary triage at the GP or in ambulance level, it can reduce the increasing burden of stroke mimics [[58,67,116](#)], and has the potential to benefit the need in monitoring patients at risk for stroke (TIA, Atrial Fibrillation, anaesthetised patients, etc.). It can alert professional when a change in SR symmetry occurs with monitoring over time.

In addition, the ability to achieve this separation using a subset of ‘dry’ electrodes locations, is supporting the possibility of creating a light and portable system based on a small number of dry electrodes which could be applied to a suspected patient within minutes.

However, in this study, both the ability to differentiate between a small stroke and a big stroke, and the ability to indicate which type of stroke is measured was not proven using any of the data types. Patients suffering from a large territory ischaemia are likely to benefit from being directed to a large stroke centre with mechanical thrombectomy abilities [[29,71,93](#)], and large ICH patients are more likely to need a surgical intervention down the road [[46](#)], hence could also benefit early identification. The ability to rule out ICH is crucial in order provide thrombolysis [[1,59,75](#)].

Nevertheless, further investigation of this database or other similar ones to achieve these goals, using additional methods, could bear fruit in the future. It is pos-

sible that additional information which is not carried by the SR exist in other parameters of the spectra, such as the shape of the average curve, amplitudes, etc. In larger future cohorts, a better characterisation of lesions dividing them into more sub-groups of types, volumes and locations will also help to better determine what are the thresholds of detection and separation. Achieving the first milestone of patients-subjects separation with these data, which has a clinical benefit itself, is a positive indication.

4.7.3 Conclusions

The two principal goals of this study were achieved. The HASU EIT stroke database, a unique, high quality, well documented brain EIT data repository is now available to researchers [69] and is already attracting attention from EIT and stroke researchers. This study has also shown that the information contained in EIS data has the potential to be used for early stroke and TBI diagnostics. The ability to rule-out ICH or to identify Large Vessel Occlusion (LVO) has not been achieved using the data and analysis in this study. The ability to identify stroke patients, and the ability to do it using a small number of electrodes located where dry electrodes might be used, was demonstrated.

The principal conclusion stemming from this study is that EIS for stroke applications has the potential to work, at least for preliminary validation of the existence of a stroke. EIS based techniques appear to offer a way forward with current understanding of impedance spectra behaviour in stroke patients and to develop MF reconstruction algorithms. EIS has the potential to be effective in all the main stroke and TBI applications: verifying structural brain injury, classifying lesion type (ischaemia vs. haemorrhagia, LVO), and monitoring for secondary injury in high risk populations.

Another important methodological conclusion of this study involves the need for continuous active co-operation between clinicians and clinical research staff. The presence of academic researchers in the clinical environment is essential for this. This kind of co-operation is potentially very productive and is required to drive the further development of medical technologies. Developing technology in the laboratory in isolation without communicating with real patients and clinicians in real settings results in misunderstandings of what clinical needs are and what is realistic to expect in a complex clinical environment.

4.7.4 Study Limitations

This study had a few substantial limitations, without forgetting the positive outcomes. A primary limitation was that the healthy subjects control group was not sufficiently well matched to the patient population. Although L-R symmetry should not be dependent on age and gender, a group of healthy controls closer in age, gender and number to the patients would have given a stronger basis to the statistical evidence presented, as age and pathological conditions are correlated with conductivity values of brain tissues [113]. Also, in future, healthy control data should be recorded with subjects in the same position as patients, half-lying on hospital beds.

A second limiting factor was the cohort size. Although this dataset is large and rich in comparison with other existing studies, a cohort which includes more cases of each lesion type, size, and location is required to improve statistics and to achieve differentiation between different brain injuries.

A third significant limitation of this study is the restriction to a relatively narrow, low frequency band. This was an unavoidable technical constraint for this pilot study. Nevertheless, as recent studies have suggested, useful information for brain injury exist in a much wider frequency band of up to 1 MHz [166,168,170]. It is strongly recommended that in future, data are recorded over a much broader spectrum.

4.7.5 Future Work

The driving forces in this project were to acquire data and to investigate the feasibility of the EIT technique for the detection of stroke and TBI. Fortunately, the study yielded some high-quality data, and some positive outcomes. Nevertheless, there are many additional worthwhile areas in this arena requiring further investigation (see Chapter 5).

5 Discussion and Future Work

5.1 Summary of Studies

In chapter 2, drift characteristics and the possible mechanisms for drift were investigated in a series of experiments on phantoms, marrows (giant zucchini), and human volunteers. Initially, this study explored the influence of electrode type on drift and noise. A comparison between three types of scalp electrode over 3.5 hours of continuous measurements found Easycap® electrodes to be the most suitable for long-term monitoring purposes in terms of changes in BV and contact impedance (CI).

In humans, with Easycap® electrodes while injecting 250 μ A at 2 KHz using the 'DE16' protocol, baseline amplitude was 5.4 ± 4.6 mV with a common reference electrode (COM). Over six hours, BV drift presented a clear and significant linear trend, and average hourly drift was 0.41 ± 0.3 %/hour. For measurements taken between adjacent electrodes (ADJ), baseline amplitude was 2.6 ± 1.7 mV, and average hourly drift was 0.5 ± 0.51 %/hour. Electrodes located in the front of the head suffered significantly larger drift than those on the sides and back. No correlation was found to changes in local temperature. Slow fluctuating noise around the baseline was the order of $\sim 1.5\%$, medium fluctuating noise (0.0015-0.015 Hz) was in the order of $\sim 0.75\%$, and fast fluctuations noise (> 0.1 Hz) was in the order of $\sim 0.4\%$. CI in human subjects was 785 ± 285 Ohms at the beginning of the recordings and demonstrated linear change over time. Averaged hourly change was 1.9 %/hour. A moderate to high correlation was found between CI change in an electrode and its related BV drift.

System drift quantified on a resistor phantom was in the order of 0.05 %/hour, and when recorded on a head-shaped tank filled with saline it increased to ~ 0.2 %/hour. When recorded on a marrow (giant zucchini), drift slightly increased with frequency and its real component was dominant. The system drift was found to be amplified by the medium but not enough to explain the whole drift phenomenon. The presence of gel between the electrode and marrow's skin effected both CI and BV drift. As expected, the CI of the electrodes with gel ('wet') was lower (half) of those without gel ('dry'), and changed significantly less over the time of recording. However, BV drift was significantly higher when injecting with wet electrodes, and only slightly lower when recording with wet electrodes.

Chapter 3 described the unique approach taken to explore the feasibility of EIT imaging of brain injury by combining simulated data with real BV drift measurements recorded over several hours. This study found a low feasibility for correctly imaging brain injury with EIT when signals are not corrected for drift. Even with low drift figures of 0.5 %/hour (0.01 mV/ hour) on average, and lesions developing to a large volume of 25 ml, the best success rates were 44% (a large ICH located in the back). The rest of the cases had even lower success rates. In general, lesion type and location had a significant effect on success rates: ICH were more detectable than ischaemic lesions as expected, while frontal lesions were least detectable from all four locations (front, side, back, and centre).

Chapter 4 describes a pilot study of EIT applied to clinical stroke patients. A unique high-quality dataset was collected and documented, which is now available to the research community [69]. This dataset contains MF EI data from 32 channels at 17 frequencies in the range 5 Hz – 2 KHz. It includes 44 recordings: 24 of acute stroke patients and 20 of healthy volunteers. MF data were analysed in the form of standing BV and spectra ratios (SR), across the whole head and as symmetry between hemispheres. Significant differences ($p < 0.05$) between healthy controls and stroke patients were found for the first time in a large cohort, while using a sub-set of electrodes located in 'dry-locations' (around the hair-line).

Using standing BV data, distinguishing between subjects and patients was possible at 1000 Hz and at 1700 Hz, but not at 100 Hz. Using SR data, separating subjects from patients was possible while using SR left-right symmetry when considering the full set of measurements, as well as when using the more sensitive subset. It was also possible when considering the 'dry locations' subset. Separation between subjects and patients, using SR L-R symmetry was also possible when considering each patients subgroup (ischaemia, haemorrhage, big or small) separately in comparison with the healthy subjects' group. No distinction between ischaemic and haemorrhagic stroke could be achieved.

5.2 Discussion

The overall objective of the work in this thesis was to bring the application of EIT in brain injury closer to clinical use. Overall, the results of this project support the feasibility of EI applied to brain injury in a clinical environment.

5.2.1 Drift in TD-EIT

Investigating the drift in TD-EIT was a fundamental part of this research. A thorough quantification of drift was established and questions regarding the nature of the drift were addressed although no mechanism has yet been found to reliably eliminate it. This study also explored the influence of electrode type choice and different measurement conditions for TD monitoring.

Drift quantified in this study was found to be very low, at least an order of magnitude lower than previously estimated [23]. It was still found to be consistent over many hours, probably accumulating to be substantial with time. Easycap electrodes suffered lower drift and noise than the other types used. The same three electrode types were formerly compared for EIT imaging in humans by Tidswell et al [150], and the Hydrogel electrodes were chosen as most suitable. However, a recent study by Yang et al [167] supports these findings by showing that a combination silver/ silver chloride electrode and low viscosity conductive gel performs best over time and frequency, so are the best combination for use in EIT.

A theoretical and simulation study by Luppi Silva et al (2016), suggested that common reference measurements are better for EIT applications [104]. In this study, comparing adjacent electrode measurements with common reference measurements found that while similar proportional drift is found in both (0.4 and 0.5 %/hour respectively), adjacent measurements suffered lower drift in terms of absolute BV change (0.02 and 0.01 mV/hour respectively). This suggests that ADJ measurements might result in less distorted images.

Initial findings regarding the mechanism causing the drift suggest a few possible causes. It was shown that drift is correlated with change in CI and is most likely to originate from drift in the injected current. In this study, electrodes in the frontal area suffered a larger drift, although a study by Yang et al [166], claimed electrodes on the forehead to have lower CI. It is still unclear whether the change in CI is causing the drift, or whether a local impedance change in the skin causes both. Temperature change near the scalp, system drift, and electrode movement were all found to be less likely to cause drift.

The main limitation of this study is that it was limited to low frequency (up to 2KHz), due to the available system's design. Another limitation was that this was a relatively crude exploration of any correlation between drift and potential mecha-

nisms. A more thorough study of the changes in the electrode-gel-skin complex over time should be the next step.

5.2.2 Feasibility of TD-EIT in Monitoring Head Injury

The feasibility question regarding the application of TD-EIT as a non-invasive bedside monitoring technique was addressed. Following this investigation, there is strong evidence to conclude that detecting even a large ICH (25 ml) which develops over a relatively short period of an hour in the human cortex is approaching 50% likelihood to be imaged with TD-EIT. The likelihood of detecting smaller bleeds, large ischemic lesions, and lesions developing over longer time periods is much less. These findings suggest that the problem of BV drift must be addressed for TD-EIT to be considered a viable clinical option.

5.2.3 The UCLH Stroke-EIT Dataset and EIS for Stroke Diagnosis

The UCLH EIT stroke dataset is unique and to the best of our knowledge the first of its kind. Its recording was high quality (SNR ~ 45 dB on average), well documented and available to all. It is the largest available dataset and contains 14 IS, 10 ICH, and 20 healthy usable recordings (including individuals recorded twice). It also has multi-frequency (17) and multi-channel (32) data, and hence is useful to both the EIT and EIS research communities.

This work yielded new evidence supporting the possibility of diagnosing brain injury using left-right asymmetry. Raw spectra of both ischaemic and haemorrhagic stroke patients was consistent with known spectra of human brain tissue [82,113] with measurements on rabbits performed by Yang et al [168] and on rats performed by Dowrick et al [49]. Stroke types could not be discriminated, similarly to the results reported by Atefi et al [140]. It is possible that classifying stroke types is difficult because both involve a similar increase in impedance when the skull is intact [41,159,168]. This also might explain the difference often observed in imaging results of simulations and animal models [50], suggesting more complex models of both stroke types are needed.

A major limitation of this dataset is its restriction to low frequencies below 3 KHz due to the available instrumentation [17]. Recent studies by Yang et al, characterizing stroke tissues in-vivo and ex-vivo in animal models and CI spectra in humans, recommended a frequency range between 10 Hz and 1 MHz for brain injury applications [166,168,170]. Further limitations of this study that should be addressed in future da-

ta collections, are the lack of matching between patients and controls for size, age, gender, race, and recording conditions, and the need for a much larger cohort.

5.3 Recommendations for Future Work

Considering all the findings of this study and recent reports in the published literature, especially recent work by Atefi et al [[11](#),[12](#),[13](#),[140](#)] and Yang et al [[166](#),[167](#),[168](#),[169](#),[170](#)], research efforts should be directed towards EIS at frequencies in the range of 0–1 MHz.

The EIT group at UCL has already devoted significant effort to exploring the application of EIT to brain imaging. It is now timely to examine how stroke and TBI patients could benefit from EI technology. EIS, instead of EIT, has the potential to assist all three main applications (diagnosing stroke, classification of stroke types, and monitoring brain injury over time), and to get there much sooner than EIT. For monitoring, a TD-EIS system could be used, similar to that described by Zhou et al (2017) [[171](#)] for a cardio-pulmonary feasibility study.

Although electrical impedance-based imaging will never replace imaging technologies such as MRI and CT, it has the potential to offer clinicians a reliable indication of whether a brain injury exists, what type of injury it is, and its approximate location in the brain. All this information could potentially be provided by EIS, without the complexity of image reconstruction, which currently consumes a major proportion of research resources. EIS also has additional technical advantages, such as reducing the number of electrodes and thereby reducing the electrode application time. The possibility of positioning electrodes solely on hairless areas (forehead, behind ears, beneath inion etc.) could permit the use of ECG-like electrodes and avoid the need for an EIT electrode cap.

If EIS is developed further for these applications, spectral patterns and symmetry/asymmetry indices could become the basic injury marker, and machine learning algorithms could use these indices when much larger datasets are recorded.

5.3.1 Drift Investigations for TD-EIT

A possible future advance would be to explore the development of statistical models to use CI changes around the electrodes, and BV drift with time, to predict future BVs from the CI data. Yang et al [[166](#)] showed that the imbalance between the CIs of two measuring electrodes affects the contribution of CI to a change in BV. Such a statistical model might use local impedance measurement to predict a drift free base-

line in measurements across the body under investigation. These predictions could then be used either to clean those measurements to benefit image reconstruction, or as a baseline in an EI- based method, enabling users to be alerted to measurements that diverge significantly from the predicted baseline (e.g. as an indication of possible developing pathology). A focused study investigating the changes in the electrode-gel-skin complex over time (hours), is also needed. Yang et al [[166](#)] studied this complex over the frequency range of 10 Hz – 1 MHz, and an equivalent investigation in the time domain would be useful.

Another potential idea is to apply and test a compensation method that has been published by the GE Global Research Centre [[26](#)]. In this paper, the researchers (who had previously worked in close collaboration with our UCL EIT group) used a Discrete CI Model to compensate for drift and improved distinguishability between two datasets without imaging.

In any case, if a method for compensating for drift is established, it is highly recommended that a feasibility study such as the one conducted in chapter 3 should be repeated.

5.3.2 EIS for Stroke and TBI Applications

Strengthening and refining the findings of this study are recommended. An example could be the quantifying of the magnitude and spatial distribution of asymmetry for different clinical cases. Determining the minimum detectable lesion is also important to assess the potential usefulness of this technique. Optimisation of data cleaning procedures for this technique would increase its sensitivity, as would scanning methods for symmetry/ a-symmetry in smaller areas of both hemispheres, similar to the approach taken by Romsauerova et al [[135](#)].

It would also be highly beneficial for advancing EIS applications to collect more data on a larger and more diverse cohort, with a matched control group of healthy volunteers to patients and with a wider frequency band.

Another direction could be to refine the method itself, i.e. reducing the number of electrodes needed, perhaps by applying PCA, ICA or similar methods to the existing data. The instrumentation could be reduced to a tablet-sized device with 4-8 ECG-like electrodes located on the forehead, temples, behind the ears and back of the head beneath the hairline. This could be applied in less than 5 minutes, and within another 5 minutes of data collection and processing a machine learning-based output would appear on the screen. This kind of device could potentially facilitate a pre-

hospital diagnosis and be used in bedside monitoring in stroke units, NICUs, and for patients at high risk of stroke.

All these opportunities for future studies are very exciting and completing them in the near future would help to bring EIT/EIS into clinical use for brain injury.

Acronyms

ADJ - Adjacent electrodes measurement

BBB - Blood-Brain Barrier

BV - Boundary Voltages

CBF - Cerebral Blood Flow

CI - Contact Impedance

COM - Common reference electrodes measurement

CPP - Cerebral Perfusion Pressure

CRF - Case Record Form

DAI - Diffused Axonal Injury

DE - Drift Elimination (reciprocity based)

EBJ - Electrode Boundary Jacobian

EDH - Extradural Haematoma

EIS - Electrical Impedance Spectroscopy

EIT - Electrical Impedance Tomography

EME - Electrode Movement Elimination

EZ electrodes - Easycap easy to apply silver-silver chloride electrodes

FD - Frequency Difference

FEM - Finite Element Model

GCS - Glasgow Coma Scale

HASU - Hyper Acute Stroke Unit

HCL - Haemorrhagic Contusions and Lacerations

HD electrodes - HydroDot Fast applying hydro-gel electrodes

HE - Haematoma Expansion

HS - Haemorrhagic Stroke

HT - Haemorrhagic Transformations

ICH - Intracerebral Haemorrhage

ICP - Intracranial Pressure
IS - Ischaemic Stroke
IVH - Interventricular Haemorrhage
MF - Multi-Frequency
MMM - Multi-Modality Monitoring
NICE - National Institute for Health and Care Excellence
NICU - Neurointensive Care Unit
NIHSS - National Institutes of Health Stroke Scale
NSU - Neuroscience Units
R&D - Research and Development
SAH - Subarachnoid Haemorrhage (SAH)
SDH - Subdural Haematoma
SNR - Signal to Noise Ratio
SVD – Singular Value Decomposition
TBI - Traumatic Brain Injury
TD - Time-Difference
TIA - Transient Ischaemic Attack
tPA - tissue Plasminogen Activator
UCLH - University College London Hospital

References

- [1] (2008). Stroke and transient ischaemic attack (TIA). In *NICE clinical guideline 68*. Retrieved from <http://www.nice.org.uk/guidance/cg68>
- [2] (2013). Stroke rehabilitation: Long-term rehabilitation after stroke. In *NICE clinical guideline 162*. Retrieved from <http://www.nice.org.uk/guidance/cg162>
- [3] (2014). Triage, assessment, investigation and early management of head injury in children, young people and adults. In *NICE clinical guideline 176*. Retrieved from <http://www.nice.org.uk/guidance/cg176>
- [4] Abascal, J.P., Arridge, S.R., Atkinson, D., Horesh, R., Fabrizi, L., De Lucia, M., Horesh, L., Bayford, R.H., & Holder, D.S. (2008). Use of anisotropic modelling in electrical impedance tomography; Description of method and preliminary assessment of utility in imaging brain function in the adult human head. *NeuroImage*, 43, 258-268. [doi: 10.1016/j.neuroimage.2008.07.023](https://doi.org/10.1016/j.neuroimage.2008.07.023)
- [5] Adler, A., & Lionheart, W. R. B. (2006). Uses and abuses of EIDORS: an extensible software base for EIT. *Physiological Measurement*, 27(5), S25–42. [doi:10.1088/0967-3334/27/5/S03](https://doi.org/10.1088/0967-3334/27/5/S03)
- [6] American Clinical Neurophysiology Society. (2006). Guidelines for standard electrode position nomenclature. *J. Clin. Neurophysiology*, 23(2), 107-110. [doi:10.1097/00004691-200604000-00006](https://doi.org/10.1097/00004691-200604000-00006)
- [7] Arimura, K., Imamura, H., Todo, K., Tani, S., Adachi, H., Hoshi, T., ... & Sakai, N. (2017). Intracranial hemorrhage after endovascular revascularization for acute ischemic stroke. *J Neuroendovascular Therapy*, 11(8), 391-397. [doi:10.5797/jnet.oa.2016-0089](https://doi.org/10.5797/jnet.oa.2016-0089)
- [8] Aristovich, K. Y., dos Santos, G. S., & Holder, D. S. (2015). Investigation of potential artefactual changes in measurements of impedance changes during evoked activity: implications to electrical impedance tomography of brain function. *Physiological Measurement*, 36(6), 1245–1259. [doi:10.1088/0967-3334/36/6/1245](https://doi.org/10.1088/0967-3334/36/6/1245)
- [9] Aristovich, K. Y., dos Santos, G. S., Packham, B. C., & Holder, D. S. (2014). A method for reconstructing tomographic images of evoked neural activity with electrical impedance tomography using intracranial planar arrays. *Physiological Measurement*, 35(6), 1095–1109. [doi:10.1088/0967-3334/35/6/1095](https://doi.org/10.1088/0967-3334/35/6/1095)

- [10] Aristovich, K. Y., Packham, B. C., Koo, H., dos Santos, G., S., McEvoy, A., & Holder, D. S. (2016). Imaging fast electrical activity in the brain with electrical impedance tomography. *NeuroImage*, 124, 204–213.
[doi:10.1016/j.neuroimage.2015.08.071](https://doi.org/10.1016/j.neuroimage.2015.08.071)
- [11] Atefi, S. R. (2015). *Electrical Bioimpedance Cerebral Monitoring: From Hypothesis and Simulations to First Experimental Evidence in Stroke Patients (PhD thesis)*. Royal Institute of Technology, Sweden. Retrieved from <http://www.diva-portal.org/smash/record.jsf?pid=diva2%3A868058&dswid=-9506>
- [12] Atefi, S. R., Seoane, F., Rosenthal, E. S., & Lev, M. H., Bonmassar, G. (2016). Intracranial hemorrhage alters scalp potential distribution in bioimpedance cerebral monitoring: Preliminary results from FEM simulation on a realistic head model and human subjects. *Medical Physics*, 43(2), 675-686.
[doi:10.1118/1.4939256](https://doi.org/10.1118/1.4939256)
- [13] Atefi, S. R., Seoane, F., Thorlin, T., & Lindecrantz, K. (2013). Stroke damage detection using classification trees on Electrical Bioimpedance Cerebral Spectroscopy measurements. *Sensors*, 13(8). 10074–10086.
[doi:10.3390/s130810074](https://doi.org/10.3390/s130810074)
- [14] Auerbach, P. S., Baine, J. G., Schott, M. L., Greenhaw, A., Acharya, M. G., & Smith, W. S. (2015). Detection of concussion using cranial accelerometry. *Clin J Sport Med*. 25(2), 126–132. [doi: 10.1097/jsm.0000000000000117](https://doi.org/10.1097/jsm.0000000000000117)
- [15] Avery, J. (2015). *Improving Electrical Impedance Tomography of brain function with a novel servo-controlled electrode helmet (PhD thesis)*. University College London, London. Retrieved from <https://discovery.ucl.ac.uk/id/eprint/1469345/3/thesis.pdf>
- [16] Avery, J., Aristovich, K., Low, B., and Holder, D. (2017). Reproducible 3D printed head tanks for electrical impedance tomography with realistic shape and conductivity distribution. *Physiological Measurement*, 38(6), 1116-1131.
[doi:10.1088/1361-6579/116586](https://doi.org/10.1088/1361-6579/116586)
- [17] Avery, J., Dowrick, T., Faulkner, M., Goren, N., & Holder, D. (2017). A versatile and reproducible multi-frequency Electrical Impedance Tomography system. *Sensors*, 17,280. [doi:10.3390/s17020280](https://doi.org/10.3390/s17020280)
- [18] Ayaz, H., Izzetoglu, M., Izzetoglu, K., Onaral, B., & Ben, B. (2019). Early diagnosis of traumatic intracranial hematomas. *Journal of Biomedical Optics* 24(5), 051411. [doi: 10.1117/1.JBO.24.5.051411](https://doi.org/10.1117/1.JBO.24.5.051411)

- [19] Bagshaw, A. P., Liston, A. D., Bayford, R. H., Tizzard, A., Gibson, A. P., Tidswell, A. T., Sparks, M.K., Dehghani, H., Binnie, C.D., & Holder, D. S. (2003). Electrical impedance tomography of human brain function using reconstruction algorithms based on the finite element method. *NeuroImage*, 20(2), 752–64. doi:
[10.1016/S1053-8119\(03\)00301-X](https://doi.org/10.1016/S1053-8119(03)00301-X)
- [20] Balami, J. S., & Buchan, A. M. (2012). Complications of intracerebral haemorrhage. *The Lancet. Neurology*, 11(1), 101–118. doi:[10.1016/S1474-4422\(11\)70264-2](https://doi.org/10.1016/S1474-4422(11)70264-2)
- [21] Balami, J. S., Chen, R. L., Grunwald, I. Q., & Buchan, A. M. (2011). Neurological complications of acute ischaemic stroke. *The Lancet Neurology*, 10(4), 357–371. doi:[10.1016/S1474-4422\(10\)70313-6](https://doi.org/10.1016/S1474-4422(10)70313-6)
- [22] Bonmassar, G., Iwaki, S., Goldmakher, G., Angelone, L. M., Belliveau J. W., & Lev, M. H. (2010). On the measurement of electrical impedance spectroscopy (EIS) of the human head, *International Journal of Bioelectromagnetism*, 12(1), 32–46. Retrieved from <https://www.ncbi.nlm.nih.gov/pmc/articles/PMC2997709/>
- [23] Boone, K. G., & Holder, D. S. (1996). Effect of skin impedance on image quality and variability in electrical impedance tomography: a model study. *Medical & Biological Engineering & Computing*, 34(5), 351–354. Retrieved from <http://www.ncbi.nlm.nih.gov/pubmed/8945858>
- [24] Boone, K., Lewis, a M., & Holder, D. S. (1994). Imaging of cortical spreading depression by EIT: implications for localization of epileptic foci. *Physiological Measurement*, 15 Suppl 2, A189–98. doi: [10.1088/0967-3334/17/4/001](https://doi.org/10.1088/0967-3334/17/4/001)
- [25] Boone, K.G., & Holder, D.S. (1996). Current approaches to analogue instrumentation design in electrical impedance tomography. *Physiological Measurement*, 17(4), 229-247. doi:[10.1088/0967-3334/17/4/001](https://doi.org/10.1088/0967-3334/17/4/001)
- [26] Boverman, G., Kao, T. J., Wang, X., Ashe, J. M., Davenport, D. M., & Amm, B. C. (2016). Detection of small bleeds in the brain with electrical impedance tomography. *Physiological Measurement*, 37(6), 727–750. doi:[10.1088/0967-3334/37/6/727](https://doi.org/10.1088/0967-3334/37/6/727)
- [27] Boyle, A., & Adler, A. (2011). The impact of electrode area, contact impedance and boundary shape on EIT images. *Physiological Measurement*, 32(7), 745–754. doi:[10.1088/0967-3334/32/7/S02](https://doi.org/10.1088/0967-3334/32/7/S02)
- [28] BrainScope Peer Review Articles. (2020). Retrieved April 29, 2020, from <https://brainscope.com/peer-review-landing>

- [29] Brandler, E. S., & Baksh, N. (2019). Emergency management of stroke in the era of mechanical thrombectomy. *Clin Exp Emerg Med*, 6(4), 273–287. doi: [10.15441/ceem.18.065](https://doi.org/10.15441/ceem.18.065)
- [30] Brott, T., Jr, H. P. A., Olinger, C. P., Marler, J. R., Barsan, W. G., Biller, J., ... & Walker, M. (1989). Measurements of acute cerebral infarction: A clinical examination scale. *Stroke*, 20(7), 864–870. doi: [10.1161/01.STR.20.7.864](https://doi.org/10.1161/01.STR.20.7.864)
- [31] Brown, B. H. (2003). Electrical impedance tomography (EIT): a review. *Journal of Medical Engineering & Technology*, 27(3), 97–108. doi: [10.1080/0309190021000059687](https://doi.org/10.1080/0309190021000059687)
- [32] Cammarata, G., Ristagno, G., Cammarata, A., Mannanici, G., Denaro, C., & Gullo, A. (2011). Ocular ultrasound to detect intracranial hypertension in trauma patients. *The Journal of Trauma*, 71(3), 779–781. doi: [10.1097/TA.0b013e3182220673](https://doi.org/10.1097/TA.0b013e3182220673)
- [33] Cao, L., Li, H., Fu, D., Liu, X., Ma, H., Xu, C., Dong, X., Yang, B., & Fu, F. (2020). Real-time imaging of infarction deterioration after ischemic stroke in rats using electrical impedance tomography. *Physiological Measurement*, 41(1), 015004. doi: [10.1088/1361-6579/ab69ba](https://doi.org/10.1088/1361-6579/ab69ba)
- [34] Carlson, A. P., & Yonas, H. (2012). Portable head computed tomography scanner- technology and applications: experience with 3421 scans. *Journal of Neuroimaging*, 22(4), 408–415. doi: [10.1111/j.1552-6569.2011.00621.x](https://doi.org/10.1111/j.1552-6569.2011.00621.x)
- [35] Chatrian, G. E., Lettich, E., & Nelson, P. L. (1988). Modified Nomenclature for the 10% Electrode System. *J. Clin. Neurophysiology*. 5(2), 183-186. Retrieved from <https://www.ncbi.nlm.nih.gov/pubmed/3250964>
- [36] Cohen, R., Abboud, S., & Arad, M. (2015). Monitoring brain damage using bioimpedance technique in a 3D numerical model of the head. *Medical Engineering & Physics*, 37(5), 453–459. doi: [10.1016/j.medengphy.2015.02.011](https://doi.org/10.1016/j.medengphy.2015.02.011)
- [37] Coles, J. P. (2007). Imaging after brain injury. *British Journal of Anaesthesia*, 99(1), 49–60. doi: [10.1093/bja/aem141](https://doi.org/10.1093/bja/aem141)
- [38] Cyrus, A., O'Neal, B., & Freeman, W. D. (2012). New approaches to bedside monitoring in stroke. *Expert Review of Neurotherapeutics*, 12(8), 915–928. doi: [10.1586/ern.12.85](https://doi.org/10.1586/ern.12.85)
- [39] Czosnyka, M., Matta, B. F., Smielewsky, P., Kirkpatrick, P. J., Pickard, J. D. (1998). Cerebral perfusion pressure in head-injured patients: a noninvasive as-

- assessment using transcranial Doppler ultrasonography. *Journal of neurosurgery*, 88: 802–808. [doi: 10.3171/jns.1998.88.5.0802](https://doi.org/10.3171/jns.1998.88.5.0802)
- [40] Dai, M., Li, B., Hu, S., Xu, C., Yang, B., Li, J., Fu, F., Fei, Z., & Dong, X. (2013). In vivo imaging of twist drill drainage for subdural hematoma: a clinical feasibility study on electrical impedance tomography for measuring intracranial bleeding in humans. *PloS One*, 8(1), e55020. [doi:10.1371/journal.pone.0055020](https://doi.org/10.1371/journal.pone.0055020)
- [41] Dai, M., Liu, X., Li, H., Xu, C., Yang, B., Wang, H., Shi, X., Dong, X., & Fu, F. (2018). EIT imaging of intracranial hemorrhage in rabbit models is influenced by the intactness of cranium. *BioMed Research International*, Vol 2018, Article ID: 1321862. [doi: 10.1155/2018/1321862](https://doi.org/10.1155/2018/1321862)
- [42] Dalbayrak, S., Gumustas, S., Bal, A., & Akansel, G. (2011). Early and delayed CT findings in patients with mild-to-moderate head trauma. *Turkish Neurosurgery*, 21(4), 591–598. [doi: 10.5137/1019-5149.JTN.3570-10.2](https://doi.org/10.5137/1019-5149.JTN.3570-10.2)
- [43] Dambinova, S. A., Bettermann, K., Glynn, T., Tews, M., Olson, D., Weissman, J. D., & Sowell, R. L. (2012). Diagnostic potential of the NMDA receptor peptide assay for acute ischemic stroke. *PLoS ONE*, 7(7), e42362. [doi:10.1371/journal.pone.0042362](https://doi.org/10.1371/journal.pone.0042362)
- [44] Dambinova, S. A., Maroon, J. C., Sufrinko, A. M., Mullins, J. D., Alexandrova, E. V., & Potapov, A. A. (2016). Functional, structural, and neurotoxicity biomarkers in integrative assessment of concussions. *Frontiers in Neurology*, 7, Article 172. [doi:10.3389/fneur.2016.00172](https://doi.org/10.3389/fneur.2016.00172)
- [45] Darde, J., Hakula, H., Hyvonen, N., & Staboulis, S. (2012). Fine-tuning electrode information in electrical impedance tomography. *Inverse Problems Imaging*, 6(3) 399-421. [doi:10.3934/ipi.2012.6.399](https://doi.org/10.3934/ipi.2012.6.399)
- [46] Dastur, C. K., & Yu, W. (2017). Current management of spontaneous intracerebral haemorrhage. *Stroke and Vascular Neurology*, 2017(2), e000047. [doi: 10.1136/svn-2016-000047](https://doi.org/10.1136/svn-2016-000047)
- [47] Dietrich, M., Ragoschke-Schumm, A., Helwig, S., Levine, S., Balucani, C., Lesmeister, M., Haass, A., Liu, Y., Lossius, H. M., & Fassbender, K. (2014). Is prehospital treatment of acute stroke too expensive? An economic evaluation based on the first trial. *Cerebrovascular diseases*, 38, 457–463. [doi:10.1159/000371427](https://doi.org/10.1159/000371427)

- [48] Domenicucci, M., Signorini, P., Strzelecki, J., & Delfini, R. (1995). Delayed post-traumatic epidermal haematoma. A review. *Neurosurgical review*, 18, 109-122. doi: [10.1007/BF00417668](https://doi.org/10.1007/BF00417668)
- [49] Dowrick, T., Blochet, C., & Holder, D. (2015). In vivo bioimpedance measurement of healthy and ischaemic rat brain: implications for stroke imaging using electrical impedance tomography. *Physiological Measurement*, 36(6), 1273-1282. doi:[10.1088/0967-3334/36/6/1273](https://doi.org/10.1088/0967-3334/36/6/1273)
- [50] Dowrick, T., Blochet, C., & Holder, D. (2016). In vivo bioimpedance changes during haemorrhagic and ischaemic stroke in rats: towards 3D stroke imaging using electrical impedance tomography. *Physiological Measurement*, 37(6), 765-784. doi:[10.1088/0967-3334/37/6/765](https://doi.org/10.1088/0967-3334/37/6/765)
- [51] Dowrick, T., Blochet, C., Chaulet, N., and Holder, D.S. (2014). A custom EIT system based on off-the-shelf equipment. In *proceedings of the 15th international conference on biomedical applications of EIT*, Ontario, Canada Retrieved from <http://www.sce.carleton.ca/faculty/adler/eit2014/EIT2014-proceedings.pdf>
- [52] Ehntholt, M. S., Parasram, M., & Mir, S. A. (2020). Mobile Stroke Units: bringing treatment to the patient. *Curr Treat Options Neurol*. 22(2), Article 5. doi: [10.1007/s11940-020-0611-0](https://doi.org/10.1007/s11940-020-0611-0)
- [53] Evans, J. W., Kundu, P., Horovitz, S. G., & Bandettini, P. A. (2015). Separating slow BOLD from non-BOLD baseline drifts using multi-echo fMRI. *NeuroImage*, 105, 189–197. doi:[10.1016/j.neuroimage.2014.10.051](https://doi.org/10.1016/j.neuroimage.2014.10.051)
- [54] Everitt, A., Root, B. K., Bauer, D. F., & Halter, R. J. (2019). Electrical impedance mapping for localizing evolving traumatic brain injury. In *Proceedings of SPIE Medical Imaging 2019: Biomedical Applications in Molecular, Structural, and Functional Imaging*, 109530W, San Diego, CA. doi: [10.1117/12.2512292](https://doi.org/10.1117/12.2512292)
- [55] Fabrizi, L., McEwan, A., Oh, T., Woo, E. J., & Holder, D. S. (2009). An electrode addressing protocol for imaging brain function with electrical impedance tomography using a 16-channel semi-parallel system. *Physiological Measurement*, 30(6), 85–101. doi:[10.1088/0967-3334/30/6/S06](https://doi.org/10.1088/0967-3334/30/6/S06)
- [56] Fabrizi, L., McEwan, A., Oh, T., Woo, E. J., & Holder, D. S. (2009). A comparison of two EIT systems suitable for imaging impedance changes in epilepsy. *Physiological Measurement*, 30(6), S103–120. doi:[10.1088/0967-3334/30/6/S07](https://doi.org/10.1088/0967-3334/30/6/S07)
- [57] Fabrizi, L., Sparkes, M., Horesh, L., Perez-Juste Abascal, J. F., McEwan, A., Bayford, R. H., Elwes, R., Binnie, C.D., & Holder, D. S. (2006). Factors limiting

- the application of electrical impedance tomography for identification of regional conductivity changes using scalp electrodes during epileptic seizures in humans. *Physiological Measurement*, 27(5), S163–S174. [doi:10.1088/90967-3334/27/5/S14](https://doi.org/10.1088/90967-3334/27/5/S14)
- [58] Faiz, K. W., Labberton, A. S., Thommessen, B., Rønning, O. M., Dahl, F. A., & Barra, M. (2018). The burden of stroke mimics: Present and future projections. *Journal of Stroke and Cerebrovascular Diseases*, 27(5), 1288–1295. [doi: 10.1016/j.jstrokecerebrovasdis.2017.12.011](https://doi.org/10.1016/j.jstrokecerebrovasdis.2017.12.011)
- [59] Fassbender, K., Grotta, J. C., Walter, S., Grunwald, I. Q., Ragoschke-schumm, A., & Saver, J. L. (2017). Mobile stroke units for prehospital thrombolysis, triage, and beyond: benefits and challenges. *The Lancet. Neurology*, 16(3), 227–237. [doi:10.1016/S1474-4422\(17\)30008-X](https://doi.org/10.1016/S1474-4422(17)30008-X)
- [60] Faulkner, M., Hannan, S., Aristovich, K., Avery, J., & Holder, D. (2018). Feasibility of imaging evoked activity throughout the rat brain using electrical impedance tomography. *NeuroImage*, 178, 1–10. [doi: 10.1016/j.neuroimage.2018.05.022](https://doi.org/10.1016/j.neuroimage.2018.05.022)
- [61] Faulkner, M., Hannan, S., Aristovich, K., Avery, J., & Holder, D. (2018). Characterising the frequency response of impedance changes during evoked physiological activity in the rat brain. *Physiological Measurement*, 39(3), 034007. [doi: 10.1088/1361-6579/aab01f](https://doi.org/10.1088/1361-6579/aab01f)
- [62] Flaherty, B., F., Moore., H., E., Riva-Cambrin., J., Bratton., S., L. (2019). Repeat head CT for expectant management of Traumatic Epidural Hematoma. *Pediatrics*, 142(3), e 20180385. [doi: 10.1542/peds.2018-0385](https://doi.org/10.1542/peds.2018-0385)
- [63] Frerichs, I. (2000). Electrical Impedance Tomography (EIT) in applications related to lung and ventilation: a review of experimental and clinical activities. *Physiological Measurement*, 21, R1-R21. [doi: 10.1088/0967-3334/21/2/201](https://doi.org/10.1088/0967-3334/21/2/201)
- [64] Fukamachi, A., Nagaseki, Y., Kohno, K., and Wakao, T. (1985). The incidence and developmental process of delayed Traumatic Intracerebral Haematomas. *Acta Neurochirurgica*. 74, 35-39. [doi: 10.1007/BF01413274](https://doi.org/10.1007/BF01413274)
- [65] Gabriel, C., Peyman, A., Grant, E. H. (2009). Electrical conductivity of tissue at frequencies below 1 MHz. *Physics in Medicine and Biology*, 54(16), 4863-4878. [doi:10.1088/0031-9155/54/16/002](https://doi.org/10.1088/0031-9155/54/16/002)
- [66] Gabriel, S., Lau, R. W., Gabriel, C. (1996). The dielectric properties of biological tissue II: Measurements in the frequency range 10 Hz to 20 GHz. *Physics in Medicine and Biology*, 41, 2251-2269. [doi:10.1088/0031-9155/41/11/002](https://doi.org/10.1088/0031-9155/41/11/002)

- [67] Gargalas, S., Weeks, R., Khan-Bourne, N., Shotbolt, P., Simblett, S., Ashraf, L., Doyle, C., Bancroft, V., & David, A. S. (2016). Incidence and outcome of functional stroke mimics admitted to a hyperacute stroke unit. *Journal of Neurology, Neurosurgery and Psychiatry*, 88(1), 2–6. Retrieved from <https://jnnp.bmj.com/content/88/1/2>
- [68] Giles, M. F., & Rothwell, P. M. (2010). Systematic review and pooled analysis of published and unpublished validations of the ABCD and ABCD2 transient ischemic attack risk scores. *Stroke*, 41(4), 667–73. [doi:10.1161/STROKEAHA.109.571174](https://doi.org/10.1161/STROKEAHA.109.571174)
- [69] Goren, N., Avery, J., Dowrick, T., Mackle, E., Witkowska-Wrobel, A., Werring, D., & Holder, D. (2018). Data Descriptor: Multi-frequency electrical impedance tomography and neuroimaging data in stroke patients. *Scientific Data*, 5, Article number: 180112. [doi: 10.1038/sdata.2018.112](https://doi.org/10.1038/sdata.2018.112)
- [70] Gottlibe, M., Rosen, O., Weller, B., Mahagney, A., Omar, N., Khuri, A., Srugo, I., & Genizi, J. (2020). Stroke identification using a portable EEG device – A pilot study. *Neurophysiologie Clinique*. [doi: 10.1016/j.neucli.2019.12.004](https://doi.org/10.1016/j.neucli.2019.12.004)
- [71] Goyal, M., Menon, B. K., Van Zwam, W. H., Dippel, D. W. J., Mitchell, P. J., Demchuk, A. M., & Jovin, T. G. (2016). Endovascular thrombectomy after large-vessel ischaemic stroke: A meta-analysis of individual patient data from five randomised trials. *The Lancet*, 387(10029), 1723–1731. [doi: 10.1016/ S0140-6736\(16\)00163-X](https://doi.org/10.1016/S0140-6736(16)00163-X)
- [72] Gracia, L., Tomas, J., Parra, L., & Lloret, J. (2019). An m-health application for cerebral stroke detection and monitoring using cloud services. *Int. Jour. of Information Management*. 45, 319-327. [doi: 10.1016/j.ijinfomgt.2018.06.004](https://doi.org/10.1016/j.ijinfomgt.2018.06.004)
- [73] Greenberg, M. S. (2006). *Handbook of neurosurgery, sixth edition*. Greenberg Graphics, Inc., Tampa, FL. Could be found at: <https://www.amazon.com/Mark-Greenberg-Handbook-Neurosurgery-sixth/dp/B008UYYH02>
- [74] Gutiérrez, J. M., Emery, R. J., Parker, S. A., Jackson, K., & Grotta, J. C. (2016). Radiation monitoring results from the first year of operation of a unique ambulance-based Computed Tomography unit for the improved diagnosis and treatment of stroke patients. *Health Physics*, 110(5), S73-S80. [doi:10.1097/HP.0000000000000502](https://doi.org/10.1097/HP.0000000000000502)

- [75] Gyrd-Hansen, D., Olsen, K. R., Kronborg, C., Ebinger, M., & Heinrich, J. A. (2015). Cost-effectiveness estimate of prehospital thrombolysis. *Neurology*, 84(11), 1090-1097. [doi: 10.1212/WNL.0000000000001366](https://doi.org/10.1212/WNL.0000000000001366)
- [76] Hamilton, S. J., Lionheart, W. R. B., & Adler, A. (2019). Comparing D-bar and common regularization-based methods for electrical impedance tomography. *Physiological Measurement*, 40(4), 044004. [doi:10.1088/1361-6579/ab14aa](https://doi.org/10.1088/1361-6579/ab14aa)
- [77] Hannan, S., Faulkner, M., Aristovich, K., Avery, J., Walker, M. C., & Holder, D. S. (2020). In vivo imaging of deep neural activity from the cortical surface during hippocampal epileptiform events in the rat brain using Electrical Impedance Tomography. *NeuroImage*, 209, 116525. [doi: 10.1016/j.neuroimage.2020.116525](https://doi.org/10.1016/j.neuroimage.2020.116525)
- [78] Hannan, S., Faulkner, M., Aristovich, K., Avery, J., Walker, M., & Holder, D. (2018). Imaging fast electrical activity in the brain during ictal epileptiform discharges with electrical impedance tomography. *NeuroImage: Clinical*, 20, 674–684. [doi: 10.1016/j.nicl.2018.09.004](https://doi.org/10.1016/j.nicl.2018.09.004)
- [79] Holder, D. (2005). Appendix A – brief introduction to bioimpedance. In Holder, D. S. (Editor), *Electrical Impedance tomography: methods, history and applications* (pp. 411–422). IOP Publishing Ltd., Bristol and Philadelphia. Retrieved from <https://biomedical-engineering-online.biomedcentral.com/articles/10.1186/1475-925X-4-27>
- [80] Holder, D. (2005). Appendix B – introduction to biomedical electrical impedance tomography. In Holder, D. S. (Editor), *Electrical Impedance tomography: methods, history and applications* (pp. 423–449). IOP Publishing Ltd., Bristol and Philadelphia. Retrieved from <https://biomedical-engineering-online.biomedcentral.com/articles/10.1186/1475-925X-4-27>
- [81] Holder, D. and Tidswell, T. (2005). Electrical impedance tomography of brain function. In Holder, D. S. (Editor), *Electrical Impedance tomography: methods, history and applications* (pp. 127–166). IOP Publishing Ltd., Bristol and Philadelphia. Retrieved from <https://biomedical-engineering-online.biomedcentral.com/articles/10.1186/1475-925X-4-27>
- [82] Horesh L. (2006). *Some Novel Approaches in Modelling and Image Reconstruction for Multi-Frequency Electrical Impedance Tomography of the Human Brain* (PhD thesis). University College London, London. Retrieved from <https://pdfs.semanticscholar.org/b99a/8256f65402b08aa4bb024cfdca29c01f89ce.pdf>

- [83] Horesh, L., Schweiger, M., Bollhöfer, M., Holder, D. S., & Arridge, S. R. (2006). Multilevel preconditioning for 3d large-scale soft-field medical applications modelling. *International journal of information and systems sciences*, 2(4), 532–556. Retrieved from <http://www.math.ualberta.ca/ijiss/SS-Volume-2-2006/No-4-06/SS-06-04-07.pdf>
- [84] Howard, R., Hirsch, N., Kitchen, N., Kullmann, D., & Walker, M. (2009). Disorders of consciousness, intensive care neurology and sleep. In Clarke, C., Howard, R., Possor, M., and Shorvon, S. (Eds), *Neurology: A Queen Square Textbook* (pp.743-748). Blackwell Publishing Ltd, Oxford, UK. Could be found at: <https://www.wiley.com/en-us/Neurology%3A+A+Queen+Square+Textbook%2C+2nd+Edition-p-9781118486177>
- [85] Hu, S., Cui, B., Mlynash, M., Zhang, X., Mehta, K. M., & Lansberg, M. G. (2020). Stroke epidemiology and stroke policies in China from 1980 to 2017: A systematic review and meta-analysis. *Int. Journal of Stroke*, 15(210), 18–28. doi: [10.1177/1747493019873562](https://doi.org/10.1177/1747493019873562)
- [86] Hui, F. K., El Mekabaty, A., Schultz, J., Hong, K., Horton, K., Urrutia, V., Naqvi, I., Brast, S., Lynch, J. K., & Nadareishvili, Z. (2018). Helistroke: neurointerventionalist helicopter transport for interventional stroke treatment: proof of concept and rationale. *J. Neuro Intervent Surg*, 10(3), 225-228. doi:[10.1136/neurintsurg-2017-013050](https://doi.org/10.1136/neurintsurg-2017-013050)
- [87] Infrascan Research and Publications. (2020). Retrieved April 29, 2020, from <https://infrascanner.com/research/>
- [88] International Electrotechnical Commission. (2002). IEC 60601-1: Medical electrical equipment: part 1: general requirements for basic safety and essential performance. Retrieved from https://www.ele.uri.edu/courses/bme484/iec60601-1ed3.0_parts.pdf
- [89] Jehl, M., & Holder, D. (2016). Correction of electrode modelling errors in Multi-Frequency EIT imaging. *Physiological Measurement*, 37(6), 893-903. doi:[10.1088/0967-3334/37/6/893](https://doi.org/10.1088/0967-3334/37/6/893)
- [90] Jehl, M., Aristovich, K., Faulkner, M., and Holder, D., (2016). Are patient specific meshes required for EIT head imaging? *Physiological Measurement*, 37(6), 879-892. doi:[10.1088/0967-3334/37/6/879](https://doi.org/10.1088/0967-3334/37/6/879)

- [91] Jehl, M., Avery, J., Malone, E., Holder, D., & Betcke, T. (2015). Correcting electrode modelling errors in EIT on realistic 3D head models. *Physiological Measurement*, 36(12), 2423–2442. [doi: 10.1088/0967-3334/36/12/2423](https://doi.org/10.1088/0967-3334/36/12/2423)
- [92] Jehl, M., Dedner, A., Betcke, T., Aristovich, K., Kloforn, R., & Holder, D. (2014). A fast parallel solver for the forward problem in Electrical Impedance Tomography. *IEEE Transactions on Bio-Medical Engineering*, 9294(c), 1–13. [doi:10.1109/TBME.2014.2342280](https://doi.org/10.1109/TBME.2014.2342280)
- [93] Kellner, C. P., Sauvageau, E., Snyder, K. V., Fargen, K. M., Arthur, A. S., Turner, R. D., & Alexandrov, A. V. (2018). The VITAL study and overall pooled analysis with the VIPS non-invasive stroke detection device. *Journal of NeuroInterventional Surgery*, 10(11), 1079–1084. [doi: 10.1136/neurintsurg-2017-013690](https://doi.org/10.1136/neurintsurg-2017-013690)
- [94] Kennedy, J. D., & Gerard, E. E. (2012). Continuous EEG monitoring in the intensive care unit. *Current Neurology and Neuroscience Reports*, 12(4), 419–28. [doi:10.1007/s11910-012-0289-0](https://doi.org/10.1007/s11910-012-0289-0)
- [95] Kim, J., Thayabaranathan, T., Donnan, G. A., Howard, G., Howard, V. J., Rothwell, P. M., ... & Thrift, A. G. (2020). Global Stroke Statistics 2019. *Int. Journal of Stroke*, 0(0), 1–20. [doi: 10.1177/1747493020909545](https://doi.org/10.1177/1747493020909545)
- [96] Koliass, A. G., Guilfoyle, M. R., Helmy, A., Allanson, J., & Hutchinson, P. J. (2013). Traumatic brain injury in adults. *Practical Neurology*, 13(4), 228-235. [doi: 10.1136/practneurol-2012-000268](https://doi.org/10.1136/practneurol-2012-000268)
- [97] Langlois, J. A., Rutland-brown, W., & Wald, M. M. (2006). The epidemiology and impact of Traumatic Brain Injury: a brief overview. *Journal for head trauma rehabilitation*, 21(5), pp.375-378. [doi: 10.1097/00001199-200609000-00001](https://doi.org/10.1097/00001199-200609000-00001)
- [98] Li, G., Ma, K., Sun, J., Jin, G., Qin, M., & Feng, H. (2017). Twenty-Four-Hour real-time continuous monitoring of cerebral edema in rabbits based on a non-invasive and noncontact system of magnetic induction. *Sensors*, 17(3), 537. [doi:10.3390/s17030537](https://doi.org/10.3390/s17030537)
- [99] Li, H., Liu, X., Xu, C., Yang, B., Fu, D., Dong, X., & Fu, F. (2020). Managing erroneous measurements of dynamic brain electrical impedance tomography after reconnection of faulty electrodes. *Physiological Measurement*, 41(3), 035002. [doi: 10.1088/1361-6579/ab71f4](https://doi.org/10.1088/1361-6579/ab71f4)
- [100] Li, Y., Zhang, D., Lin, B., Jin, Z., Duan, W., Dong, X., Fu, F., Yu, S., & Shi, X. (2018). Noninvasive cerebral imaging and monitoring using Electrical Impedance Tomography during Total Aortic Arch Replacement. *Journal of*

Cardiothoracic and Vascular Anesthesia. 32(6), 2469–2476. [doi: 10.1053/j.jvca.2018.05.002](https://doi.org/10.1053/j.jvca.2018.05.002)

- [101] Ljungqvist, J., Candefjord, S., Persson, M., Skoglund, T., & Elam, M. (2017). Clinical evaluation of a microwave-based device for detection of traumatic Intracranial hemorrhage. *J Neurotrauma*, 34(13), 2176–2182. [doi:10.1089/neu.2016.4869](https://doi.org/10.1089/neu.2016.4869)
- [102] Losseff, N., Brown, M., Grieve, J. (2009). Stroke and Cerebrovascular Diseases. In Clarke, C., Howard, R., Possor, M., and Shorvon, S. (Eds), *Neurology: A Queen Square Textbook* (pp.109-154). Blackwell Publishing Ltd, Oxford, UK. Could be found at: <https://www.wiley.com/en-us/Neurology%3A+A+Queen+Square+Textbook%2C+2nd+Edition-p-9781118486177>
- [103] Lowtherl, D. A., Throne, R. D., Olson, L. G., & Windle, J. R. (2001). A comparison of zero and first order Tikhonov regularization for an Inhomogeneous volume. *Computers in Cardiology*, 28, 541-544. [doi: 10.1109/CIC.2001.977712](https://doi.org/10.1109/CIC.2001.977712)
- [104] Luppi, O., Gonzalez, R., Castro, T., Silva, F., Seiji, R., & Tsuzuki, G. (2016). Influence of current injection pattern and electric potential measurement strategies in electrical impedance tomography. *Control Engineering Practice*, 58(C), 276-286. doi.org/10.1016/j.conengprac.2016.03.003
- [105] Ma, H., Li, H., Liu, X., Li, W., Xia, J., Liu, B., Shi, X., Dong, X., & Fu, F. (2019). Real-time monitoring of Contact Impedance from multiple electrode – scalp interfaces during cerebral Electrical Impedance Tomography. *IEEE Access*, 7, 95186-95196. [doi: 10.1109/ACCESS.2019.2928580](https://doi.org/10.1109/ACCESS.2019.2928580)
- [106] Ma, J., Xu, C., Dai, M., You, F., Shi, X., Dong, X., & Fu, F. (2014). Exploratory study on the methodology of fast imaging of human heads, 2014. *The Scientific World Journal*. Article ID 534012. [doi:10.1155/2014/534012](https://doi.org/10.1155/2014/534012)
- [107] Malone, E., Jehl, M., Arridge, S., Betcke, T., & Holder, D. (2014). Stroke type differentiation using spectrally constrained multifrequency EIT: evaluation of feasibility in a realistic head model. *Physiological Measurement*, 35(6), 1051–1066. [doi:10.1088/0967-3334/35/6/1051](https://doi.org/10.1088/0967-3334/35/6/1051)
- [108] Malone, E., Sato Dos Santos, G., Holder, D., & Arridge, S. (2014). Multifrequency electrical impedance tomography using spectral constraints. *IEEE Transactions on Medical Imaging*, 33(2), 340–350. [doi: 10.1109/TMI.2013.2284966](https://doi.org/10.1109/TMI.2013.2284966)

- [109] Manwaring, P. K., Moodie, K. L., Hartov, A., Manwaring, K. H., & Halter, R. J. (2013). Intracranial electrical impedance tomography: a method of continuous monitoring in an animal model of head trauma. *Anesthesia and Analgesia*, 117(4), 866–75. [doi:10.1213/ANE.0b013e318290c7b7](https://doi.org/10.1213/ANE.0b013e318290c7b7)
- [110] Marsh, E. B., Llinas, R. H., Schneider, A. L. C., Hillis, A. E., Lawrence, E., Dziedzic, P., & Gottesman, R. F. (2016). Predicting Hemorrhagic Transformation of acute ischemic stroke prospective validation of the HeRS score. *Medicine*, 95(2), e2430. [doi:10.1097/MD.0000000000002430](https://doi.org/10.1097/MD.0000000000002430)
- [111] Matsuda, W., Sugimoto, K., Sato, N., Watanabe, T., Fujimoto, A., & Matsumura, A. (2008). Delayed onset of posttraumatic acute subdural hematoma after mild head injury with normal computed tomography: a case report and brief review. *The Journal of Trauma*, 65(2), 461–463. [doi: 10.1097/01.ta.0000202465.13784.2a](https://doi.org/10.1097/01.ta.0000202465.13784.2a)
- [112] McAdams, E. T., Jossinet, J., Lackermeier, A., & Risacher, F. (1996). Factors affecting electrode-gel-skin interface impedance in electrical impedance tomography. *Medical & Biological Engineering & Computing*, 34(6), 397–408. Retrieved from <http://www.ncbi.nlm.nih.gov/pubmed/9039740>
- [113] McCann, H., Pisano, G., & Beltrachini, L. (2019). Variation in reported human head tissue electrical conductivity values. *Brain Topography*, 32, 825-858. [doi: 10.1007/s10548-019-00710-2](https://doi.org/10.1007/s10548-019-00710-2)
- [114] McDermott, B., O'Halloran, M., Porter, E., & Santorelli, A. (2020). Brain haemorrhage detection using a SVM classifier with electrical impedance tomography measurement frames. *PLoS ONE*, 13(7), e0200469. [doi: 10.1371/journal.pone.0200469](https://doi.org/10.1371/journal.pone.0200469)
- [115] McDermott, B., Porter, E., Jones, M., McGinley, B., & O'Halloran, M. (2018). Symmetry difference electrical impedance tomography- A novel modality for anomaly detection. *Physiological Measurement*, 39(4), 044007. [doi: 10.1088/1361-6579/aab656](https://doi.org/10.1088/1361-6579/aab656)
- [116] Merino, J. G., Luby, M., Benson, R. T., Davis, L. A., Hsia, A. W., Latour, L. L., Lynch, J. K., & Warach, S. (2013). Predictors of acute stroke mimics in 8187 patients referred to a stroke service. *Journal of Stroke and Cerebrovascular Diseases*, 22(8), 397–403. [doi: 10.1016/j.jstrokecerebrovasdis.2013.04.018](https://doi.org/10.1016/j.jstrokecerebrovasdis.2013.04.018)

- [117] Meyer, B. C., & Lyden, P., D. (2010). The modified National Institutes of Health Stroke Scale (mNIHSS): Its time has come. *Int J Stroke*, 4(4), 267–273. [doi:10.1111/j.1747-4949.2009.00294.x](https://doi.org/10.1111/j.1747-4949.2009.00294.x)
- [118] Mohammed, B. J., Abbosh, A., Bialkowski, K., & Mustafa, S. (2014). Investigation of noise effect on image quality in microwave head imaging systems. *IET Microwaves, Antennas & Propagation*, 9(3), 200-205. [doi:10.1049/iet-map.2014.0109](https://doi.org/10.1049/iet-map.2014.0109)
- [119] Moreau, F., Yang, R., Nambiar, V., Demchuk, A. M., & Dunn, J. F. (2016). Near-infrared measurements of brain oxygenation in stroke. *Neurophotonics*, 3(3), 031403. [doi: 10.1117/1.NPh.3.3.031403](https://doi.org/10.1117/1.NPh.3.3.031403)
- [120] Muir, K. W. (2017). Stroke in the acute setting. *Medicine*, 45(3), 163–168. [doi: 10.1016/j.mpmed.2016.12.008](https://doi.org/10.1016/j.mpmed.2016.12.008)
- [121] Mukherjee, D., & Patil, C. G. (2011). Epidemiology and the global burden of stroke. *World Neurosurgery*, 76(6 Suppl), S85–90. [doi: 10.1016/j.wneu.2011.07.023#](https://doi.org/10.1016/j.wneu.2011.07.023#)
- [122] Murphy, D., Burton, P., Coombs, R., Tarassenko, L., & Rolfe, P. (1987). Impedance imaging in the newborn. *Clinical Physics and Physiological Measurement*, 8(4A), 131–140. [doi:10.1088/0143-0815/8/4A/017](https://doi.org/10.1088/0143-0815/8/4A/017)
- [123] Nor, A. M., Davis, J., Sen, B., Shipsey, D., Louw, S. J., Dyker, A. G., Davis, M., & Ford, G. a. (2005). The Recognition of Stroke in the Emergency Room (ROSIER) scale: development and validation of a stroke recognition instrument. *The Lancet. Neurology*, 4(11), 727–734. [doi:10.1016/S1474-4422\(05\)70201-5](https://doi.org/10.1016/S1474-4422(05)70201-5)
- [124] Nor, A. M., McAllister, C., Louw, S. J., Dyker, A. G., Davis, M., Jenkinson, D., & Ford, G. A. (2004). Agreement between ambulance paramedic- and physician-recorded neurological signs with Face Arm Speech Test (FAST) in acute stroke patients. *Stroke*, 35(6), 1355–1359. [doi:10.1161/01.STR.0000128529.63156.c5](https://doi.org/10.1161/01.STR.0000128529.63156.c5)
- [125] Oostenveld, R., & Praamstra, P. (2001). The five percent electrode system for high-resolution EEG and ERP measurements. *Clin. Neurophysiology*, 112, 713-719. [doi:10.1016/S1388-2457\(00\)00527-7](https://doi.org/10.1016/S1388-2457(00)00527-7)
- [126] Orlando, A., Wagner, J. C., Fanale, C. V., Whaley, M., McCarthy, K. L., & Bar-Or, D. (2016). A Four-year experience of symptomatic intracranial hemorrhage following intravenous tissue Plasminogen Activator at a Comprehensive Stroke Center. *Journal of Stroke and Cerebrovascular Diseases*, 25(4), 969–976. [doi: 10.1016/j.jstrokecerebrovasdis.2016.01.003](https://doi.org/10.1016/j.jstrokecerebrovasdis.2016.01.003)

- [127] Oziel, M., Hjouj, M., Rubinsky, B., & Korenstein, R. (2020). Multifrequency analysis of single inductive coil measurements across a gel phantom simulation of internal bleeding in the brain, *Bioelectromagnetics*, 41(1),21-33. [doi: 10.1002/bem.22230](https://doi.org/10.1002/bem.22230)
- [128] Oziel, M., Korenstein, R., & Rubinsky, B. (2020). A brain phantom study of a noncontact single inductive coil device and the attendant algorithm for first stage diagnosis of internal bleeding in the head. *J. Med. Devices*. 14(1): 011102. [doi: 10.1115/1.4045489](https://doi.org/10.1115/1.4045489)
- [129] Packham, B., Koo, H., Romsauerova, A., Ahn, S., McEwan, A., Jun, S. C., & Holder, D. S. (2012). Comparison of frequency difference reconstruction algorithms for the detection of acute stroke using EIT in a realistic head-shaped tank. *Physiological Measurement*, 33(5), 767–786. [doi: 10.1088/0967-3334/33/5/767](https://doi.org/10.1088/0967-3334/33/5/767)
- [130] Persson, M., Fhager, A., Dobř, H., Karlsson, J., & Elam, M. (2014). Microwave-based stroke diagnosis making global pre-hospital thrombolytic treatment possible. *IEEE Transactions on Biomedical Engineering*, 61(11), 2806-2817. [doi:10.1109/TBME.2014.2330554](https://doi.org/10.1109/TBME.2014.2330554)
- [131] Qureshi, A. I., Malik, A. A., Adil, M. M., Defillo, A., Sherr, G. T., & Suri, M. F. K. (2015). Hematoma Enlargement among patients with Traumatic Brain Injury: analysis of a prospective multicentre clinical trial. *J Vasc. and Inter Neurology*. 8(3), 42–49. Retrieved from <https://www.ncbi.nlm.nih.gov/pmc/articles/PMC4535606/>
- [132] Rahman, T., Hasan, M. M., Farooq, A., & Uddin, M. Z. (2013). Extraction of cardiac and respiration signals in electrical impedance tomography based on independent component analysis. *Journal of Electrical Bioimpedance*, 4(1), 38–44. [doi:10.5617/jeb.553](https://doi.org/10.5617/jeb.553)
- [133] Ravagli, E., Mastitskaya, S., Thompson, N., Aristovich, K., & Holder, D. (2019). Optimization of the electrode drive pattern for imaging fascicular compound action potentials in peripheral nerve with fast neural electrical impedance tomography. *Physiological Measurement*, 40(11), 115007. [doi: 10.1088/1361-6579/ab54eb](https://doi.org/10.1088/1361-6579/ab54eb)
- [134] Romsauerova A., McEwan A., Horesh L., Oh T.I., Woo E.J., & Holder D.S. (2007) A comparison of Multi-Frequency EIT systems intended for acute stroke imaging. In: Magjarevic R., Nagel J.H. (Eds), *World Congress on Medical Physics and Biomedical Engineering 2006*. IFMBE Proceedings,

14(5), 3777–3779. Springer, Berlin, Heidelberg. [doi: 10.1007/978-3-540-36841-0_991](https://doi.org/10.1007/978-3-540-36841-0_991)

- [135] Romsauerova, A., McEwan, A., Horesh, L., Yerworth, R., Bayford, R. H., & Holder, D. S. (2006). Multi-frequency electrical impedance tomography (EIT) of the adult human head: initial findings in brain tumours, arteriovenous malformations and chronic stroke, development of an analysis method and calibration. *Physiological Measurement*, 27(5), S147–161. [doi:10.1088/0967-3334/27/5/S13](https://doi.org/10.1088/0967-3334/27/5/S13)
- [136] S. Khan, P. Manwaring, A. Borsic and R. Halter. (2015). FPGA-based voltage and current dual drive system for high frame rate Electrical Impedance Tomography. *IEEE Transactions on Medical Imaging*. 34(4), 888-901. [doi: 10.1109/TMI.2014.2367315](https://doi.org/10.1109/TMI.2014.2367315)
- [137] Samandouras, G. (2010). *The neurosurgeon's handbook*. Oxford University Press, Oxford. [doi: 10.1093/med/9780198570677.001.0001](https://doi.org/10.1093/med/9780198570677.001.0001)
- [138] Scapatucci, R., Bucci, O. M., Catapano, I., & Crocco, L. (2014). Differential microwave imaging for brain stroke followup. *International Journal of Antennas and Propagation*, Article ID 312528, 1–11. [doi:10.1155/2014/312528](https://doi.org/10.1155/2014/312528)
- [139] Sekhon, M. S., Griesdale, D. E., Robba, C., McGlashan, N., Needham, E., Walland, K., Shook, A. C., Smielewski, P., Czosnyka, M., Gupta, A. K., & Menon, D. K. (2014). Optic nerve sheath diameter on computed tomography is correlated with simultaneously measured intracranial pressure in patients with severe traumatic brain injury. *Intensive Care Medicine*, 40(9), 1267–1274. [doi:10.1007/s00134-014-3392-7](https://doi.org/10.1007/s00134-014-3392-7)
- [140] Seoane, F., Atefi, S. R., Tomner, J., Kostulas, K., & Lindecrantz, K. (2015). Electrical Bioimpedance Spectroscopy on acute unilateral stroke patients: Initial observations regarding differences between sides. *BioMed Research International*. Article ID 613247. [doi:10.1155/2015/613247](https://doi.org/10.1155/2015/613247)
- [141] Smith, M. (2011). Shedding light on the adult brain: a review of the clinical applications of near-infrared spectroscopy. *Philosophical Transactions. Series A, Mathematical, Physical, and Engineering Sciences*, 369(1955), 4452–69. [doi:10.1098/rsta.2011.0242](https://doi.org/10.1098/rsta.2011.0242)
- [142] Smith, W. S., Browne, J. L., & Ko, N. U. (2015). Cranial accelerometry can detect cerebral vasospasm caused by Subarachnoid Hemorrhage. *Neurocrit Care*, 23, 364–369. [doi: 10.1007/s12028-015-0118-9](https://doi.org/10.1007/s12028-015-0118-9)

- [143] Stanca, M. D., Marginean, I. C., Soritau, O., Dragos, C., Marginean, M., Muresanu, D. F., Vester, J. C., & Rafila, A. (2015). GFAP and antibodies against NMDA receptor subunit NR2 as biomarkers for acute cerebrovascular diseases. *J. Cell. Mol. Med.* 19(9), 2253–2261. [doi:10.1111/jcmm.12614](https://doi.org/10.1111/jcmm.12614)
- [144] Stocker, R. A. (2019). Intensive care in Traumatic Brain Injury including Multi-Modal Monitoring and Neuroprotection. *Med. Sci*, 7(3), 37. [doi: 10.3390/medsci7030037](https://doi.org/10.3390/medsci7030037)
- [145] Subramaniam, M., Singh, D., Park, S. J., Kim, S. E., Kim, D. J., Im, J. N., Lee, K. S., & Min, S. N. (2018). IoT based wake-up stroke prediction - Recent trends and directions. In *IOP Conf. Ser.: Mater. Sci. Eng.* 402, 012045. [doi: 10.1088/1757-899X/402/1/012045](https://doi.org/10.1088/1757-899X/402/1/012045)
- [146] Sussman, E. S., & Connolly, E. S. (2013). Haemorrhagic transformation: a review of the rate of haemorrhage in the major clinical trials of acute ischemic stroke. *Frontiers in Neurology*, 4, 69. [doi:10.3389/fneur.2013.00069](https://doi.org/10.3389/fneur.2013.00069)
- [147] Tagliaferri, F., Compagnone, C., Korsic, M., Servadei, F., & Kraus, J. (2006). A systematic review of brain injury epidemiology in Europe. *Acta Neurochirurgica*, 148(3), 255–268. [doi: 10.1007/s00701-005-0651-y](https://doi.org/10.1007/s00701-005-0651-y)
- [148] Tang, C., You, F., Cheng, G., Gao, D., Fu, F., Yang, G., & Dong, X. (2008). Correlation Between Structure and Resistivity Variations of the Live Human Skull. *IEEE Transactions on Biomedical Engineering.* 55(9), 2286-2292. [doi: 10.1109/TBME.2008.923919](https://doi.org/10.1109/TBME.2008.923919)
- [149] Teasdale, G., and Jennett, B. (1974). Assessment of coma and impaired consciousness. A practical scale. *Lancet* 13 (2): 81–84. [doi: 10.1016/S0140-6736\(74\)91639-0](https://doi.org/10.1016/S0140-6736(74)91639-0)
- [150] Tidswell, A. T., Bagshaw, A. P., Holder, D. S., Yerworth, R. J., Eadie, L., Murray, S., Morgan, L., Bayford, R. H. (2003). A comparison of headnet electrode arrays for electrical impedance tomography of the human head. *Physiological Measurement*, 24(2), 44- 527. [doi: 10.1088/0967-3334/24/2/363](https://doi.org/10.1088/0967-3334/24/2/363)
- [151] Tidswell, T., Gibson, A., Bayford, R. H., & Holder, D. S. (2001). Three-dimensional electrical impedance tomography of human brain activity. *NeuroImage*, 13(2), 283–294. [doi:10.1006/nimg.2000.0698](https://doi.org/10.1006/nimg.2000.0698)
- [152] Tikhonov, A. N., Goncharsky A., Stepanov, V. V., & Yagola A. (1995). *Numerical Methods for the Solution of Ill-Posed Problems*, Springer, Berlin. Retrieved from <https://www.springer.com/gp/book/9780792335832>

- [153] Tisdall, M. M., & Smith, M. (2007). Multimodal monitoring in traumatic brain injury: current status and future directions. *British Journal of Anaesthesia*, 99(1), 61–67. [doi:10.1093/bja/aem143](https://doi.org/10.1093/bja/aem143)
- [154] Vauhkonen, M., Vadász, D., Karjalainen, P. a, Somersalo, E., & Kaipio, J. P. (1998). Tikhonov regularization and prior information in electrical impedance tomography. *IEEE Transactions on Medical Imaging*, 17(2), 285–293. [doi:10.1109/42.700740](https://doi.org/10.1109/42.700740)
- [155] Vonach, M., Marson, B., Yun, M., Cardoso, J., Modat, M., Ourselin, S., & Holder, D. (2012). A method for rapid production of subject specific finite element meshes for electrical impedance tomography of the human head. *Physiological Measurement*, 33(5), 801–816. [doi:10.1088/0967-3334/33/5/801](https://doi.org/10.1088/0967-3334/33/5/801)
- [156] Vongerichten, A. N., dos Santos, G. S., Aristovich, K., Avery, J., McEvoy, A., Walker, M., & Holder, D. S. (2016). Characterisation and imaging of cortical impedance changes during interictal and ictal activity in the anaesthetised rat. *NeuroImage*, 124, 813–823. [doi:10.1016/j.neuroimage.2015.09.015](https://doi.org/10.1016/j.neuroimage.2015.09.015)
- [157] Vongerichten, A., dos Santos, G. S., Avery, J., Walker, M., & Holder, D. S. (2014). Electrical Impedance Tomography (EIT) of epileptic seizures in rat models – a potential new tool for diagnosis of seizures. *Clinical Neurophysiology*. 125, S282–S283. [doi: 10.1016/S1388-2457\(14\)50924-8](https://doi.org/10.1016/S1388-2457(14)50924-8)
- [158] Walsh, K. B. (2019). Non-invasive sensor technology for prehospital stroke diagnosis: Current status and future directions. *International Journal of Stroke*, 14(6), 592–602. [doi: 10.1177/1747493019866621](https://doi.org/10.1177/1747493019866621)
- [159] Wang, L., Liu, W., Yu, X., Xu, C., Dong, X., & Gao, F. (2006). Image monitoring for head phantom of Intracranial Hemorrhage using electrical impedance tomography. In *Proceedings of Progress in Electromagnetic Research Symposium (PIERS)*, 1408-1411, Shanghai, China. [doi:10.1109/PIERS.2016.7734663](https://doi.org/10.1109/PIERS.2016.7734663)
- [160] Wi, H., Sohal, H., McEwan, A. L., Woo, E. J., & Oh, T. I. (2014). Multi-Frequency Electrical Impedance Tomography system with automatic self-calibration for long-term monitoring. *IEEE Transactions on Biomedical Circuits and Systems*. 8(1), 119-128. [doi: 10.1109/TBCAS.2013.2256785](https://doi.org/10.1109/TBCAS.2013.2256785)
- [161] Witkowska-Wrobel, A., Aristovich, K., Faulkner, M., Avery, J., & Holder, D. (2018). Feasibility of imaging epileptic seizure onset with EIT and depth electrodes. *NeuroImage*, 173, 311–321. [doi: 10.1016/j.neuroimage.2018.02.056](https://doi.org/10.1016/j.neuroimage.2018.02.056)

- [162] Xu, S., Dai, M., Xu, C., Chen, C., Tang, M., Shi, & Dong, X. (2011). Performance evaluation of five types of Ag / AgCl bio-electrodes for cerebral Electrical Impedance Tomography. *Ann Biomed Eng* 39(7), 2059–2067. [doi: 10.1007/s10439-011-0302-9](https://doi.org/10.1007/s10439-011-0302-9)
- [163] Yamal, J., Rajan, S. S., Parker, S. A., Jacob, A. P., Gonzalez, M. O., Gonzales, N. R., ..., & Grotta, J. C. (2017). Benefits of stroke treatment delivered using a mobile stroke unit trial. *Journal of stroke*. 13(3), 321-327. [doi:10.1177/1747493017711950](https://doi.org/10.1177/1747493017711950)
- [164] Yan, Q., Jin, G., Ma, K., Qin, M., Zhuang, W., & Sun, J. (2017). Magnetic inductive phase shift: A new method to differentiate hemorrhagic stroke from ischemic stroke on rabbit, *BioMed Eng OnLine*, 16, 63. [doi: 10.1186/s12938-017-0354-7](https://doi.org/10.1186/s12938-017-0354-7)
- [165] Yang, B., Li, B., Xu, C., Hu, S., Dai, M., Xia, J., Lou, P., Shi, X., Zhao, Z., Dong, X., Fei, Z., & Fu, F. (2019). Comparison of electrical impedance tomography and intracranial pressure during dehydration treatment of cerebral edema. *NeuroImage: Clinical*, 23, 101909. [doi: 10.1016/j.nicl.2019.101909](https://doi.org/10.1016/j.nicl.2019.101909)
- [166] Yang, L., Dai, M., Xu, C., Zhang, G., Li, W., Fu, F., Shi, X., & Dong, X. (2017). The frequency spectral properties of Electrode-Skin Contact Impedance on human head and its frequency-dependent effects on Frequency-Difference EIT in stroke detection from 10Hz to 1MHz. *PLoS ONE*, 12(1), e0170563. [doi:10.1371/journal.pone.0170563](https://doi.org/10.1371/journal.pone.0170563)
- [167] Yang, L., Li, H., Ding, J., Li, W., Dong, X., Wen, Z., & Shi, X. (2018). Optimal combination of electrodes and conductive gels for brain electrical impedance tomography. *BioMedical Engineering Online*, 17, 186. [doi: 10.1186/s12938-018-0617-y](https://doi.org/10.1186/s12938-018-0617-y)
- [168] Yang, L., Liu, W., Chen, R., Zhang, G., Li, W., Fu, F., & Dong, X. (2017). In vivo bio-impedance spectroscopy characterization of healthy, hemorrhagic and ischemic rabbit brain within 10 Hz–1 MHz. *Sensors*, 17, 791. [doi:10.3390/s17040791](https://doi.org/10.3390/s17040791)
- [169] Yang, L., Xu, C., Dai, M., Fu, F., Shi, X., & Dong, X. (2016). A novel multi-frequency electrical impedance tomography spectral imaging algorithm for early stroke detection. *Physiological Measurement*, 37(12), 2317-2335. [doi:10.1088/1361-6579/37/12/2317](https://doi.org/10.1088/1361-6579/37/12/2317)

- [170] Yang, L., Zhang, G., Song, J., Dai, M., Xu, C., Dong, X., & Fu, F. (2016). Ex-vivo characterization of bioimpedance spectroscopy of normal, ischemic and hemorrhagic rabbit brain tissue at frequencies from 10 Hz to 1 MHz. *Sensors*, 16(11), 1942-1957. [doi:10.3390/s16111942](https://doi.org/10.3390/s16111942)
- [171] Zhou, Y., & Li, X. (2017). Biomedical signal processing and control Multifrequency time difference EIT imaging of cardiac activities. *Biomedical Signal Processing and Control*, 38, 128–135. [doi:10.1016/j.bspc.2017.05.012](https://doi.org/10.1016/j.bspc.2017.05.012)
- [172] Zhou, Z., dos Santos, G. S., Dowrick, E., Avery, j., Li, N., Sun, Z., Xu, X., & Holder, D. (2015). Comparison of total variation algorithms for electrical impedance tomography. *Physiological Measurement*, 36(6),1193-1209. [doi:10.1088/0967-3334/36/6/1193](https://doi.org/10.1088/0967-3334/36/6/1193)
- [173] Zhou, Z., Dowrick, T., Malone, E., Avery, j., Li, N., Sun, Z., Xu, X., & Holder, D. (2015). Multifrequency electrical impedance tomography with total variation regularization. *Physiological Measurement*, 36(9), 1943-1961. [doi:10.1088/0967-3334/36/9/1943](https://doi.org/10.1088/0967-3334/36/9/1943)
- [174] Zhukov, L., & Weinstein, D. (2000). Independent Component Analysis for EEG Source Localization. *IEEE engineering in medicine and biology*, 19(3), 87–96. [doi:10.1109/51.844386](https://doi.org/10.1109/51.844386)